AWARD NUMBER: W81XWH-14-1-0073

TITLE: Prevention and Treatment of Neurofibromatosis Type 1-Associated Malignant Peripheral Nerve Sheath Tumors

PRINCIPAL INVESTIGATOR: Kevin A. Roth, MD, PhD

CONTRACTING ORGANIZATION: Columbia University
New York, NY 10032

REPORT DATE: July 2018

TYPE OF REPORT: Final

PREPARED FOR: U.S. Army Medical Research and Materiel Command
Fort Detrick, Maryland 21702-5012

REPORT DOCUMENTATION PAGE

Form Approved
OMB No. 0704-0188

1. REPORT DATE	2. REPORT TYPE	3. DATES COVERED
July 2018	Final	1Apr2014 - 31Mar2018

4. TITLE AND SUBTITLE
Prevention and Treatment of Neurofibromatosis Type 1-Associated Malignant Peripheral Nerve Sheath Tumors

5a. CONTRACT NUMBER

5b. GRANT NUMBER
W81XWH-14-1-0073

5c. PROGRAM ELEMENT NUMBER

6. AUTHOR(S)
Kevin A. Roth, MD, PhD

E-Mail:karoth@columbia.edu

5d. PROJECT NUMBER

5e. TASK NUMBER

5f. WORK UNIT NUMBER

7. PERFORMING ORGANIZATION NAME(S) AND ADDRESS(ES)

Columbia University Department
of Pathology and Cell Biology
630 West 168th St.
New York, NY 10032

8. PERFORMING ORGANIZATION REPORT NUMBER

9. SPONSORING / MONITORING AGENCY NAME(S) AND ADDRESS(ES)

U.S. Army Medical Research and Materiel Command
Fort Detrick, Maryland 21702-5012

10. SPONSOR/MONITOR'S ACRONYM(S)

11. SPONSOR/MONITOR'S REPORT NUMBER(S)

12. DISTRIBUTION / AVAILABILITY STATEMENT

Approved for Public Release; Distribution Unlimited

13. SUPPLEMENTARY NOTES

14. ABSTRACT

The most common cause of death in Neurofibromatosis Type 1 (NF1) patients is malignant peripheral nerve sheath tumor (MPNST). MPNSTs are aggressive Schwann cell-derived neoplasms that typically arise from precursor lesions such as plexiform neurofibromas. Although gross total resection of MPNSTs is potentially curative, this occurs in only a small minority of cases. Radiotherapy and chemotherapy have almost no effect on patient mortality. NF1 patients have an approximate 10% lifetime risk of developing an MPNST. Thus, development of safe and effective MPNST preventative therapies could have an important impact on NF1 patient morbidity and mortality. In this grant, we are testing the hypothesis that chronic administration of agents that promote apoptosis and/or inhibit pro-survival autophagy will inhibit MPNST formation and progression in transgenic mouse models of MPNST. Specifically, we are examining the mechanisms of action and *in vivo* utility of two classes of drugs, BH3 mimetics and lysosomotropic agents, on MPNSTs. The drugs that we are testing are approved for human use and could be rapidly advanced into human MPNST clinical trials if our pre- clinical testing yields positive results.

15. SUBJECT TERMS
Apoptosis; autophagy; lysosomotropic agents; Bcl2 family members

16. SECURITY CLASSIFICATION OF:			17. LIMITATION OF ABSTRACT	18. NUMBER OF PAGES	19a. NAME OF RESPONSIBLE PERSON
a. REPORT	b. ABSTRACT	c. THIS PAGE			USAMRMC
U	U	U	UU	73	19b. TELEPHONE NUMBER *(include area code)*

Table of Contents

Title of Grant: Prevention and Treatment of Neurofibromatosis Type 1- Associated Malignant Peripheral Nerve Sheath Tumors

Award #: W81XWH-14-1-0073
Principal Investigator: Kevin A. Roth, MD, PhD
Final Report: 04/01/2014– 03/31/2018

1. Introduction

Neurofibromatosis type 1 (NF1) has a frequency of approximately one in 3,000 humans and decreases life expectancy by ten to twenty years. Malignant peripheral nerve sheath tumors (MPNSTs) are the leading cause of death in NF1 patients and typically arise from NF1-associated precursor lesions. NF1 patients have an approximate 10% lifetime risk of developing a MPNST and this risk may be as high as 30% in NF1 patients with symptomatic plexiform neurofibromas. MPNSTs afflict NF1 patients in the prime of their lives, median age at diagnosis being approximately 40 years, and have a poor prognosis with median disease specific survival of approximately five to eight years. Gross total surgical resection is the only curative therapy and is unobtainable in the vast majority of patients. Radiotherapy and chemotherapy have proven largely ineffective in extending MPNST patient survival. Tumor formation and malignant progression are both dependent on the ability of tumor cells to evade normal cell death inducing stimuli. Numerous studies have shown that overexpression of anti-apoptotic Bcl-2 family members such as Bcl-2, Bcl-XL and MCL-1 can decrease tumor cell sensitivity to both radiotherapy and chemotherapy. Small molecule inhibitors of anti-apoptotic Bcl-2 proteins which have a functional BH3 domain, so called "BH3 mimetics", can potentiate tumor cell sensitivity to standard chemotherapeutic agents. Similarly, cytoprotective autophagy is commonly increased in tumor cells permitting these cells to survive in nutrient poor and hypoxic conditions that would kill normal cells. Cytoprotective autophagy can be inhibited by lysosomotropic agents such as chloroquine (CQ) that inhibit lysosome degradation of autophagic vacuoles and their contents. To date, no studies of combined BH3 mimetic and lysosomotropic agents have examined their potential utility as MPNST chemopreventive agents in either animal models or in NF1 patients.

2. Keywords

Apoptosis
Autophagy
Bcl2 family members
Lysosomotropic agents
Usp9X

3. Accomplishments

What were the major goals of the project?

1. To determine therapeutic effects of BH3 mimetics and lysosomotropic agents to inhibit Schwann cell hyperproliferation, MPNST formation and progression in transgenic mouse models.
2. To determine the effects and mechanisms of action of BH3 mimetics and lysosomotropic agents, alone and in combination, on NF1 patient-derived MPNST cell lines *in vitro*.

What was accomplished under these goals?

Over the course of this project, we addressed all of our original aims and extended our research scope to identify novel regulators of MPNST initiation and progression. Overall, our work was divided into three main areas: first, an examination of the effects of BH3 mimetics and lysosomtropic agents on MPNST cells

in vitro and *in vivo*; second, identification of CXCL12 as a possible mediator of BH3 mimetic effects on MPNST cells; and third, our most recent discovery that Usp9X is a potential target for MPNST therapy. A comprehensive description of all three areas of research effort and supporting data is presented below.

Key Research Accomplishments:

Topic One: Effects of BH3 Mimetics and Lysosomotropic Agents on MPNST cells *in vitro* and *in vivo*.

- Combined treatment with lysosomotropic agents and BH3-mimetics enhances MPNST cell death.

We previously reported that both chloroquine and AT-101 decrease MPNST cell survival. We extended these observations to examine other lysosomotropic agents, such as quinacrine (QA), and BH3-mimetics, such as ABT-263, and to determine if combinations of these drugs might be more effective in killing MPNST cells *in vitro*. As shown in figure 1, we observed cytotoxic effects of both quinacrine and ABT-263 on MPNST cells and that enhanced cytotoxicity was found if the two drugs were given in combination.

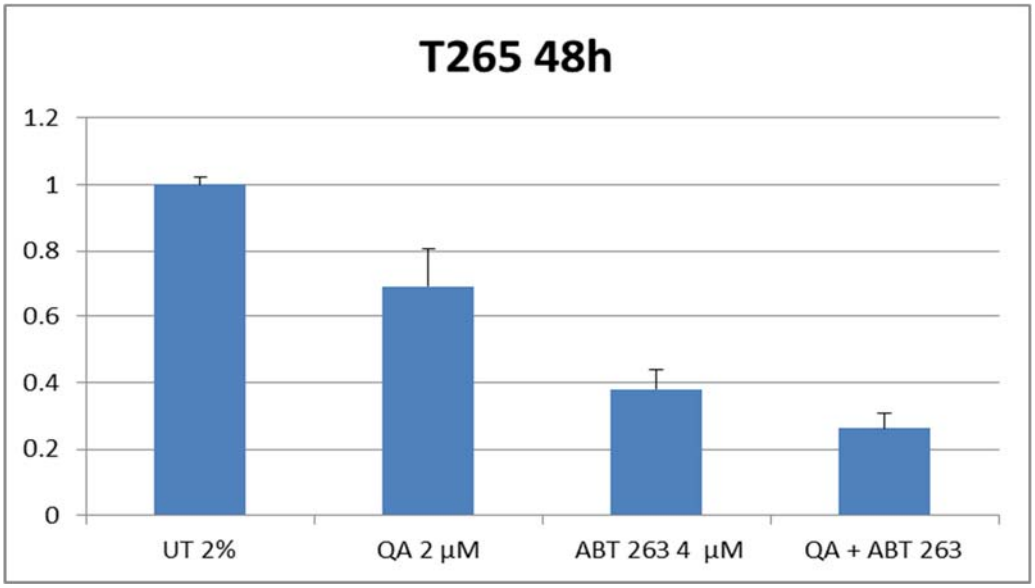

Figure 1. Treatment of T265 MPNST cells with the lysosomotropic drug quinacrine (QA) or with the BH3-mimetic ABT 263 results in decreased cell viability (y-axis: fractional cell viability). Combined administration of the two drugs further decreases MPNST cell survival.

- Cytotoxic effects of combined BH3-mimetic and lysosomotropic agents may be due to suppression of USP9X.

To investigate the mechanisms by which lysosomotropic agents and BH3-mimetics enhance MPNST cell death, we first examined markers of apoptotic cell death by western blot analysis of MPNST cells. As expected from our previous studies, we found a significant increase in cleaved PARP, cleaved caspase-9 and cleaved caspase-3 following treatment of MPNST cells (8814 cell line) with either quinacrine (QA) or ABT-263 (Figure 2). The combination of QA with ABT-263 produced an even more dramatic increase in apoptotic markers.

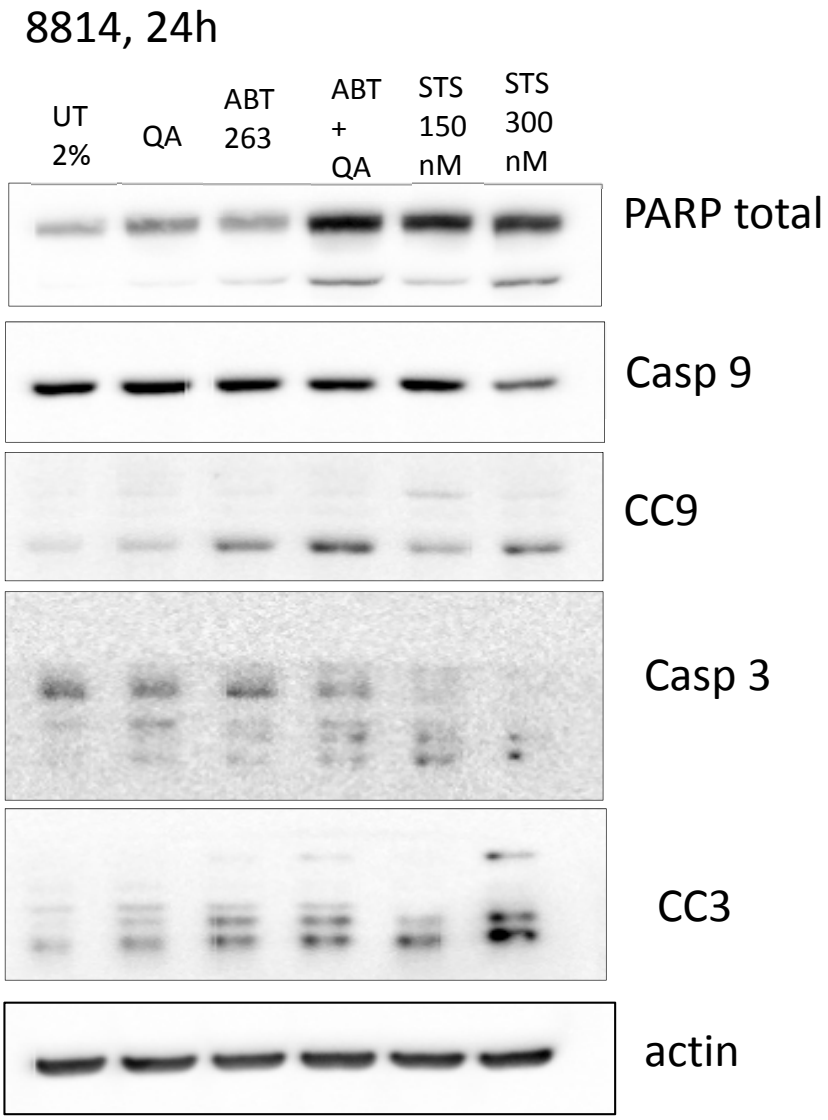

Figure 2. MPNST 8814 cells were treated with QA and ABT-263 alone or in combination for 24 hours and protein extracts were subjected to Western blot analysis for PARP (total is the upper band, cleaved is the lower band), caspase 9

(Casp 9), cleaved caspase 9 (CC9), caspase 3 (Casp 3), cleaved caspase 3 (CC3), and actin (loading control). Staurosporine served as a positive control for apoptosis induction.

To explore the possible molecular mechanism for the pro-apoptotic action of quinacrine and ABT-263, we examined the levels of several Bcl2 family members and USP9X in control and treated MPNST cell lines. USP9X is a deubiquitinating enzyme that plays an important role in regulating the degradation of multiple proteins. USP9X has been implicated in regulating multiple signaling pathways including Notch, Wnt, EGF and mTOR. USP9X has been shown to also regulate stem cell maintenance and it is expressed in the nervous system. Of note, USP9X has been reported to directly affect MCL1 stability which is a key regulator of apoptosis.
We treated 8814 and T265 MPNST cells with quinacrine, ABT-263, or the combination of the two drugs for 24 hours and examined levels of USP9X, MCL1, and Noxa (a BH3-only, pro-apoptotic Bcl2 family member). We found that quinacrine had minimal effect on USP9X, MCL1 and Noxa; ABT-263 decreased USP9X and increased Noxa levels, and this effect was markedly enhanced by combined treatment with quinacrine and ABT-263 (Figure 3). Interestingly, levels of MCL1 were relatively unaffected by these treatments suggesting an MCL1-independent cell death pathway.

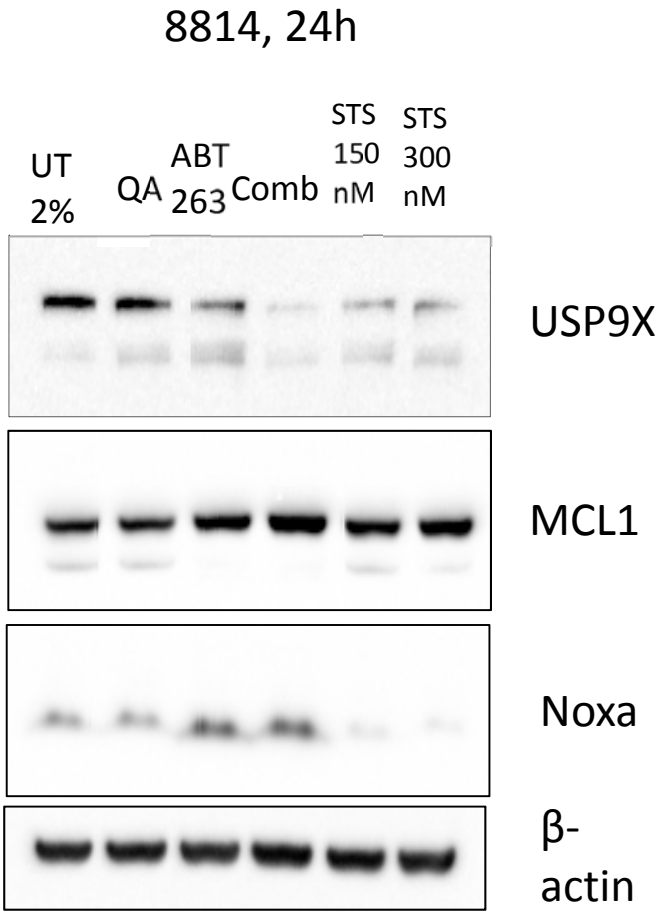

Figure 3. MPNST cells (8814) were treated for 24 hours with quinacrine (QA), ABT-263, or combined QA and ABT-

263 (Comb) and levels of USP9X, MCL1 and Noxa were measured by Western blot. Staurosporine (STS) served as a positive control for apoptosis induction. Beta-actin is a loading control.

Based upon these observations, we next went on to determine if USP9X might serve as a regulator of MPNST cell death. We tested the effects of USP9X-siRNA versus non-targeting-siRNA treatment on MPNST cell viability over time. In both T265 and 8814 cell lines, we observed a time dependent loss of cell viability following USP9X-siRNA treatment (Figure 4). In particular, the 8814 cell line showed rapid cell death following USP9X knockdown.

8814-Viability **T265-Viability**

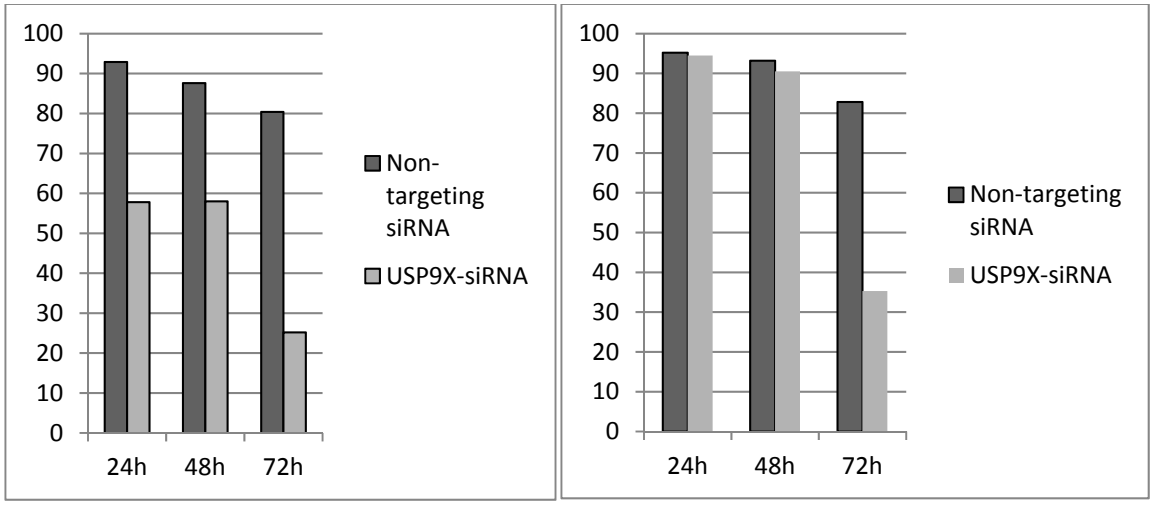

Figure 4. MPNST cells, T265 and 8814, were treated with USP9X targeting or non-targeting siRNA and cell viability (y-axis) was measured over time. Both MPNST cell lines exhibited time-dependent decreased viability after USP9X-siRNA treatment with the 8814 cells showing enhanced sensitivity.

In total, the studies performed over the entire project period suggest that BH3-mimetics, alone and in combination with lysosomotropic agents, induce MPNST cell apoptosis. In addition, our studies suggest that USP9X may be an important regulator of MPNST cell death although the precise mechanism of death requires additional investigation.

- ***In Vivo* Studies of BH3 Mimetics and Lysosomotropic Agents in a Transgenic Mouse MPNST Model:**

During the overall funding period, we completed two experiments involving chronic *in vivo* administration of BH3 mimetics and/or lysosomotropic agents to animals in a transgenic (GGF beta 3 x p53 +/-) mouse model of MPNST. In the first experiment, we chronically administered the BH3 mimetic AT101 alone or in combination with the lysosomotropic agent chloroquine (CQ) beginning at weaning and monitored the mice for one year for the development of MPNSTs and survival in our transgenic mouse model of MPNST (Figure 5). This large study involved multiple weekly injections to over 100 mice and a detailed histopathological analysis of the nervous system of all animals. We found that chronic CQ administration slightly prolonged median survival from approximately 210 days to approximately 250 days but this effect was not statistically significant. Disappointingly, the BH3 mimetic AT101 did not increase median survival and we found no survival promoting

effect of combined CQ and AT101. None of the treatments had an effect on the incidence, distribution or histopathological grade of the observed MPNSTs.

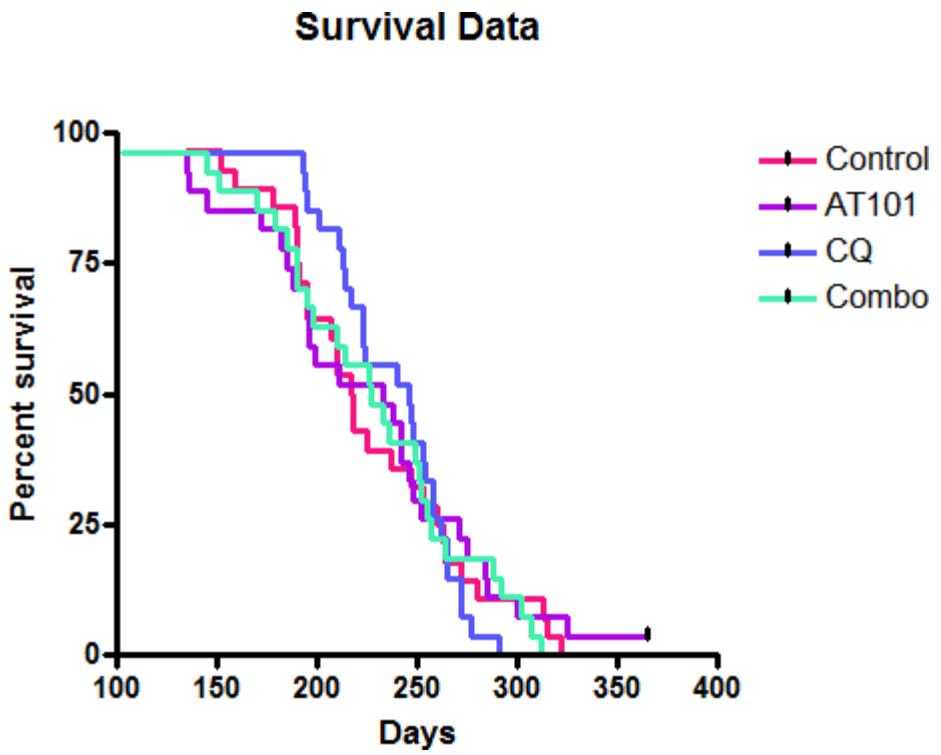

Fig. 5: Chronic administration of AT101 and CQ, alone or in combination, failed to affect survival in an *in vivo* MPNST transgenic mouse model.

In a second experiment, we used the BH3 mimetic (ABT-263) and the lysosomotropic agent quinacrine and examined tumor formation and survival in the same transgenic mouse model. Unfortunately, once again the results were negative (data not shown). Neither ABT-263 nor quinacrine, alone or in combination, had any effect on mouse survival, the occurrence of MPNSTs, their location or histological grade. Given the promising results we had obtained with all of these agents *in vitro*, these *in vivo* results are disappointing.

Topic Two: Identification of CXCL12 as a possible mediator of BH3 mimetic effects on MPNST cells.

During the course of the grant, we studied and published a study of the potential role of CXCL12 as a mediator of MPNST survival. Our manuscript is included as an appendix item and summarized below.

- We determined that BH3 mimetics suppress CXCL12 expression in MPNST cells *in vitro*.

Malignant peripheral nerve sheath tumors (MPNSTs) are aggressive, Schwann cell-derived neoplasms of the peripheral nervous system that have recently been shown to possess an autocrine CXCL12/CXCR4 signaling loop that promotes tumor cell proliferation and survival. Importantly, the CXCL12/CXCR4 signaling axis is driven by availability of the CXCL12 ligand rather than CXCR4 receptor levels alone. Therefore, pharmacological reduction of CXCL12 expression could be a potential chemotherapeutic target for patients with MPNSTs or other pathologies wherein the CXCL12/CXCR4 signaling axis is active. AT101 is a well-established BCL-2 homology domain 3 (BH3) mimetic that we have recently demonstrated to also function as an iron chelator and therefore acts as a hypoxia mimetic. In this study, we found that AT101 significantly reduces CXCL12 mRNA and secreted protein in established human MPNST cell lines *in vitro* (Figure 6). This effect was recapitulated by other BH3 mimetics [ABT-737 (ABT), obatoclax (OBX) and sabutoclax (SBX)] but not by desferrioxamine (DFO), an iron chelator and known hypoxia mimetic (Figure 7). These data suggest that CXCL12 reduction is a function of AT101's BH3 mimetic property rather than its iron chelation ability (Figure 8). Additionally, this study investigates a potential mechanism of BH3 mimetic-mediated CXCL12 suppression: liberation of a negative CXCL12 transcriptional regulator, poly (ADP-Ribose) polymerase I (PARP1) from its physical interaction with BCL-2. These data suggest that clinically available BH3 mimetics might prove therapeutically useful at least in part by virtue of their ability to suppress CXCL12 expression.

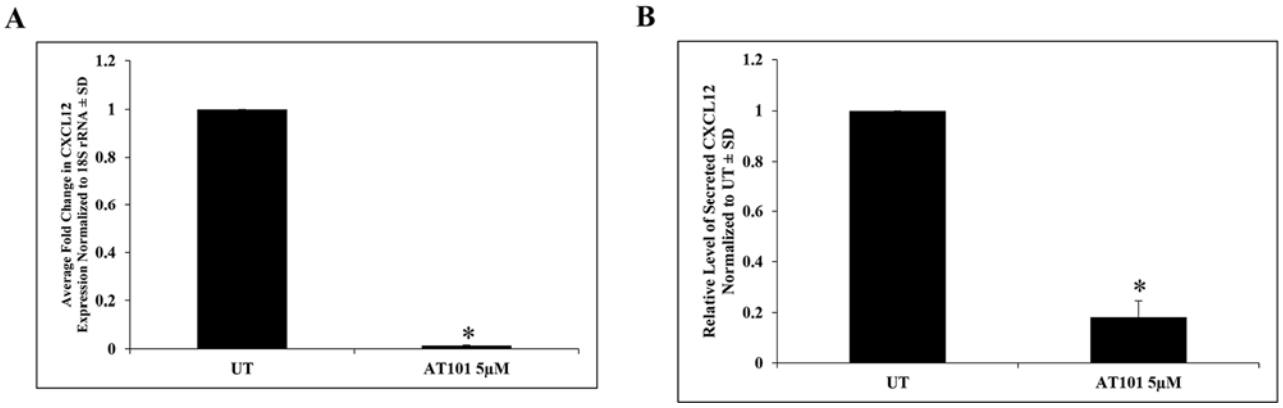

Figure 6: AT101 down-regulates CXCL12 in MPNST cells. A. qRT-PCR analysis of AT101-treated T265-2c cells (5μM, 24h). **B.** AT101 treatment (5μM, 24h) resulted in a significant reduction of secreted CXCL12 protein in T265-2c cells as demonstrated by an ELISA. **p*-value <0.05.

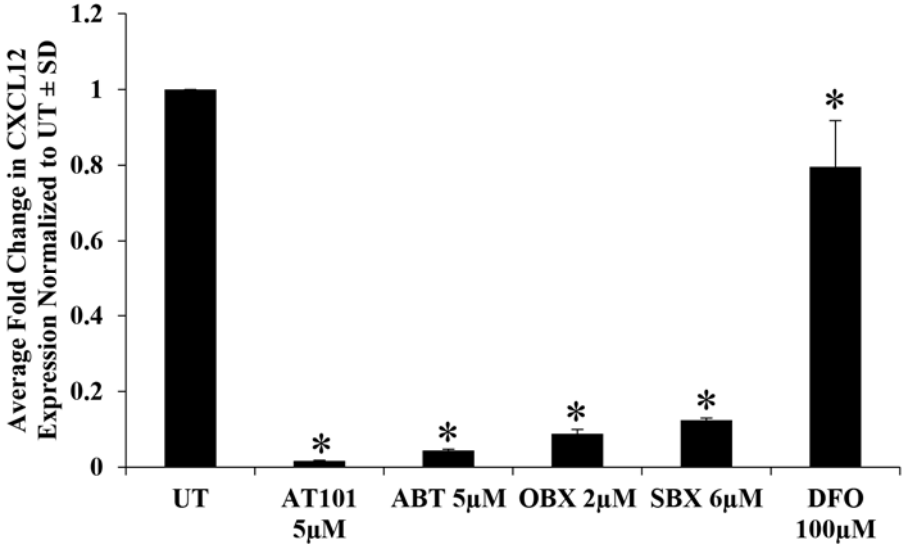

Figure 7: BH3 mimetics recapitulate the effects of AT101 on CXCL12 expression. T265-2c cells treated with AT101, ABT, OBX, SBX or DFO significantly suppress CXCL12 mRNA levels compared to no treatment as demonstrated by qRT-PCR. **p*-value <0.05. Comparison of DFO with AT101, ABT, OBX or SBX treatment resulted in a statistically significant difference in CXCL12 expression (*p*-value <0.01).

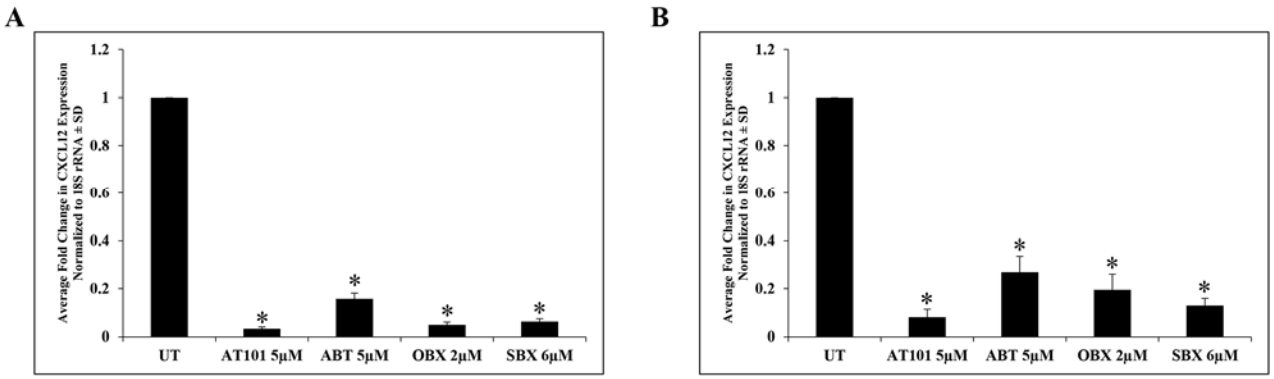

Figure 8: BH3 mimetic suppression of CXCL12 is conserved among multiple MPNST cell lines. BH3 mimetics suppress CXCL12 mRNA levels in an NF1-derived (90-8) **A.** and sporadic (STS26T) **B.** MPNST cell line as demonstrated by qRT-PCR. **p*-value <0.05.

Topic Three: Usp9X is a potential target for MPNST therapy.

- **Usp9X Regulates Cell Death in Malignant Peripheral Nerve Sheath Tumors:**

Usp9X is a deubiquitinating enzyme that is overexpressed in various human cancers, including nervous system tumors, such as glioblastoma (GBM). Genetic and/or pharmacological inhibition of Usp9X activity has been shown to induce tumor cell death in both *in vitro* and *in vivo* models of GBM. Previous studies have demonstrated that down-regulation of Usp9X is followed by enhanced degradation of the anti-apoptotic Bcl-2 family member, myeloid cell leukemia 1 (Mcl-1). Furthermore, Mcl-1 down-regulation is known to be an important determinant of apoptosis in sarcomas. Our findings, described below, suggest that Usp9X and Mcl-1 are novel targets for the treatment of MPNSTs and that paraptosis, a caspase-independent type of regulated cell death, may play a role in MPNST cell death induced by Usp9X inhibition.

Usp9X inhibition causes massive reduction in MPNST cell viability.

To investigate the potential role of Usp9X in regulating MPNST cell survival, we first examined the effects of inhibiting Usp9X enzymatic activity with the deubiquitinase inhibitor, WP1130, a pharmacological inhibitor of Usp9X known also as Degrasyn, on three NF1 patient-derived MPNST cell lines (ST88-14, T265-2c and 90-8). WP1130 caused a concentration-dependent decrease in cell viability after 72h in all three cell lines, with ST88-14 cells being particularly sensitive (Fig. 2 a, b, c). In all three cell lines, Usp9X gene silencing resulted in a significant reduction in viable cell numbers after 72h (Fig. 2 d, e, f). Consistent with the results obtained with pharmacological inhibition of Usp9X activity, ST88-14 cells were most strongly affected by Usp9X silencing, with a significant reduction in cell viability observed after just 24h treatment (Fig. 2d). These data support the conclusion that Usp9X is critical for the survival of MPNST cells.

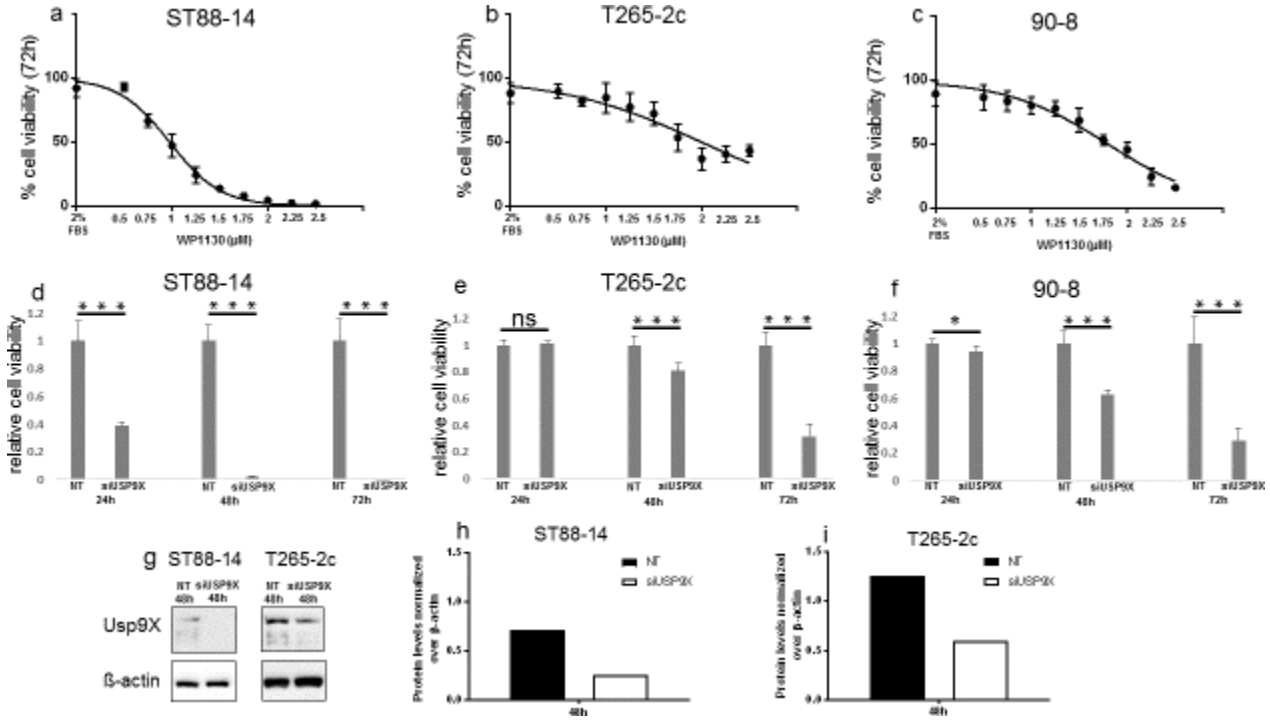

Fig. 2: Usp9X inhibition causes massive reduction in cellular viability in MPNST cell lines. (a-c) ST88-14 (a), T265-2c (b), 90-8 cells (c) were treated with increasing concentrations of WP1130 for 72h. Cellular viability was determined by CellTiter-Glo® assay and the IC_{50}-values were calculated based on a non-linear regression analysis. Data are presented as mean and SD, n=3. **(d-f)** Usp9X was silenced in ST88-14 (d), T265-2c (e), 90-8 cells (f) with non-targeting (NT) RNA or siUsp9X for 24, 48 and 72h. Cellular viability was determined by CellTiter-Glo® assay and relative cell viability was calculated. Data are presented as mean and SD, n=3. * = 0.0129 *** ≤ 0.001. **(g-i)** Usp9X knock down was performed in ST88-14 and T265-2c cells for 48h. Whole-cell extracts were examined by Western blot for Usp9X. ß-actin Western blot analysis was performed to confirm equal protein loading. Data are presented as mean and SD, n=3.

Usp9X knock-down causes MPNST cell death with variable caspase activation and features of apoptosis.

To determine if Usp9X inhibition induced apoptosis of MPNST cells, we inhibited Usp9X pharmacologically with WP1130 and silenced it by siRNA, as well, in ST88-14 and T265-2c cell lines and examined various biochemical indicators of apoptosis. Usp9X pharmacological inhibition resulted in several features of apoptosis (Fig. 3 a, b), including a time-dependent decrease in mitochondrial membrane potential (Fig. 3 c, d), in both cell lines. Consistent with the viability data, ST88-14 cells were more rapidly and strongly affected by Usp9X inhibition, than T265-2c cells. As with pharmacological inhibition of Usp9X activity, Usp9X knock-down produced biochemical features of apoptotic cell death including a significant loss in mitochondrial membrane potential (Fig. 3 a, b, c, d). ST88-14 cells consistently showed more dramatic effects after Usp9X interference, compared to T265-2c cells (Fig 3 a-d) and caspase 3-like enzymatic activity was more pronounced after Usp9X knock-down or WP1130 treatment in ST88-14 cells compared to T265-2c cells (Fig. 3 e, f, g).

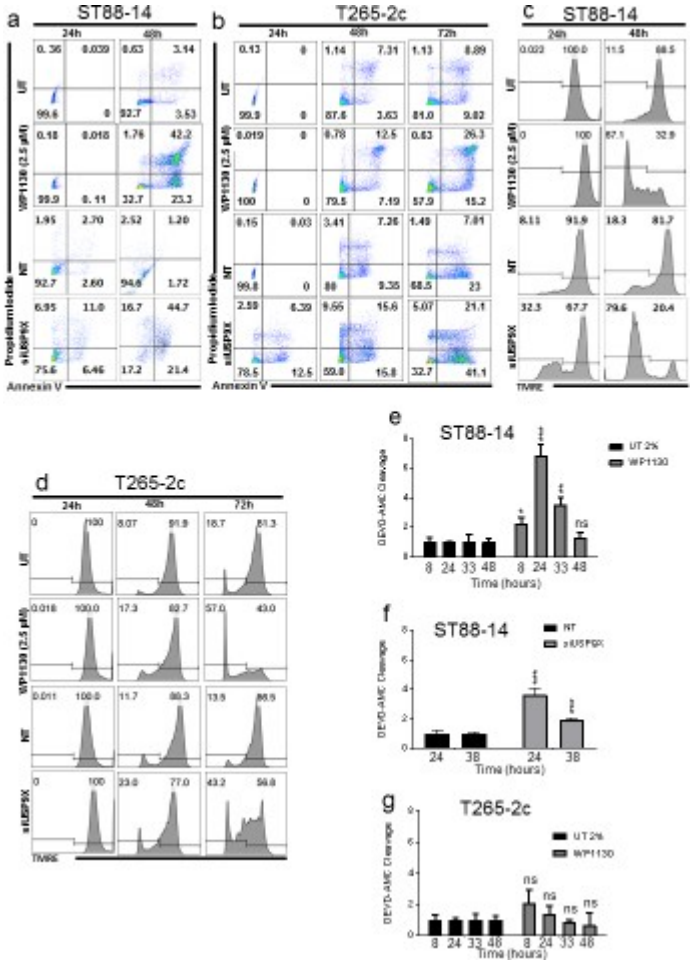

Fig. 3: Usp9X inhibition induces cell death with features of apoptosis and loss of membrane potential in MPNST cell lines. (a-d) ST88-14 (a, c) and T265-2c cells (b, d) were treated with WP1130 at the concentration of 2.5 μM, or transfected either with non-targeting (NT)-siRNA or Usp9X-siRNA. **(a, b)** Staining for annexin V/Propidium Iodide was performed prior to flow cytometric analysis. Representative flow plots are shown. N=3. **(c,d)** Cells were stained with TMRE, then flow cytometric analysis was performed. N=3. **(e-f)** ST88-14 cells were treated with WP1130 at the concentration of 2.5μM (e) or transfected either with non-targeting (n.t.)-siRNA or Usp9X-siRNA (f), then caspase 3-like enzymatic activity was measured at different time points. Column: mean. Error bar: SD, n=3. * = 0.0209 ** = 0.0026 *** ≤ 0.001. **(g)** T265-2c cells were treated with WP1130 at the concentration of 2.5μM prior to caspase 3-like activity measurement at different time points.

Ultrastructural examination of MPNST cells following Usp9X inhibition reveals evidence of paraptosis.

We used transmission electron microscopy (TEM) to determine if there was ultrastructural evidence of apoptosis and/or ER stress in MPNST cells following Usp9X inhibition. T265-2c cells were treated with vehicle or 2.5 µM WP1130 for 24h and processed for TEM. Vehicle treated cells showed intact organelles and normal ER structure (Fig. 4 c, d, e). In contrast, WP1130 treated T265-2c cells exhibited significant morphological changes including reduced cell size and altered cell shape (Fig. 4 f). In addition, following WP1130 treatment T265-2c cells exhibited numerous small and large clear cytoplasmic vacuoles (Fig. 4 f). The typical ultrastructural features of apoptosis, e.g. chromatin condensation and margination and membrane blebbing were only rarely observed in treated cells (Fig. 4 f, g, h). Striking changes in ER and mitochondrial ultrastructure previously described in paraptotic cell death were seen following WP1130 treatment of T265- 2c cells. Compared with vehicle treated cells, WP1130 exposed cells showed significant swelling and disruption of normal ER structure with dramatic expansion of the ER lumina (Fig. 4 d and g). Similarly, in contrast with normal appearing mitochondria in vehicle treated cells, numerous mitochondria in the WP1130 treated cells were markedly enlarged, edematous, disorganized and fragmented (Fig. 4 e and h). Taken together, these results suggest that WP1130 induces paraptosis in T265-2c cells.

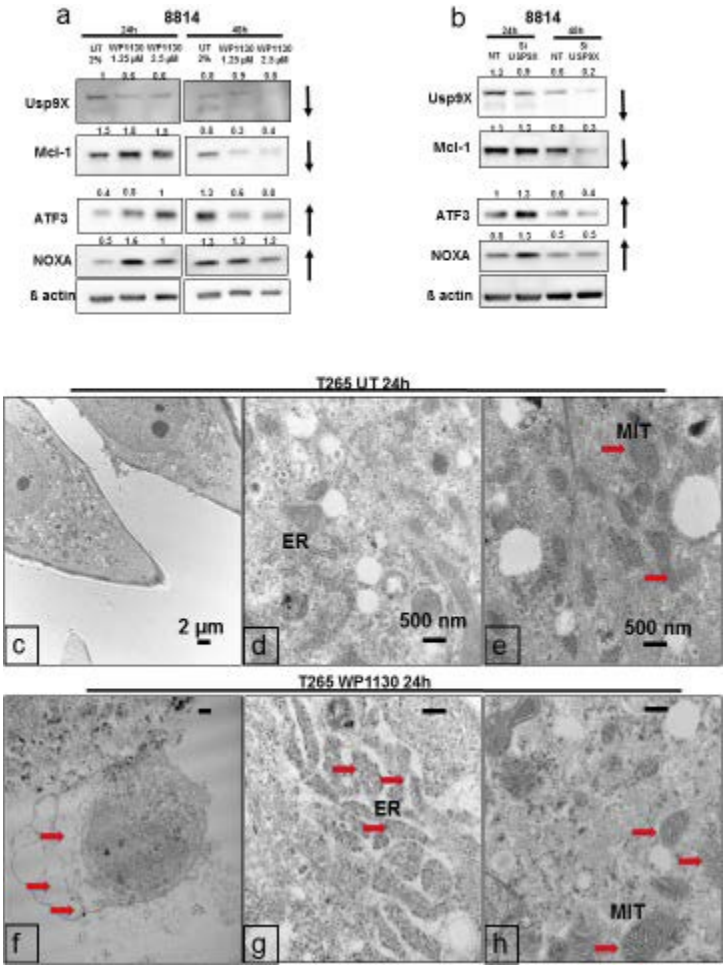

Fig. 4: Usp9X inhibition causes Noxa increase, Mcl-1 depletion and ER stress in MPNST cell lines. Ultrastructural analysis shows features of paraptosis. (a, b) ST88-14 cells were treated for 24 and 48 h with WP1130 at the concentration of 1.25 and 2.5 µM (a), or transfected either with non-targeting (n.t.)-siRNA or Usp9X-siRNA (b). Whole cell extracts were collected prior to Western blot analysis for Usp9X, Mcl-1, ATF3, Noxa. ß-actin served as loading control. Numbers shows protein quantification analyzed through ImageJ. N=2. **(c-e)** provided untreated cells control, pictures acquired using TEM. **(f-h)** After treatment with WP1130 at the concentration of 2.5 µM (f, g, h) T265-2c cells showed extensive cytosolic vacuolization (f, red arrows) and swelling of ER (g, red arrowheads) and mitochondria (h, red arrows).

WP1130 inhibits MPNST tumor growth *in vivo.*

To assess the potential efficacy of Usp9X inhibition in treating MPNSTs *in vivo*, we tested WP1130 in a heterotopic xenograft MPNST model. ST88-14 cells were implanted subcutaneously and animals were divided into three groups receiving either vehicle or two different concentrations of WP1130 (12.5 and 25 mg/kg intraperitoneally) (Fig. 5). In our initial *in vivo* experiment, treatment was initiated eight days after implantation and injections were given three times/week for four weeks (Fig. 5 a-f). WP1130 at 25 mg/kg per dose produced a statistically significant growth reduction with partial regression of tumors compared to vehicle treated controls (Fig. 5 a). The day after the last injection, tumors were resected and the tumor volume and weight measured. WP1130 produced a significant decrease in tumor volume at both concentrations (Fig. 5 b) and a statistically significant decrease in tumor weight in the 25 mg/kg dose group (Fig. 5 c and d). The regression of the tumors' size suggested that this treatment not only attenuated tumor growth but induced tumor cell death. Histopathological analysis of the resected tumors in the vehicle treated control group showed densely cellular, highly pleomorphic tumors with brisk mitotic activity (fig. 5 e). In contrast, mice treated with WP1130 showed tumors with reduced cellularity and mitotic activity, multi-focal necrotic areas and the presence of scattered apoptotic nuclei throughout the tumors at both concentrations (fig. 5 f). To preliminarily assess potential *in vivo* toxic effects of WP1130, we performed body weight measurements on vehicle and WP1130 treated animals throughout the experiment and found no differences between the three groups (data not shown) suggesting that WP1130 does not have obvious toxic effects. These results are consistent with several previous *in vivo* studies of WP1130.

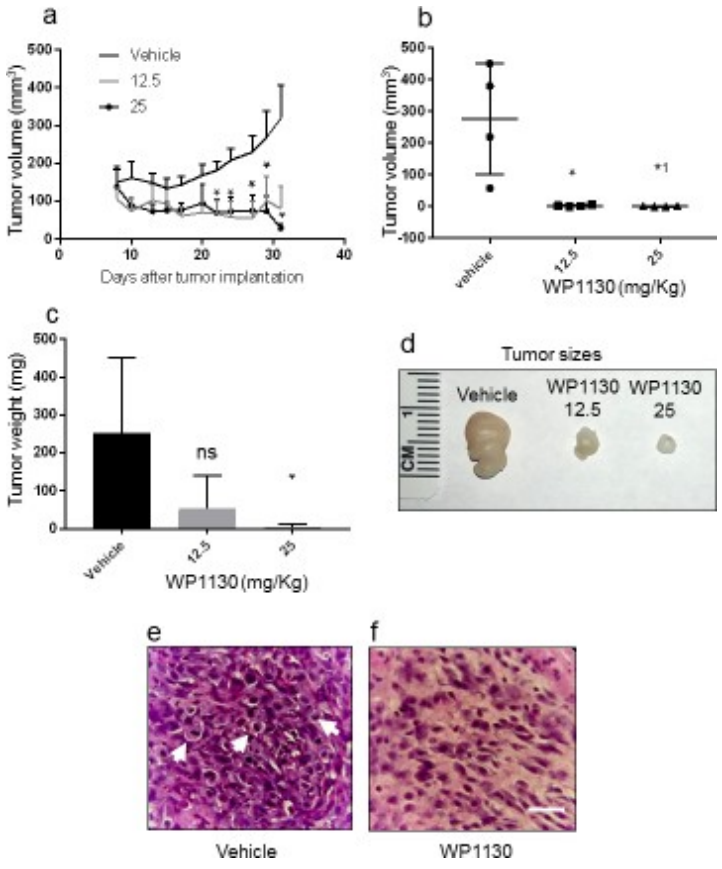

Fig. 5: Treatment with WP1130 reduces tumor size in a mouse MPNST model generated by orthotopic injection of ST88-14 cell line. (a) Tumor growth curves showing the increase in tumor size for each treatment group. Data are presented as mean and SEM. Asterisks shown only for 25 mg/Kg dose, compared to control group. Asterisks values, from left to right: 0.0413, 0.0321, 0.0409, 0.0479 and 0.0162. **(b)** Quantification of the tumors volume among different treatment groups 35 days after tumor implantation. * = 0.0202, *[1] = 0.0198. **(c)** Quantification of the tumors weight among different treatment groups 35 days after tumor implantation. * = 0.0458. **(d)** Representative photographs of the tumors. **(e, f)** Representative photomicrographs showing the histological morphology (H & E staining) of tumors from mice receiving either vehicle or WP1130 at the concentration of 12.5 mg/Kg. Arrows indicate mitotic figures. Scale bar, 50 μm.

In total, our studies of Usp9X and its pharmacological inhibition with WP1130 in MPNSTs suggest interesting new therapeutic options for the treatment, and possible prevention, of NF1-associated MPNSTs. Future studies will be required to fully explore this novel therapeutic target in human patients.

What opportunities for training and professional development has the project provided?
Dr. Roth met with students, post-docs, trainees and senior scientists at several venues over the last year to discuss this project including Experimental Biology 2017 in Chicago, Illinois April 22-26, 2017; the Association of Pathology Chairs Meeting in Washington D.C. July 25-28, 2017; and at the Northeast Association of Pathology Chairs Meeting in Bermuda September 13-17, 2017.

How were the results disseminated to communities of interest?
In addition to discussion of our results at the meetings described above, Dr. Roth and Dr. Bianchetti also presented the findings of this project at various neuroscience, neuro-oncology, and cell biology laboratory meetings throughout the year at Columbia University. Our findings were discussed at the lab meetings of Dr. Markus Siegelin (Pathology and Cell Biology), Dr. Michael Shelanski (Pathology and Cell Biology), Dr. Lloyd Greene (Pathology and Cell Biology), Dr. Jeffrey Bruce (Neurosurgery) and Dr. Peter Canoll (Neuropathology).

What do you plan to do during the next reporting period to accomplish the goals?
The grant has been completed and this is the final report. However, we have one manuscript currently under review and will revise and resubmit it for publication if it is not accepted in its current form.

4. Impact

What was the impact on the development of the principal discipline(s) of the project?
Our discovery that Usp9X inhibition has a potent cytotoxic effect on human MPNST cell lines both *in vitro* and *in vivo* is very exciting. MPNSTs are the leading cause of death in patients with neurofibromatosis type 1 (NF1). Current treatment modalities have been largely unsuccessful in improving MPNST patient survival, making the identification of new therapeutic targets urgent. Our observation that pharmacological inhibition of Usp9X with WP1130 was able to significantly reduce human MPNST growth and induce tumor cell death in an *in vivo* xenograft model suggests that future studies of NF1-patient derived MPNSTs are needed. Similarly, the original goal of this grant was to develop prophylactic strategies for preventing MPNST formation from lower grade nerve sheath tumors. Thus, future studies of the effects of WP1130 in the *in vivo* transgenic mouse model of MPNST formation are required to fully assess this novel target.

What was the impact on other disciplines?
Nothing to Report

What was the impact on technology transfer?
Nothing to Report

What was the impact on society beyond science and technology?
Nothing to Report

5. Changes/Problems

Nothing to Report

6. Products

Publications, conference papers, and presentations

Bibliography/Journal publications:
Graham CD, Kaza N, Pruitt HC, Gibson LM, Klocke BJ, Shevde LA, Carroll SL, Roth KA. BH3 mimetics suppress CXCL12 expression in human malignant peripheral nerve sheath tumor cells. Oncotarget, 2017 Jan 31;8(5):8670-8678. Doi: 10.18632/oncotarget.14398.

The following manuscript has been submitted and is under review:

Bianchetti, E, Siegelin, MD, Carroll, SL, and Roth KA. Usp9X regulates cell death in malignant peripheral nerve sheath tumors.

Books or other non-periodical, one-time publications:
Nothing to Report

Other publications, conference papers, and presentations:
Dr. Roth discussed his research at Experimental Biology 2017 in Chicago, Illinois April 23, 2017; at the Association of Pathology Chairs Meeting in Washington D.C. on July 26, 2017; and at the Northeast Association of Pathology Chairs Meeting in Bermuda on September 14, 2017.

Website(s) or other Internet site(s)
Nothing to Report

Technologies or techniques
Nothing to Report

Inventions, patent applications, and/or licenses
Nothing to Report

Other Products
Nothing to Report

7. Participants & Other Collaborating Organizations

What individuals have worked on the project?
Kevin A. Roth, M.D., Ph.D.
Elena Bianchetti, Ph.D.
Hai Tang, M.D.

Researcher Identifier (e.g. ORCID ID):	0000-0002-0643-995X
Nearest person month worked:	1 Calendar Months
Contribution to Project:	Dr. Roth supervised all aspects of the project.
Name:	Elena Bianchetti, Ph.D
Project Role:	Post Doctoral Researcher
Researcher Identifier (e.g. ORCID ID):	NA
Nearest person month worked:	3 Calendar Months
Contribution to Project:	Dr. Bianchetti performed all the in vitro tissue culture studies.
Name:	Hai Tang, M.D
Project Role:	Technician
Researcher Identifier (e.g. ORCID ID):	NA
Nearest person month worked:	1 Calendar Months
Contribution to Project:	Dr. Tang performed all in vivo studies.

Has there been a change in the active other support of the PD/PI(s) or senior/key personnel since the last reporting period?
Nothing to Report

What other organizations were involved as partners?
None

8. Special Reporting Requirements
None

9. Bibliography and Appendices
Graham CD, Kaza N, Pruitt HC, Gibson LM, Klocke BJ, Shevde LA, Carroll SL, Roth KA. BH3 mimetics suppress CXCL12 expression in human malignant peripheral nerve sheath tumor cells. Oncotarget, 2017 Jan 31;8(5):8670-8678. Doi: 10.18632/oncotarget.14398.

The following manuscript has been submitted and is under review:

Bianchetti, E, Siegelin, MD, Bates, S, Carroll, SL, and Roth KA. Usp9X regulates cell death in malignant peripheral nerve sheath tumors.

10. Personnel Receiving Pay from the Research Effort:

Kevin A. Roth, M.D., Ph.D. (Principle Investigator)

Steven L. Carroll, M.D., Ph.D. (Investigator; subcontract to MUSC)

Elena Bianchetti, Ph.D. (Post Doctoral Researcher)

Hai Tang, M.D. (Technician)

Barbara J. Klocke, M.S. (Technician)

www.impactjournals.com/oncotarget/ Oncotarget, 2017, Vol. 8, (No. 5), pp: 8670-8678

Research Paper

BH3 mimetics suppress CXCL12 expression in human malignant peripheral nerve sheath tumor cells

Christopher D. Graham[1], Niroop Kaza[1], Hawley C. Pruitt[1], Lauren M. Gibson[1], Barbara J. Klocke[1], Lalita A. Shevde[1], Steven L. Carroll[1,2], Kevin A. Roth[1,3]

[1]Department of Pathology, University of Alabama at Birmingham, Birmingham, Alabama, United States of America

[2]Current Address: Medical University of South Carolina, Department of Pathology and Laboratory Medicine, Charleston, South Carolina, United States of America

[3]Current Address: Columbia University Medical Center, Department of Pathology and Cell Biology, New York, United States of America

Correspondence to: *Kevin A. Roth,* ***email:*** *kar2208@cumc.columbia.edu*

Keywords: *MPNST, BH3 mimetic, CXCL12, PARP1, AT101*

Received: *July 13, 2016* ***Accepted:*** *December 05, 2016* ***Published:*** *December 31, 2016*

ABSTRACT

Malignant peripheral nerve sheath tumors (MPNSTs) are aggressive, Schwann cell-derived neoplasms of the peripheral nervous system that have recently been shown to possess an autocrine CXCL12/CXCR4 signaling loop that promotes tumor cell proliferation and survival. Importantly, the CXCL12/CXCR4 signaling axis is driven by availability of the CXCL12 ligand rather than CXCR4 receptor levels alone. Therefore, pharmacological reduction of CXCL12 expression could be a potential chemotherapeutic target for patients with MPNSTs or other pathologies wherein the CXCL12/CXCR4 signaling axis is active. AT101 is a well-established BCL-2 homology domain 3 (BH3) mimetic that we recently demonstrated functions as an iron chelator and thus acts as a hypoxia mimetic. In this study, we found that AT101 significantly reduces CXCL12 mRNA and secreted protein in established human MPNST cell lines *in vitro*. This effect was recapitulated by other BH3 mimetics [ABT-737 (ABT), obatoclax (OBX) and sabutoclax (SBX)] but not by desferrioxamine (DFO), an iron chelator and known hypoxia mimetic. These data suggest that CXCL12 reduction is a function of AT101's BH3 mimetic property rather than its iron chelation ability. Additionally, this study investigates a potential mechanism of BH3 mimetic-mediated CXCL12 suppression: liberation of a negative CXCL12 transcriptional regulator, poly (ADP-Ribose) polymerase I (PARP1) from its physical interaction with BCL-2. These data suggest that clinically available BH3 mimetics might prove therapeutically useful at least in part by virtue of their ability to suppress CXCL12 expression.

INTRODUCTION

MPNSTs arise sporadically or in patients affected by neurofibromatosis type 1 (NF1) [1]. NF1 is the most commonly inherited cancer predisposition syndrome of the human nervous system, affecting 1 in 3500 newborns [2]. NF1 patients typically exhibit numerous benign neurofibromas, and 8 – 13% of patients will develop more aggressive MPNSTs [1]. Despite increased understanding of the underlying molecular mechanisms driving the development of MPNSTs, treatment advances have been limited. Surgery is the standard of care; however, complete tumor excision is often impossible as MPNSTs aggressively invade adjacent tissues and metastasize [3]. Further, radiation and chemotherapy are largely ineffective at promoting MPNST patient survival [4]. These factors result in a <50% five-year survival rate for MPNST patients [1] and MPNSTs remain the leading cause of death in patients with NF1 [5].

CXCL12 (stromal cell-derived factor-1, SDF-1) belongs to a class of small (8-12 kilodalton [kD]) cytokines, known as chemokines (chemotactic cytokines). Based on structure, CXCL12 is a member of the C-X-C sub-group of chemokines possessing a single,

non-conserved amino acid residue (X) between the first N-terminal cysteine residues. Originally described as a homeostatic chemokine with a prominent role in the trafficking of hematopoietic cells, CXCL12 is now recognized to modulate multiple physiological processes via activation of its receptor, CXCR4 [5, 6]. Such pathways include activation of phospholipase C (PLC), regulation of adenylate cyclase and stimulation of kinase cascades such as phosphoinositide 3-kinase (PI3K), mitogen-activated protein kinase (MAPK) and c-Jun N-terminal kinase (JNK) [7, 8, 9, 10]. In addition to its physiological role, CXCL12/CXCR4 signaling has been implicated in driving tumor cell proliferation, survival and migration in various solid tumors [11, 12]. The original view of stromal cell-secreted CXCL12 acting on CXCR4-expressing tumor cells in a paracrine manner has evolved in recent years. Several studies have shown that some tumor cells, in addition to expressing CXCR4, can secrete CXCL12 and so activate an autocrine loop promoting growth and metastasis [6, 13]. Parada, *et al*'s discovery of this autocrine signaling axis' involvement in NF1-derived MPNST cells provides an exciting opportunity to explore novel therapies targeting CXCL12/CXCR4 autocrine signaling to treat MPNST patients [6].

In addition to CXCR4, CXCL12 also binds a "decoy" receptor, CXCR7 [14]. While it is thought that CXCR7 does not induce the same cascade of signals mediated by CXCR4, CXCR7 has been shown to significantly increase cell proliferation and adhesion in various conditions [14, 15, 16, 17]. Speculation abounds as to the biological role(s) of CXCR7, from the idea that it sequesters CXCL12 to create a gradient leading to differential signaling through CXCR4 [18, 19], to the hypothesis that CXCR7 serves as a co-receptor for CXCR4 [20, 21]. Accordingly, inhibition of CXCR7 function may serve to increase the clinical efficacy of CXCR4 inhibitors such as AMD3100, as blockage of CXCR4 only partially inhibits tumor cell response to CXCL12 gradients in multiple animal models [22, 23, 24]. These observations strengthen the argument that inhibition of CXCL12 expression may complement or enhance the efficacy of clinically available CXCR4 antagonists such as AMD3100.

AT101 [(-)-gossypol acetic acid] is a modified enantiomer of the naturally occurring polyphenolic aldehyde gossypol, and has received significant attention as a potential chemotherapeutic agent in multiple tumor types [25]. The basis for AT101's anti-neoplastic activity has been largely attributed to its BH3 mimetic activity, which results in interaction and inhibition of anti-apoptotic B-Cell Lymphoma 2 (BCL-2) family proteins such as BCL-2, BCL-X_L and MCL-1 [25]. This BH3 mimetic property of AT101 has been shown to promote both apoptotic and non-apoptotic tumor cell death, *in vitro* and *in vivo* [26, 27]. We recently reported that AT101, independent of its BH3 mimetic property, acts as an iron chelator in established human MPNST cell lines [4].

In this report, we show that AT101 causes a significant reduction in CXCL12 mRNA and secreted protein in established human MPNST cell lines. This effect results from AT101's BH3 mimetic property rather than its iron chelation ability. Finally, we show that the BH3 mimetic ABT robustly increases PARP1 binding to the *CXCL12* promoter.

RESULTS

AT101 suppresses CXCL12 expression

Because an active CXCL12/CXCR4 signaling pathway has been shown to mediate tumor cell proliferation, survival and migration in several tumor types including MPNSTs [6, 11, 12] and BH3 mimetics have been demonstrated to modulate CXCL12 transcription [28, 33], we sought to assess CXCL12 mRNA levels in T265-2c cells treated with AT101 (5μM for 24h) by quantitative real time PCR. We found that AT101 treatment resulted in a dramatic reduction of CXCL12 mRNA expression in T265-2c cells (Figure 1A, Supplementary Figure 4). CXCL12 is a chemotactic cytokine and is rapidly secreted, making it difficult to measure levels of intracellular CXCL12 in cell extracts. Accordingly, we performed an Enzyme-Linked ImmunoSorbent Assay (ELISA) on T265-2c culture media that had been treated with or without AT101 to assess whether treatment suppressed CXCL12 protein secretion as well as mRNA expression. Our data demonstrate that AT101 treatment (5μM for 24h) significantly decreased levels of secreted CXCL12 protein compared to untreated cells (Figure 1B Supplementary Figure 5). Our findings indicate that AT101 suppresses both CXCL12 expression and secretion in T265-2c MPNST cells. ABT, OBX, SBX and DFO had varying effects on CXCL12 secretion (Supplementary Figure 10).

AT101-induced suppression of CXCL12 is a function of its BH3 mimetic property

Because AT101 has both BH3 mimetic and hypoxia mimetic effects [4], we sought to address which mechanism, if either, was responsible for the observed suppression of CXCL12 expression. We compared the effects of three BH3 mimetics (ABT, OBX, SBX) and a hypoxia mimetic (DFO) with AT101 on CXCL12 mRNA levels in T265-2c cells. BH3 mimetic drug concentrations were chosen because of the comparable reduction in viable cell number after 24h treatment. We found that all BH3 mimetics tested dramatically reduced CXCL12 mRNA levels after 24h (Figure 2, Supplementary Figure 6). DFO produced only a slight, albeit statistically significant, reduction in CXCL12 mRNA that was substantially less than that of BH3 mimetics (Figure 2, Supplementary Figure 6). These results suggest that BH3 mimetics as a class suppress CXCL12 expression and that

AT101-mediated suppression of CXCL12 is not dependent on its ability to chelate iron. Further, to determine if CXCL12 suppression was a unique effect of BH3 mimetics on T265-2c cells or represented a more general response of MPNST cells, an additional NF1-derived (90-8) and a sporadic MPNST cell line (STS26T) were treated with AT101, ABT, OBX and SBX for 24h followed by qRT-PCR analysis of CXCL12. Both the NF1-derived (Figure 3A, Supplementary Figure 7) and sporadic (Figure 3B, Supplementary Figure 8) MPNST cell lines exhibited suppression of CXCL12 similar to T265-2c cells. These results suggest that BH3 mimetics possess a conserved function of CXCL12 suppression in MPNST cells. It is important to note that the BH3 mimetics tested exhibited conserved effects in U251 established human glioblastoma cells (Supplementary Figure 9). Further, BH3 mimetics reduced cell viability in all MPNST cell lines tested (Figure 4, Supplementary Figure 1/2/3) while DFO resulted in a less robust and reproducible effect (Supplementary Figure 11/12/13) Because CXCL12 is known to stimulate autocrine cell cycle progression via induction of cyclin D1, we evaluated cyclin D1 protein levels following AT101 or ABT treatment and observed an AT101- but not ABT-dependent reduction in cyclin D1 (Supplementary Figure 14).

BH3 mimetics and PARP1

The single most defining characteristic of Type 1 diabetes (T1D) is loss of pancreatic insulin-producing beta cells [28]. Because CXCL12 has demonstrated anti-diabetogenic capability by promoting pancreatic beta cell survival [31, 32], interest in the regulatory mechanism(s) of CXCL12 transcription has increased. A recent investigation into the transcriptional regulation of CXCL12 in rat pancreatic beta cells identified PARP1 as a negative transcriptional regulator of CXCL12 [28]. Interestingly, ABT has been shown to displace PARP1 from its interaction with the BCL-2 family member BCL-2 [33]. Considered together with the observation that PARP1 is known to have a negative regulatory effect on CXCL12 transcription [28], we hypothesized that at least some BH3 mimetic-mediated suppression of CXCL12 expression may result from liberation of a negative CXCL12 transcriptional regulator (PARP1). To test this hypothesis, we developed PCR primers flanking a putative PARP1 binding site within the CXCL12 promoter (Supplementary Figure 15) and performed ChIP analysis of T265-2c cells using antibodies against PARP1 or rabbit IgG following treatment with ABT. qRT-PCR analysis of ChIP products revealed a robust increase in PARP1 interaction with the *CXCL12* promoter (Figure 5A).

DISCUSSION

The BCL-2 family of proteins mediates cellular life and death in part by regulating mitochondrial membrane integrity [34]. This regulation results from a delicate balance of interactions between BH domains of pro- and anti-apoptotic proteins within the BCL-2 family. Following various pro-death stimuli including DNA damage [35], growth factor deprivation [36] and oncogene activation [37], the balance of physical interactions between BH domains of pro- and anti-apoptotic proteins is disrupted by BH3-only proteins. This results in activation of pro-apoptotic multi-domain BCL-2 proteins (BAX/BAK) and subsequent apoptosis. It is estimated that roughly 50% of all human cancers exhibit elevated gene expression of anti-apoptotic BCL-2 family members [38], contributing to resistance to standard apoptosis-inducing therapies. Consequently, molecules possessing only the BH3 domain of BCL-2 proteins (termed BH3 mimetics), have received significant attention as potentially useful cancer therapeutic agents either alone or in combination with other drugs [34].

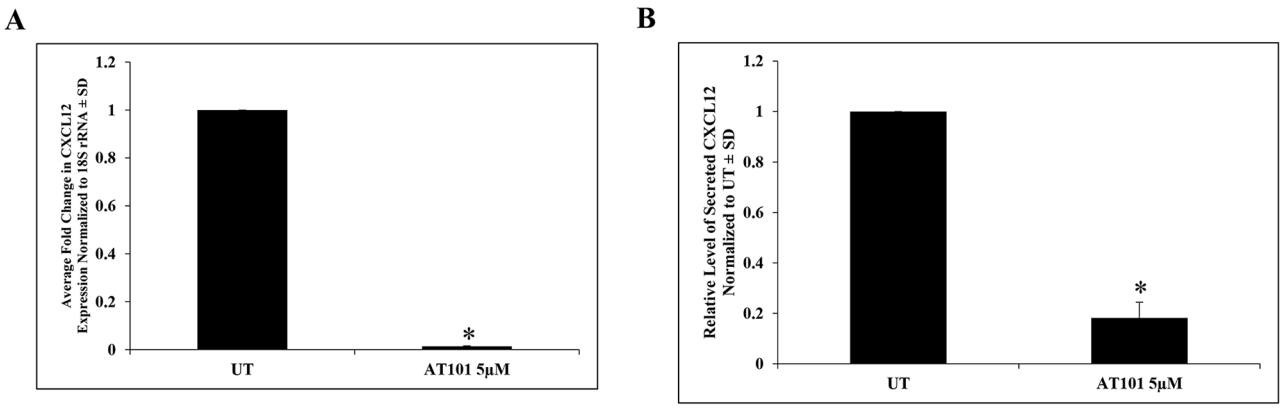

Figure 1: AT101 down-regulates CXCL12 in MPNST cells. A. qRT-PCR analysis of AT101-treated T265-2c cells (5μM, 24h). **B.** AT101 treatment (5μM, 24h) resulted in a significant reduction of secreted CXCL12 protein in T265-2c cells as demonstrated by an ELISA. **p*-value <0.05.

We have been investigating AT101, a well-known BH3 mimetic, as an alternative chemotherapeutic option for patients with MPNSTs. Previously published studies from our lab have demonstrated that AT101 can also chelate intracellular iron and induce a hypoxia-like state *in vitro*. qRT-PCR analysis demonstrated that AT101-induced suppression of CXCL12 transcription in all three MPNST cell lines tested. To gain insight into the mechanism by which AT101 exerts its suppressive effects on CXCL12, we compared AT101 with three BH3 mimetics (ABT, OBX, SBX) and a hypoxia mimetic (DFO). We found that BH3 mimetics, but not DFO, robustly suppressed CXCL12 in all three MPNST cell lines tested. These results suggest that AT101's ability to suppress CXCL12 is largely a function of its BH3 mimetic property rather than its iron chelation ability.

Understanding the mechanism behind BH3 mimetic-induced reduction of CXCL12 is critical to appropriate clinical application. To this end, we have investigated an interesting hypothesis based on the observation that ABT has been shown to displace PARP1 from BCL-2 [33] and that PARP1 exerts a strong inhibitory effect on CXCL12 transcription [28]. Our ChIP data, which demonstrates a robust BH3 mimetic-mediated increase in PARP1 binding to the *CXCL12* promoter, supports the hypothesis that disruption of the BCL-2:PARP1 interaction via BH3 mimetics results in increased negative regulation of CXCL12 transcription by PARP1. These data suggest that BH3 mimetic-mediated suppression of CXCL12 expression is, at least in part, mediated by displacement of PARP1 from its interaction with BCL-2 and subsequent binding of PARP1 to the

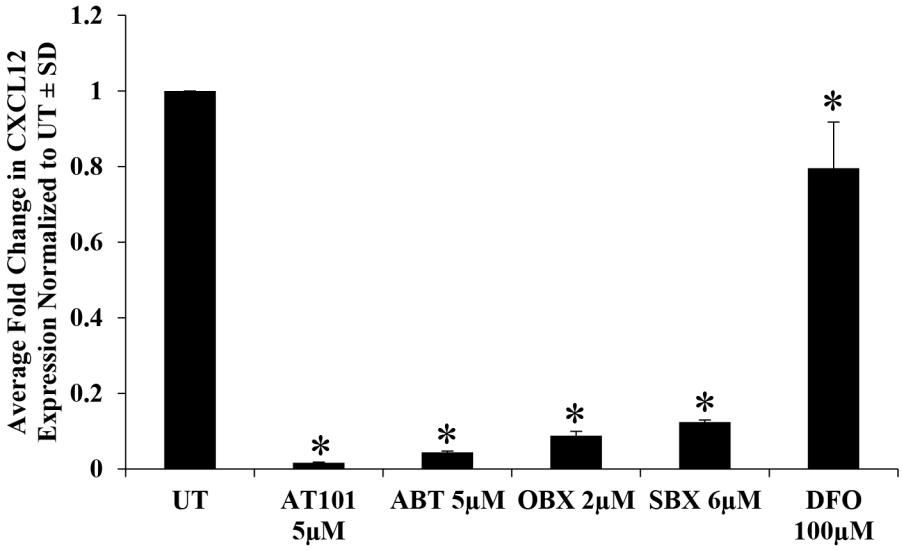

Figure 2: BH3 mimetics recapitulate the effects of AT101 on CXCL12 expression. T265-2c cells treated with AT101, ABT, OBX, SBX or DFO significantly suppress CXCL12 mRNA levels compared to no treatment as demonstrated by qRT-PCR. **p*-value <0.05. Comparison of DFO with AT101, ABT, OBX or SBX treatment resulted in a statistically significant difference in CXCL12 expression (*p*-value <0.01).

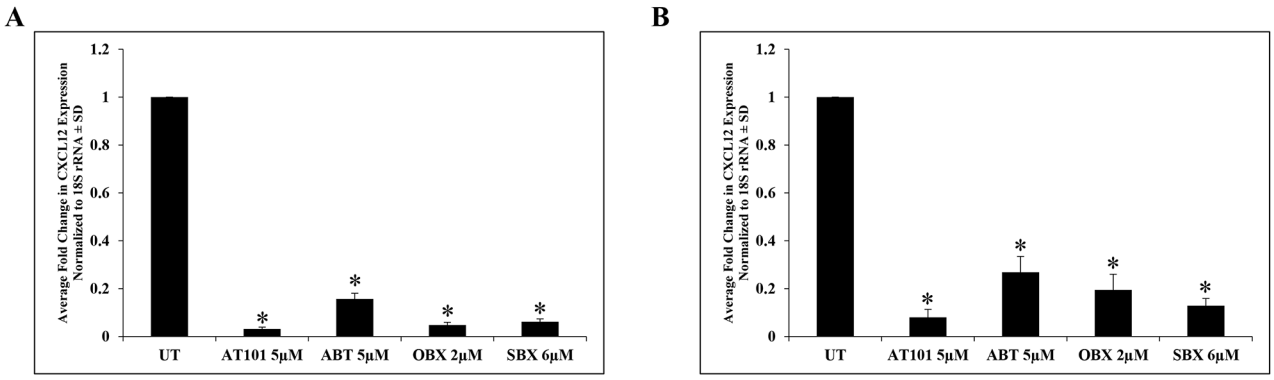

Figure 3: BH3 mimetic suppression of CXCL12 is conserved among multiple MPNST cell lines. BH3 mimetics suppress CXCL12 mRNA levels in an NF1-derived (90-8) **A.** and sporadic (STS26T) **B.** MPNST cell line as demonstrated by qRT-PCR. **p*-value <0.05.

CXCL12 promoter resulting in transcriptional down-regulation (Figure 5B, proposed model).

Targeting tumor-specific growth promoting pathways is important for successful cancer therapy, and the CXCL12/CXCR4 signaling axis is involved in tumor progression and migration in multiple tumor types [12, 39, 40]. The physiological role for chemotactic cytokines is to direct the homing of hematopoietic cells to specific sites within the body via interaction with cell-surface receptors [41–47]. This physiological role may help explain the observation that organs possessing the highest frequency of breast cancer metastasis also have the most abundant secretion of these chemotactic ligands, suggesting a significant role for these molecules in breast cancer metastasis [11]. Supporting this notion is the observation that CXCL12 expression is elevated in multiple tissues

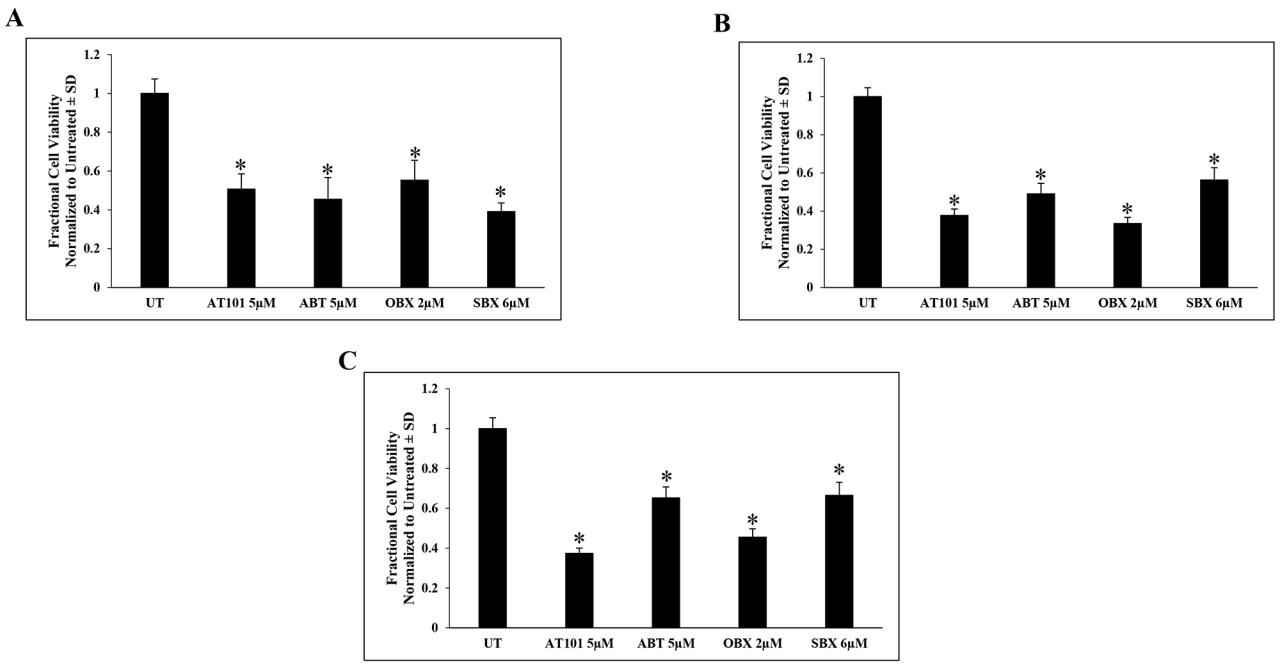

Figure 4: AT101 and BH3 mimetics mediate reduction in MPNST cell viability. AT101- or BH3 mimetic-treated T265 **A.** 90-8 **B.** and STS26 **C.** MPNST cells demonstrate a decrease in viable cell number after 24h. **p*-value <0.01.

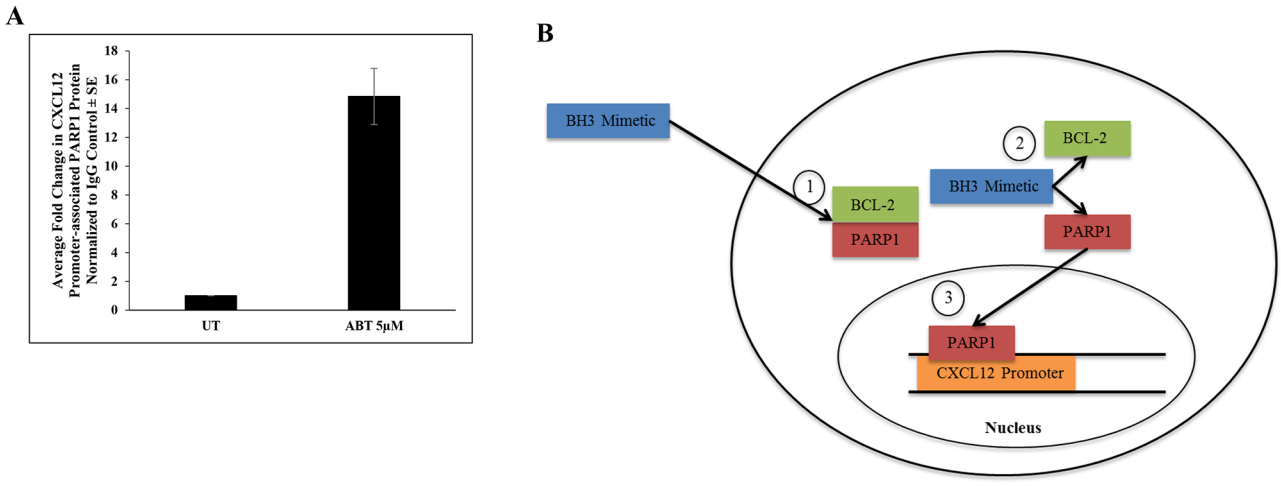

Figure 5: ABT increases PARP1 binding to the *CXCL12* promoter. A. T265-2c cells treated with ABT for 24h exhibit increased PARP1 binding to the *CXCL12* promoter as demonstrated by qRT-PCR of Chromatin Immunoprecipitation (ChIP) with PARP1 antibody or IgG control. **B.** Proposed mechanism: PARP1 dimerizes with BCL-2 under normal physiological conditions (Step 1) (ref 33, ref 55). BH3 mimetics disrupt the BCL-2:PARP1 complex via the BH3 domain (Step 2) (ref 33), freeing PARP1 to bind the CXCL12 proximal promoter and exert transcriptional repression (Step 3).

known to harbor breast cancer metastases (lymph nodes, lung, liver, bone marrow) and relatively lower in tissues not typically associated with such metastases (small intestine, kidney, skin, brain, skeletal muscle) [11]. Further, *in vivo* neutralization of the CXCL12/CXCR4 interaction in breast cancer has been shown to significantly inhibit lung and lymph node metastasis [11]. Outside the context of cancer, reduction of CXCL12 has potential significance in the field of autoimmune disorders, as neutralization of chemokines is thought to have a restraining effect on the autoimmune response [48]. Conversely, disruption of the CXCL12/CXCR4 interaction has been shown to promote hematopoietic stem cell mobilization, promoting immunologic response of patients with non-Hodgkin lymphoma and multiple myeloma [49]. Additional studies are required to determine if BH3 mimetic suppression of CXCL12 is limited to MPNST and related tumor cells or is a general phenomenon with implications for other tumor types.

Affecting the CXCL12 signaling axis has potential for significant therapeutic benefit, as CXCR4 is over-expressed in more than 20 human cancers [50]. Accordingly, CXCR4 has been targeted by numerous antagonists including AMD3100, TN14003, T22, CTCE-9908 and ALX40-4C, all of which are CXCL12 N-terminus peptide analogs [51]. The ligand-dependent nature of this signaling axis relative to other cancer-relevant pathways of which ligand-independent signal transduction occurs via means such as receptor dimerization provides additional therapeutic targeting at the ligand level. This approach has potential for therapeutic benefit alone or as a combination approach to shut down the pathway at multiple levels. Here we demonstrate that BH3 mimetics as a class have the capability to robustly suppress CXCL12 expression and secretion in MPNSTs and set a precedent for further studies into the clinical utility of targeting the CXCL12 signaling axis by ligand ablation.

MATERIALS AND METHODS

Antibodies and other reagents

PARP1 primary antibody (#sc-7150 [H-250]) and rabbit IgG (sc-2027) were obtained from Santa Cruz (Dallas, TX). Other reagents were obtained from the following sources: ABT-737 [ABT] and Obatoclax [OBX] (Selleck Chemicals, Houston, TX S1002 and S1057, respectively), desferrioxamine [DFO] (Sigma D9533), sabutoclax [SBX] (AdooQ Biosciences, Irvine, CA A12823), AT101 (Ascenta Therapeutics, Malvern, PA).

Cell culture

We have previously described the source of human NF1-derived MPNST cell lines (T265-2c, 90-8) utilized in this study [29]. STS26T sporadic MPNST cells were a gift from Dr. Steven Carroll whose source is described by Dahlberg *et al*. [30]. All cell lines were cultured in DMEM containing 1% penicillin/streptomycin (Invitrogen, Carlsbad, CA), 1% L-glutamine (Sigma), and 10% fetal bovine serum (Fisher Scientific). All cells were incubated at 37°C in a humidified 5% CO2, 95% air atmosphere. Based on cellular size and in order to achieve relative confluence, cell lines were plated at varying densities. For DNA, RNA and protein collection, cells were plated on 100mm dishes at a density of: 1×10^6/dish- 90-8, STS26T; 1.5×10^6/dish- T265-2c. Cultures were used in experiments 24 hours post-plating. Drug treatments were performed in respective media supplemented with 2% FBS.

Cell viability assay

The calcein-AM conversion assay (Life Technologies, Carlsbad, CA C3100MP) was employed to quantify viable cell number after drug treatment as previously described [54, 55].

ELISA

T265-2c cells were plated in 100mm dishes at previously described densities and were treated 24h post plating in media containing 2% FBS with or without AT101. Conditioned media was collected 24 hours after treatment and concentrated ~80-fold using Amicon Ultra-4 centrifugal filters with a molecular size exclusion of 3kD (Millipore, Billerica, MA UFC800324) and stored at -80°C. Following protein quantification, 375µg total protein was loaded per well (in duplicate) using a human CXCL12/SDF-1 ELISA kit (R&D Systems, Minneapolis, MN DSA00) per the manufacturer's instructions.

Reverse transcription and real-time quantitative PCR analysis

RNA was isolated using the RNeasy Plus mini kit (Qiagen, Germany #74134). cDNA was subsequently synthesized using the High Capacity cDNA Reverse Transcription kit (Applied Biosystems, Foster City, CA #4368814). Real-time quantitative PCR was performed using the Maxima SYBR Green/ROX qPCR master mix (Thermo Scientific, Waltham, MA #K0221) and probes were obtained from Life Technologies (Carlsbad, CA). Amplifications were run in a StepOne Plus Real-Time PCR System (Applied Biosystems). The following sense/antisense primers and probes were selected from the Harvard PrimerBank and used for detecting: human CXCL12 (5'-ATTCTCAACACTCCAAACTGTGC-3' and 5'-ACTTTAGCTTCGGGTCAATGC-3') and human 18S rRNA (5'-GTAACCCGTTGAACCCCATT-3' and 5'-CCATCCAATCGGTAGTAGCG-3'). Analysis was performed using the ΔΔCT method [52] and values were adjusted using 18S rRNA levels as reference.

Chromatin immunoprecipitation (ChIP)

T265-2c cells were plated in 100mm dishes at densities described above in the *Cell Culture* section and drug treatments were performed after 24h. To account for loss of total cell number resulting from cytotoxic effects of BH3 mimetic treatment, twice as many 100mm dishes were used for each treatment condition versus untreated and each dish of respective cells was combined after fixation. ChIP using antibodies against PARP1 (Santa Cruz H-250 [sc-7150]) (12µg/ml) or rabbit IgG (Santa Cruz sc-2027) (12µg/ml) was performed using the ChIP-IT Express Enzymatic kit from Active Motif (Carlsbad, CA #53009) per the manufacturer's instructions. DNA was amplified using primers flanking the putative PARP1 ["A/GNNA/TCAAA" [53] binding site within the *CXCL12* promoter. Negative control primers were obtained from Active Motif (#103708).

Primer sequence:
Forward: 5′-GAATCTCCCGTCCCACTCC-3′
Reverse: 5′-GCCGAGCCTCAGTTTCCT-3′

Statistics

All data points represent the mean ± standard deviation (S.D.) except for ChIP qRT-PCR data, which represents mean ± standard error (S.E.). All experiments were repeated at least 3 times (except for T265-2c ChIP and STS26T qRT-PCR) and representative data is shown; all biological replicates are included in supplementary material. Each real-time quantitative PCR was performed in triplicate and the average and S.D. (or S.E. for ChIP qRT-PCR) was used for statistical analysis. Each ELISA was performed in duplicate and averages from three biological and technical replicates were used to obtain an average and S.D. for statistical analysis. ELISA data is presented as a compilation of three replicate experiments. Statistical significance was determined by ANOVA followed by Dunnett's post-hoc test. A p-value < 0.05 was considered significant.

Abbreviations

Malignant Peripheral Nerve Sheath Tumor (MPNST); Neurofibromatosis Type 1 (NF1); ABT-737 (ABT); obatoclax (OBX); sabutoclax (SBX); desferrioxamine (DFO); B-Cell Lymphoma 2 (BCL-2); BCL-2 Homology domain 3 (BH3); Poly (ADP-Ribose) Polymerase 1 (PARP1); Phospholipase C (PLC); PhosphoInositide 3-Kinase (PI3K); Mitogen-Activated Protein Kinase (MAPK); c-Jun N-terminal Kinase (JNK).

ACKNOWLEDGEMENTS

We wish to thank the UAB Heflin Center for Genomic Studies (supported by grant CA013148) and UAB Molecular Detection Core (supported by grant NS47466) for technical assistance as well as Ascenta Therapeutics for supplying AT101. This work was supported by United States Department of Defense (DOD) grant W81XWH-14-1-0073.

CONFLICTS OF INTEREST

None.

FUNDING

This work was supported by Department of Defense grant W81XWH-14-1-0073 (K.A.R). Funding sources for this study had no involvement in study design, collection/analysis/interpretation of data, writing of the report, or decision to publish.

Author contributions

CDG, SLC, KAR conceived study; CDG, NK, HCP, LAS, SLC, KAR designed experiments; CDG, NK, HCP, LMG, BJK performed experiments; CDG, KAR, NK, HCP, LAS analyzed data; CDG, KAR wrote manuscript; CDG, NK, BJK, LMG, HCP, LAS, SLC, KAR reviewed manuscript.

REFERENCES

1. Evans DG, Baser ME, McGaughran J, Sharif S, Howard E, Moran A. Malignant peripheral nerve sheath tumours in neurofibromatosis 1. J Med Genet 2002; 39:311-314.
2. Zhu Y, Parada LF. Neurofibromin, a tumor suppressor in the nervous system. Exp Cell Res 2001; 264:19-28.
3. Ferner RE, Gutmann DH. International consensus statement on malignant peripheral nerve sheath tumors in neurofibromatosis. Cancer Res 2002; 62:1573-77.
4. Kaza N, Kohli L, Graham CD, Klocke BJ, Carroll SL, Roth KA. BNIP3 regulates AT101 [(-)-gossypol] induced death in malignant peripheral nerve sheath tumor cells. PLOS ONE 2014; 9:e96733.
5. Ma Q, Jones D, Borghesani PR, Segal RA, Nagasawa T, Kishimoto T, Bronson RT, Springer TA. Impaired B-lymphopoiesis, myelopoiesis, and derailed cerebellar neuron migration in CXCR4- and SDF-1-deficient mice. Proc Natl Acad Sci U.S.A. 1998; 95:9448-53.
6. Mo W, Chen J, Patel A, Zhang L, Chau V, Li Y, Cho W, Lim K, Xu J, Lazar AJ, Creighton CJ, Bolshakov S, McKay RM, Lev D, Le LQ, Parada LF. CXCR4/CXCL12 mediate autocrine cell-cycle progression in NF1-associated malignant peripheral nerve sheath tumors. Cell 2013; 152:1077-90.
7. Lattin J, Zidar DA, Schroder K, Kellie S, Hume DA, Sweet MJ. G-protein-coupled receptor expression, function, and signaling in macrophages. J Leukoc Biol 2007; 82:16-32.

8. Mellado M, Rodríguez-Frade JM, Mañes S, Martínez-A C. Chemokine signaling and functional responses: the role of receptor dimerization and TK pathway activation. Annu Rev Immunol 2001; 19:397-421.
9. New DC, Wong YH. Molecular mechanisms mediating the G protein-coupled receptor regulation of cell cycle progression. J Mol Signal 2007; 2:2.
10. Pierce KL, Premont RT, Lefkowitz RJ. Seven-transmembrane receptors. Nat Rev Mol Cell Biol 2002; 3:639-50.
11. Müller A, Homey B, Soto H, Ge N, Buchanan ME, McClanahan T, Murphy E, Yuan W, Wagner SN, Barrera JL, Mohar A, Verastequi E, Zlotnik A. Involvement of chemokine receptors in breast cancer metastasis. Nature 2001; 410:50-56.
12. Rempel SA, Dudas S, Ge S, Gutiérrez JA. Identification and localization of the cytokine SDF1 and its receptor, CXC chemokine receptor 4, to regions of necrosis and angiogenesis in human glioblastoma. Clin Cancer Res 2000; 6:102-111.
13. Gatti M, Pattarozzi A, Bajetto A, Würth R, Daga A, Fiaschi P, Zona G, Florio T, Barbieri F. Inhibition of CXCL12/CXCR4 autocrine/paracrine loop reduces viability of human glioblastoma stem-like cells affecting self-renewal ativity. Toxicology 2013; 314:209-20.
14. Burns JM, Summers BC, Wang Y, Melikian A, Berahovich R, Miao Z, Penfold ME, Sunshine MJ, Littman DR, Kuo CJ, Wei K, McMaster BE, Wright K, *et al*. A novel chemokine receptor for SDF-1 and I-TAC involved in cell survival, cell adhesion, and tumor development. J Exp Med 2006; 203:2201-13.
15. Raggo C, Ruhl R, McAllister S, Koon H, Dezube BJ, Früh K, Moses AV. Novel cellular genes essential for transformation of endothelial cells by Kaposi's sarcoma-associated herpesvirus. Cancer Res 2005; 65:5084-95.
16. Miao Z, Luker KE, Summers BC, Berahovich R, Bhojani MS, Rehemtulla A, Kleer CG, Essner JJ, Nasevicius A, Luker GD, Howard MC, Schall TJ. CXCR7 (RDC1) promotes breast and lung tumor growth *in vivo* and is expressed on tumor-associated vasculature. Proc Natl Acad Sci U.S.A. 2007; 104:15735-40.
17. Begley LA, MacDonald JW, Day ML, Macoska JA. CXCL12 activates a robust transcriptional response in human prostate epithelial cells. J Biol Chem 2007; 282:26767-74.
18. Boldajipour B, Mahabaleshwar H, Kardash E, Reichman-Fried M, Blaser J, Minina S, Wilson D, Xu Q, Raz E. Control of chemokine-guided cell migration by ligand sequestration. Cell 2008; 132:463-73.
19. Dambly-Chaudière C, Cubedo N, Ghysen A. Control of cell migration in the development of the posterior lateral line: antagonistic interactions between the chemokine receptors CXCR4 and CXCR7/RDC1. BMC Dev Biol 2007; 7:23.
20. Levoye A, Balabanian K, Baleux F, Bachelerie F, Lagane B. CXCR7 heterodimerizes with CXCR4 and regulates CXCL12-mediated G protein signaling. Blood 2009; 113:6085-93.
21. Sierro F, Biben C, Martínez-Muñoz L, Mellado M, Ransohoff RM, Li M, Woehl B, Leung H, Groom J, Batten M, Harvey RP, Martinez-A C, Mackay CR, *et al*. Disrupted cardiac development but normal hematopoiesis in mice deficient in the second CXCL12/SDF1 receptor, CXCR7. Proc Natl Acad Sci U.S.A. 2007; 104:14759-64.
22. Jankowski K, Kucia M, Wysoczynski M, Reca R, Zhao D, Trzyna E, Trent J, Peiper S, Zembala M, Ratajczak J, Houghton P, Janowska-Wieczorek A, Ratajczak MZ. Both hepatocyte growth factor (HGF) and stromal-derived factor-1 regulate the metastatic behavior of human rhabdomyosarcoma cells, but only HGF enhances their resistance to radiochemotherapy. Cancer Res 2003; 63:7926-35.
23. Wysoczynski M, Kucia M, Ratajczak J, Ratajczak MZ. Cleavage fragments of the third complement component (C3) enhance stromal derived factor-1 (SDF-1)-mediated platelet production during reactive postbleeding thrombocytosis. Leukemia 2007; 21:973-82.
24. Wysoczynski M, Miekus K, Jankowski K, Wanzeck J, Bertolone S, Janowska-Wieczorek A, Ratajczak J, Ratajczak MZ. Leukemia inhibitor factor: a newly identified metastatic factor in rhabdomyosarcomas. Leukemia 2007; 67:2131-40.
25. Hu W, Wang F, Tang J, Liu X, Yuan Z, Nie C, Wei Y. Proapoptotic protein Smac mediates apoptosis in cisplatin-resistant ovarian cancer cells when treated with the anti-tumor agent AT101. J Biol Chem 2012; 287:68-80.
26. Goff DJ, Court Recart A, Sadarangani A, Chun HJ, Barrett CL, Krajewska M, Leu H, Low-Marchelli J, Ma W, Shih AY, Wei J, Zhai D, Geron I, *et al*. A Pan-BCL2 inhibitor renders bone-marrow-resistant human leukemia stem cells sensitive to tyrosine kinase inhibition. Cell Stem Cell 2013; 12:316-28.
27. Voss V, Senft C, Lang V, Ronellenfitsch MW, Steinbach JP, Seifert V, Kogel D. The pan-Bcl-2 inhibitor (-)-gossypol triggers autophagic cell death in malignant glioma. Mol Cancer Res 2010; 8:1002-16.
28. Marković J, Grdović N, Dinić S, Karan-Djurašević T, Uskoković A, Arambašić J, Mihailovic M, Pavlovic S, Poznanovic G, Vidakovic M. PARP-1 and YY1 are important novel regulators of CXCL12 gene transcription in rat pancreatic beta cells. PLOS ONE 2013; 8:e59679.
29. Stonecypher MS, Byer SJ, Grizzle WE, Carroll SJ. Activation of the neuregulin-1/ErbB signaling pathway promotes the proliferation of neoplastic Schwann cells in human malignant peripheral nerve sheath tumors. Oncogene 2005 24:5589-605.
30. Dahlberg WK, Little JB, Fletcher JA, Suit HD, Okunieff P. Radiosensitivity *in vitro* of human soft tissue sarcoma cell

lines and skin fibroblasts derived from the same patients. Int J Radiat Biol 1993; 63:191-98.

31. Yu L, Cecil J, Peng SB, Schrementi J, Kovacevic S, Paul D, Su EW, Wang J. Identification and expression of novel isoforms of human stromal cell-derived factor 1. Gene 2006; 374:174-79.
32. Yano T, Liu Z, Donovan J, Thomas MK, Habener JF. Stromal cell derived factor-1 (SDF-1)/CXCL12 attenuates diabetes in mice and promotes pancreatic beta-cell survival by activation of the prosurvival kinase Akt. Diabetes 2007; 56:2946-57.
33. Dutta C, Day T, Kopp N, van Bodegom D, Davids MS, Ryan J, Bird L, Kommajosyula N, Weigert O, Yoda A, Fung H, Brown JR, Shapiro GI, *et al*. BCL2 suppresses PARP1 function and nonapoptotic cell death. Cancer Res 2012; 72:4193-203.
34. Ni Chonghaile T, Letai A. Mimicking the BH3 domain to kill cancer cells. Oncogene 2008; 27:S149-57.
35. Evan GI, Wyllie AH, Gilbert CS, Littlewood TD, Land H, Brooks M, Waters CM, Penn LZ, Hancock DC. Induction of apoptosis in fibroblasts by c-myc protein. Cell 1992; 69:119-28.
36. Oda E, Ohki R, Murasawa H, Nemoto J, Shibue T, Yamashita T, Tokino T, Taniquchi T, Tanaka N. Noxa, a BH3-only member of the Bcl-2 family and candidate mediator of p53-induced apoptosis. Science 2000; 288:1053-58.
37. Nakano K, Vousden KH. PUMA, a novel proapoptotic gene, is induced by p53. Mol Cell 2001; 7:683-94.
38. Yip KW, Reed JC. Bcl-2 family proteins and cancer. Oncogene 2008; 27:6398-406.
39. Shakir M, Tang D, Zeh HJ, Tang SW, Anderson CJ, Bahary N, Lotze MT. The chemokine receptors CXCR4/CXR7 and their primary heterodimeric ligands CXCL12 and CXCL12/high mobility group box 1 in pancreatic cancer growth and development: finding flow. Pancreas 2015; 44:528-34.
40. Yadav SS, Prasad SB, Das M, Kumari S, Pandey LK, Singh S, Pradhan S, Narayan G. Epigenetic silencing of CXCR4 promotes loss of cell adhesion in cervical cancer. Biomed Res Int 2014; 2014:581403.
41. Zlotnik A, Yoshie O. Chemokines: a new classification system and their role in immunity. Immunity 2000; 12:121-27.
42. Campbell JJ, Butcher EC. Chemokines in tissue-specific and microenvironment-specific lymphocyte homing. Curr Opin Immunol 2000; 12:336-41.
43. Butcher EC, Williams M, Youngman K, Rott L, Briskin M. Lymphocyte trafficking and regional immunity. Adv Immunol 1999; 72:209-53.
44. Morales J, Homey B, Vicari AP, Hudak S, Oldham E, Hedrick J, Orozco R, Copeland NG, Jenkins NA, McEvoy LM, Zlotnik A. CTACK, a skin-associated chemokine that preferentially attracts skin-homing memory T cells. Proc Natl Acad Sci U.S.A. 1999; 96:14470-75.
45. Homey B, Wang W, Soto H, Buchanan ME, Wiesenborn A, Catron D, Muller A, McClanahan TK, Dieu-Nosjean MC, Orozco R, Ruzicka T, Lehmann P, Oldham E, *et al*. Cutting edge: the orphan chemokine receptor G protein-coupled receptor-2 (GPR-2, CCR10) binds the skin-associated chemokine CCL27 (CTACK/ALP/ILC). J Immunol 2000; 164:3465-70.
46. Peled A, Petit I, Kollet O, Magdid M, Ponomaryov T, Byk T, Nagler A, Ben-hur H, Many A, Schultz L, Lider O, Alon R, Zipori D, *et al*. Dependence of human stem cell engraftment and population of NOD/SCID mice on CXCR4. Science 1999; 283:845-48.
47. Förster R, Schubel A, Breitfeld D, Kremmer E, Renner-Müller I, Wolf E, Lipp M. CCR7 coordinates the primary immune response by establishing function microenvironments in secondary lymphoid organs. Cell 1999; 99:23-33.
48. Karin N. The multiple faces of CXCL12 (DF-1alpha) in the regulation of immunity during health and disease. J Leukoc Biol 2010; 88:463-73.
49. Damon LE, Damon LE. Mobilization of hematopoietic stem cells into the peripheral blood. Expert Rev Hematol 2009; 2:717-33.
50. Balkwill F. Cancer and the chemokine network. Nat Rev Cancer 2004; 4:540-50.
51. Sun X, Cheng G, Hao M, Zheng J, Zhou X, Zhang J, Taichman RS, Pienta KJ, Wang J. CXCL12/CXCR4/CXCR7 chemokine axis and cancer progression. Cancer Metastasis Rev 2010; 29:709-22.
52. Livak KL, Schmittgen TD. Analysis of relative gene expression data using real-time quantitative PCR and the 2(-Delta C(T)) Method. Methods 2001; 25:402-08.
53. Ko HL, Ren EC. (2011) Novel poly (ADP-ribose) polymerase 1 binding motif in hepatitis B virus core promoter impairs DNA damage repair. Hepatology 54:1190-98 (PMID 21721027).
54. Geng Y, Kohli L, Klocke BJ, Roth KA. (2010) Chloroquine-induced autophagic vacuole accumulation and cell death in glioma cells is p53 independent. Neuro Oncol 12:473-81 (PMID 20406898).
55. Oltersdorf T, Elmore SW, Shoemaker AR, Armstrong RC, Augeri DJ, Belli BA, *et al*. (2005) An inhibitor of Bcl-2 family proteins induces regression of solid tumours. Nature 435:677-81 (PMID 15902208).

To be submitted to: Scientific Reports

Usp9X Regulates Cell Death in Malignant Peripheral Nerve Sheath Tumors.

Bianchetti E[1*], Bates SJ[1], Carroll SL[2], Siegelin MD[1], Roth KA[1]

1 Department of Pathology & Cell Biology, Columbia University Vagelos College of Physicians and Surgeons, New York, New York, USA.

2 Medical University of South Carolina, Department of Pathology and Laboratory Medicine, Charleston, South Carolina, USA.

[*]Corresponding author: Elena Bianchetti, PhD
Email: eb2985@cumc.columbia.edu

Keywords: MPNST, Usp9X, Mcl-1, deubiquitinase, paraptosis

ABSTRACT

Malignant peripheral nerve sheath tumors (MPNSTs) are the leading cause of death in neurofibromatosis type 1 (NF1) patients. Current treatment modalities have been largely unsuccessful in improving MPNST patient survival, making the identification of new therapeutic targets urgent. In this study, we found that interference with Usp9X, a deubiquitinating enzyme which is overexpressed in nervous system tumors, or Mcl-1, an anti-apoptotic member of the Bcl-2 family whose degradation is regulated by Usp9X, causes rapid death in human MPNST cell lines. Although both Usp9X and Mcl-1 knockdown elicited some features of apoptosis, broad spectrum caspase inhibition was ineffective in preventing knockdown-induced MPNST cell death suggesting that caspase-independent death pathways were also activated. Ultrastructural

examination of MPNST cells following either Usp9X interference or pharmacological inhibition showed extensive cytoplasmic vacuolization and swelling of endoplasmic reticulum (ER) and mitochondria most consistent with paraptotic cell death. Finally, the Usp9X pharmacological inhibitor WP1130 significantly reduced human MPNST growth and induced tumor cell death in an *in vivo* xenograft model. In total, these findings indicate that Usp9X and Mcl-1 play significant roles in maintaining human MPNST cell viability and that pharmacological inhibition of Usp9X deubiquitinase activity could be a therapeutic target for MPNST treatment.

INTRODUCTION

Neurofibromatosis type 1 (NF1) is a genetic neurocutaneous disease with an incidence of 1:3000 [1,2] characterized by a predisposition to multiple peripheral nerve sheath tumors [3]. The vast majority of NF1-associated nerve sheath tumors are benign, but malignant peripheral nerve sheath tumors (MPNSTs) are the leading cause of death in NF1 patients. MPNSTs are aggressive Schwann cell-derived soft tissue sarcomas and occur in 5 to 10% of patients with NF1 [4]. Approximately half of MPNSTs are associated with NF1 and often arise from benign plexiform neurofibromas [5]. Currently, standard MPNST therapy is tumor resection with wide surgical margins, but patient prognosis is poor due to variables such as tumor size, anatomic location, propensity to metastasis and limited tumor cell sensitivity to chemotherapy and radiation [1]. Therefore, identification of new therapeutic targets to treat this aggressive neoplasm is a high clinical priority.

Usp9X is a deubiquitinating enzyme which is overexpressed in various human cancers, including nervous system tumors, such as glioblastoma (GBM) [6]. Genetic and/or pharmacological inhibition of Usp9X activity has been shown to induce tumor cell death in both *in vitro* and *in vivo* models of GBM [6-8]. Previous studies have demonstrated that down-regulation of Usp9X is followed by

enhanced degradation of the anti-apoptotic Bcl-2 family member, myeloid cell leukemia 1 (Mcl-1) [7,9]. Furthermore, Mcl-1 down-regulation is known to be an important determinant of apoptosis in sarcomas [10]. Our findings suggest that Usp9X and Mcl-1 are novel targets for the treatment of MPNSTs and that paraptosis, a caspase-independent type of regulated cell death, may play a role in MPNST cell death induced by Usp9X inhibition.

RESULTS

Usp9X is expressed in human MPNST cell lines

Usp9X expression in MPNSTs has not previously been reported. Thus to ensure potential human clinical relevance, we first examined Usp9X expression levels in a panel of human MPNST cell lines (Suppl. Fig. 1 a). All MPNST cells showed Usp9X protein expression, albeit at different levels. The results confirm that the Usp9X protein is expressed in MPNST cells, reinforcing the notion that Usp9X is a viable, potential therapeutic target for MPNST.

Usp9X inhibition causes massive reduction in MPNST cell viability.

To investigate the potential role of Usp9X in regulating MPNST cell survival, we first examined the effects of inhibiting Usp9X enzymatic activity with the deubiquitinase inhibitor, WP1130, a pharmacological inhibitor of Usp9X known also as Degrasyn [6], on three NF1 patient-derived MPNST cell lines (ST88-14, T265-2c and 90-8). WP1130 caused a concentration-dependent decrease in cell viability after 72h in all three cell lines, with ST88-14 cells being particularly sensitive (Fig. 1 a, b, c). In these experiments, we used a concentration range between 0.5 and 2.5 μM, established from preliminary results (Suppl. Fig. 1 b, c). In addition to Usp9X, WP1130

inhibits the enzymatic activity of multiple deubiquitinases; thus, to more selectively determine the effects of Usp9X inhibition on MPNST cell survival *in vitro*, we silenced Usp9X gene using siRNA. Suppression of Usp9X was confirmed by immunoblotting (Fig. 1 g-j). In all three cell lines, Usp9X gene silencing resulted in a significant reduction in viable cell numbers after 72h (Fig. 1 d-f). Consistent with the results obtained with pharmacological inhibition of Usp9X activity, ST88-14 cells were most strongly affected by Usp9X silencing, with a significant reduction in cell viability observed after just 24h treatment (Fig. 1d). These data support the conclusion that Usp9X is critical for the survival of MPNST cells.

Usp9X inhibition depletes Mcl-1

Based on our previously published observation that Usp9X induces a decline of Mcl-1 protein levels in GBM cells [9,11], we hypothesized that similar effects would be observed in MPNST cells. To test this hypothesis, ST88-14 cells were treated with WP1130 at two different concentrations (Suppl. Fig. 1 e) and Mcl-1 levels were assessed by Western blot after 24 and 48h. Usp9X interference decreased endogenous Mcl-1 protein levels at both concentrations after treatment for 48h (Suppl. Fig. 1 e). Consistent with these results, Usp9X knock-down in ST88-14 cells resulted in decreased Mcl-1 levels at 48h as well (Suppl. Fig. 1 d).

Usp9X knock-down causes MPNST cell death with variable caspase activation and features of apoptosis.

To determine if Usp9X inhibition induced apoptosis of MPNST cells, we inhibited Usp9X pharmacologically with WP1130 and silenced it by siRNA, as well, in ST88-14 and T265-2c cell

lines and examined various biochemical indicators of apoptosis. Usp9X pharmacological inhibition resulted in several features of apoptosis (Fig. 2 a, b), including a time-dependent decrease in mitochondrial membrane potential (Fig. 2 c, d), in both cell lines. Consistent with the viability data, ST88-14 cells were more rapidly and strongly affected by Usp9X inhibition, than T265-2c cells. As with pharmacological inhibition of Usp9X activity, Usp9X knock-down produced biochemical features of apoptotic cell death including a significant loss in mitochondrial membrane potential (Fig. 2 a-d). ST88-14 cells consistently showed more dramatic effects after Usp9X interference, compared to T265-2c cells (Fig 2 a-d) and caspase 3-like enzymatic activity was more pronounced after Usp9X knock-down or WP1130 treatment in ST88-14 cells compared to T265-2c cells (Fig. 2 e-g).

Interference with Mcl-1 produces cell death with apoptotic features in MPNST cell lines.

Usp9X regulates cell survival through both Mcl-1-dependent and –independent processes. To determine if Mcl-1 is a regulator of MPNST survival, we examined the effects of Mcl-1 knockdown on the three MPNST cell lines. As with Usp9X pharmacological inhibition or knock-down, Mcl-1 knock-down resulted in significant cell death in all cell lines tested (Fig. 3 a-g), most prominently in T265-2c and 90-8 cell lines (Fig. 3 d-g). All three cell lines showed time-dependent apoptotic features with enhanced DNA fragmentation, annexin V staining (Fig. 3 b, f), and loss in mitochondrial membrane potential (Fig. 3 c, g) with maximal response at 72h after transfection. T265-2c cells were more sensitive to Mcl-1 depletion (Fig. 3 d, e), compared to ST88-14 cells (Fig. 3 a), with strong features of apoptosis (Fig. 3 f, g). Suppression of Mcl-1 was confirmed by immunoblotting (Fig. 3 h, i). Consistent with these results, pharmacological inhibition of Mcl-1

with A-1210477 [12], caused a concentration-dependent decrease in cellular viability after 72h in all tested cell lines (Suppl. Fig. 2). These data indicate that in addition to being sensitive to Usp9X inhibition, MPNST cell lines are also susceptible to Mcl-1 loss, which appears to activate apoptosis, most prominently in the T265-2c cell line.

Caspase-inhibition provides minimal protection from cell death after Usp9X or Mcl-1 depletion.

To determine if caspase-dependent apoptosis is the main cell death pathway activated by Usp9X or Mcl-1 depletion, we tested the ability of ZVAD, a broad-spectrum caspase inhibitor, to inhibit Usp9X and Mcl-1 knock-down induced MPNST cell death. Despite producing a complete inhibition of caspase 3-like enzymatic activity (Fig. 4 c), ZVAD failed to significantly attenuate cell death after Usp9X or Mcl-1knock-down at 72h in ST88-14 (Fig. 4 a) or T265-2c cells (Fig. 4 b), indicating that other caspase-independent death pathways are likely activated in parallel with apoptosis following Usp9X or Mcl-1 inhibition.

Usp9X inhibition causes ER stress in MPNST cell lines.

Interestingly, both Usp9X pharmacological inhibition and silencing in MPNST cells elicited a significant increase in ATF3, a typical marker of ER-stress (Fig. 5 a, b) and in the pro-apoptotic BH3-only protein Noxa (Fig. 5 a, b). The protein expression level of a second ER stress marker, ATF4, was similarly increased in ST88-14 cells after Usp9X disruption (data not shown). Given that ATF3 and ATF4 are downstream regulators of the ER-stress response [7] and are capable of

activating Noxa [7], we hypothesized that cell death induced by Usp9X inhibition may in part be mediated through an ER stress response.

Ultrastructural examination of MPNST cells following Usp9X inhibition reveals evidence of paraptosis.

We used transmission electron microscopy (TEM) to determine if there was ultrastructural evidence of ER stress in MPNST cells following Usp9X inhibition. T265-2c cells were treated with vehicle or 2.5 μM WP1130 for 24h and processed for TEM. Vehicle treated cells showed intact organelles and normal ER structure (Fig. 5 c-e). In contrast, WP1130 treated T265-2c cells exhibited significant morphological changes including reduced cell size and altered cell shape (Fig. 5 f). In addition, following WP1130 treatment T265-2c cells exhibited numerous small and large clear cytoplasmic vacuoles (Fig. 5 f). The typical ultrastructural features of apoptosis, e.g. chromatin condensation and margination and membrane blebbing were only rarely observed in treated cells (Fig. 5 f-h). Striking changes in ER and mitochondrial ultrastructure previously described in paraptotic cell death [13,14] were seen following WP1130 treatment of T265-2c cells. Compared with vehicle treated cells, WP1130 exposed cells showed significant swelling and disruption of normal ER structure with dramatic expansion of the ER lumina (Fig. 5 d and g). Similarly, in contrast with normal appearing mitochondria in vehicle treated cells, numerous mitochondria in the WP1130 treated cells were markedly enlarged, edematous, disorganized and fragmented (Fig. 5 e and h). Taken together, these results suggest that WP1130 induces paraptosis [13] in T265-2c cells.

WP1130 inhibits MPNST tumor growth *in vivo.*

To assess the potential efficacy of Usp9X inhibition in treating MPNSTs *in vivo*, we tested WP1130 in a heterotopic xenograft MPNST model. ST88-14 cells were implanted subcutaneously and animals were divided into three groups receiving either vehicle or two different concentrations of WP1130 (12.5 and 25 mg/kg intraperitoneally) (Fig. 6 and Suppl. Fig. 3). In our initial *in vivo* experiment, treatment was initiated eight days after implantation and injections were given three times/week for four weeks (Fig. 6 a-f). WP1130 at 25 mg/kg per dose produced a statistically significant growth reduction with partial regression of tumors compared to vehicle treated controls (Fig. 6 a). The day after the last injection, tumors were resected and the tumor volume and weight measured. WP1130 produced a significant decrease in tumor volume at both concentrations (Fig. 6 b) and a statistically significant decrease in tumor weight in the 25 mg/kg dose group (Fig. 6 c and d). The regression of the tumors' size suggested that this treatment not only attenuated tumor growth but induced tumor cell death. Histopathological analysis of the resected tumors in the vehicle treated control group showed densely cellular, highly pleomorphic tumors with brisk mitotic activity (fig. 6 e). In contrast, mice treated with WP1130 showed tumors with reduced cellularity and mitotic activity, multi-focal necrotic areas and the presence of scattered apoptotic nuclei throughout the tumors at both concentrations (fig. 6 f). WP1130 inhibition of Usp9X leads to the inhibition of Usp9X function and thus, an expected decrease in the levels of Usp9X substrates [15]. To verify the *in vivo* effectiveness of WP1130 treatment, we tested the protein levels of Mcl-1 in xenografts from vehicle and WP1130 treated mice and found a significant reduction in Mcl-1 levels *in vivo* (Fig. 6 g). To extend these findings, we performed a second *in vivo* experiment in which we allowed the tumors to grow to a significant size before initiating WP1130 therapy to better model the human situation. Therefore, we implanted ST88-14 cells and waited

one month before initiating daily injections of WP1130 for five days per week for two weeks (Suppl. Fig. 3). WP1130 treatment resulted in a significant attenuation in tumor growth when compared to the vehicle treated group (Suppl. Fig. 3 a). Histopathological analysis of the resected tumors showed features similar to those observed in the initial *in vivo* study. WP1130 reduced cellularity and induced cell death, with multiple areas of necrosis and presence of frequent apoptotic nuclei, at both concentrations (Suppl. Fig. 3 c), compared to the control group (Suppl. Fig. 3 b). WP1130 treatment also resulted in a marked increase in cleaved caspase 3 immunoreactivity and TUNEL labeling compared to tumors of the vehicle group (Suppl. Fig. 4 a-d). To preliminarily assess potential *in vivo* toxic effects of WP1130, we performed body weight measurements on vehicle and WP1130 treated animals throughout the experiment and found no differences between the three groups (data not shown) suggesting that WP1130 does not have obvious toxic effects. These results are consistent with several previous *in vivo* studies of WP1130 [6 16 17].

DISCUSSION

The goal of this study was to determine if Usp9X and/or Mcl-1 play(s) a role in MPNST cell survival and thus, serve as potential therapeutic targets for MPNST treatment. Usp9X is a deubiquitinating enzyme [18] that plays a role in regulating protein degradation by modulation of ubiquitin conjugation to its targets and thereby controlling their proteasomal turnover [19]. It is well established that Usp9X plays a pivotal role in various malignant tumors affecting the nervous system, including GBM [6,11,20]. Mechanistically, Usp9X exerts its effects on cell survival at least in part by controlling the levels of anti-apoptotic Bcl-2 family members, including Mcl-1, or inhibitor of apoptosis proteins, such as XIAP [8]. Interference with Usp9X results in degradation of these

survival promoting proteins [8,19]. Studies related to other malignancies, such as pancreatic cancer, demonstrated that Usp9X is necessary to drive tumor growth by inhibition of cell death [21]. However, it should be noted that the effects of Usp9X on tumors are likely to be context dependent since at least one study, involving a transgenic mouse model of pancreatic cancer, suggested that Usp9X played a tumor suppressive role [22]. Such observations do not void Usp9X as a cancer therapeutic target, but they remind us that some proteins have tumor type-specific biological roles that must be determined experimentally before advancing to human trials for any given cancer type. There might also be "context" dependent and functional differences between tumor initiation and the propagation of established malignancies. This is the first study that we are aware of examining the potential role of Usp9X in MPNST survival. Given that anti-apoptotic Bcl-2 family members are important cell death mediators in the context of MPNST and that Mcl-1 is a central regulator of apoptosis in sarcomas [10], a pivotal role of Usp9X as a potential therapeutic target in MPNSTs appears likely.

The current study offers evidence to support the hypothesis that targeting Usp9X might significantly impact MPNST viability. In our report, by both pharmacological and genetic targeting of Usp9X *in vitro*, we detected not only inhibition of cell growth, but also massive cell death. WP1130 inhibits Usp9X deubiquitinase activity as well as that of several other deubiquitinases such as Usp5, Usp14, and UCH37 [23]. First, we showed that WP1130, in a concentration- and time-dependent manner, decreases the viability of three different human NF1 patient-derived MPNST cell lines, ST88-14, T265-2c and 90-8. To determine the specific role of Usp9X in MPNST cell survival, we silenced Usp9X by siRNA. The selective knock-down of Usp9X caused a significant reduction in cell viability in all three MPNST cell lines tested. Both pharmacological inhibition and Usp9X knock down, caused time-dependent MPNST cell death

with some features of apoptosis, including loss in mitochondrial membrane potential. However, the extent of caspase-3 enzymatic activity varied between cell lines being most robust in ST88-14 cells with minimal caspase activation observed in T265-2c cells. Thus, the extent of caspase-3 enzymatic activity after WP1130 in our cell lines seems to be dependent on cell-specific factors that remain to be determined. Interestingly, treatment of MPNST cell lines with a broad caspase inhibitor failed to significantly attenuate cell death after Usp9X knock-down suggesting that caspase-independent death pathways are also activated. In all MPNST cell lines tested, but most prominently in the T265-2c cell line, Mcl-1 knock-down-induced death displayed features of apoptosis such as increased annexin V staining and decreased mitochondrial membrane potential but, as in Usp9X knock-down cells, broad caspase inhibition did not protect MPNST cells from Mcl-1 knock-down-induced death. We also tested a novel small-molecule inhibitor of Mcl-1, A1210477, since these compounds are currently in preparation for human clinical application, and our results suggest that this compound exerts anti-proliferative activity against MPNST cells. From these data, we conclude that Usp9X and Mcl-1 are central cell death regulators in MPNSTs and that although caspases may be activated following their inhibition, caspase-independent pathways contribute significantly to the MPNST cell death promoting effects of Usp9X and Mcl-1 inhibition *in vitro*.

The mechanism by which Usp9X interference induced massive reduction of viability in MPNST cell lines appears to be multiple. Biochemical analysis showed that Usp9X inhibition caused an ER stress response with an increase of ATF3 and ATF4, two markers of ER stress, followed by an increase in pro-apoptotic Noxa and a subsequent decrease in Mcl-1 protein levels. Similar to our *in vitro* observations, ST88-14 xenografts following treatment with WP1130 showed a significant reduction in Mcl-1 protein levels *in vivo*.

According to previous publications [24], upon ER stress, the ER lumen is remarkably enlarged in cells, which can be detected by electron microscopic examination. Ultrastructural examination of MPNST cells following WP1130 treatment showed features of ER stress and paraptosis, a type of caspase-independent cell death associated with ER damage. These results suggest for the first time a relation between Usp9X and ER stress in the context of MPNST. In addition, we noted an increase in pro-apoptotic Noxa, which is known to be regulated by ATF3 and ATF4 [25,26] and which preceded the down-regulation of Mcl-1 [7]. Although a relationship between Noxa induction and Usp9X inhibition has not been described before in MPNST cells, these results suggest that Noxa might be implicated in the death produced by Usp9X inhibition. As explained above, we found a decline in Mcl-1 levels upon Usp9X inhibition, which is in keeping with earlier findings in other model systems [7,18,27,28]. However, our study demonstrated that Noxa up-regulation precedes Mcl-1 down-regulation, suggesting that the Noxa increase is proximal of Mcl-1 with respect to cell death induction. Given that Noxa is an inhibitor of Mcl-1 and has been known to stimulate Mcl-1 mediated proteasomal degradation, Usp9X inhibition might in part lead to a reduction of Mcl-1 levels through Noxa mediated destabilization of Mcl-1. However, taking this speculation aside, at the minimum, increased Noxa levels will facilitate release of BAK and BIM from Mcl-1, thereby driving BAX/BAK mediated intrinsic apoptosis.

In seeking to identify others forms of cell death produced by Usp9X inhibition in MPNST cells, TEM analysis showed morphological features of paraptosis with extensive cytoplasmic vacuolization, swelling of ER and mitochondria and only minimal features of apoptosis [13,14]. To the best of our knowledge, presence of paraptosis has never been described before in relation to MPNSTs or in the context of Usp9X inhibition.

To determine if Usp9X inhibition has therapeutic potential *in vivo*, we tested WP1130 in a heterotopic MPNST xenograft model. WP1130 treatment resulted in a statistically significant growth reduction and partial regression of tumors. These results suggest that WP1130 might be useful for MPNST treatment. Our findings are in keeping with the results of others that have observed anti-cancer effects of WP1130 in various xenograft model systems [6,16,17]. While we found single agent efficacy with Usp9X and Mcl-1 inhibitors in MPSNT model systems, it is tempting to speculate as to whether these effects may be further enhanced by drug combination therapies. The literature suggests that in other tumor entities, including GBM, the efficacy of Mcl-1 inhibitors is dramatically increased in the presence of other drug compounds [11,29]. Similar results have been found with regards to Usp9X inhibition [15]. For instance, Bcl-2/Bcl-xL- inhibition coupled with the inhibitor WP1130 showed synergistic anti-cancer effects in several preclinical model systems [18,30] . In conclusion, our study demonstrates that MPNST cell lines are susceptible to both Usp9X and Mcl-1 loss which appears to activate both apoptotic and caspase-independent death pathways, such as paraptosis.

MATERIALS AND METHODS

Ethics statement

All procedures were in accordance with Animal Welfare Regulations and approved by the Institutional Animal Care and Use Committee at the Columbia University Irving Medical Center. The study was reviewed and approved by the institutional review board at the Columbia University Irving Medical Center.

Reagents

Primary antibodies were obtained from the following sources: Usp9X (Cell Signaling,

Danvers, MA #5751), Mcl-1 (Cell Signaling, Danvers, MA #5453), Noxa (Calbiochem, San Diego, CA #OP180), ATF4 (Cell Signaling, Danvers, MA #11815), ATF3 (Novus Biologicals, Littleton, CO #NBP1-85816), β-actin (Sigma, St. Louis, MO #A5316). Secondary antibodies were HRP-conjugated goat anti-rabbit (Thermo Scientific, Waltham, MA #31460) and goat anti-mouse (Thermo Scientific, Waltham, MA #31430). Degrasyn [WP1130] was obtained from Selleckchem (Houston, TX #S2243). A-1210477 was purchased from APExBIO (Houston, TX #B6011). Tunicamycin [TUN] and Staurosporine [STS] were purchased from Sigma (St. Louis, MO; TUN #T7765, STS #S5921).

Cell culture

The human NF1-associated MPNST lines used in this study are: T265-2c cells, ST88-14 cells and 90-8 cells, obtained and maintained as described [31,32]. Morphology and doubling times of cells were routinely assessed, according to the guidelines contained in the ATCC Technical Bulletin 8. The identity of cells was verified by short tandem repeat analyses. The short tandem repeat profile of each sporadic MPNST cell line was determined by examining 15 markers standardly used by the American Type Culture Collection and the amelogenin locus (included to verify the sex of the patient from which the tumor was derived) with an AmpFLSTR system (Applied Biosystems; Foster City, CA). Cells were regularly tested for Mycoplasma infection, as well. Cells were maintained in Dulbecco's modified Eagle's medium (DMEM, Corning, Manassas, VA), containing 1% penicillin/streptomycin (Invitrogen, Carlsbad, CA), 1% L-glutamine (Sigma, St. Louis, MO), and 10% fetal bovine serum (FBS;Hyclone, Logan, UT) and incubated at 37°C in a humidified 5% CO2, 95% air atmosphere. For cell viability studies, cells were plated on uncoated 96 well plates at a density of 4,000/well. For caspase 3-like enzymatic activity assays, on uncoated

48 well plates at a density of 20,000/well. For flow analyses and lysate collection, on uncoated 12 well plates at a density of 50,000/well, and in 100 mm dishes at a density of 10^6 cells/dish. Cultures were used in experiments 24 hours post-plating unless stated otherwise. Drug treatments were performed in media supplemented with 2% FBS.

RNAi

SignalSilence Usp9X siRNA I #6308 was purchased from Cell Signaling. Non-targeting siRNA-pool (ON-TARGETplus Non-targeting Pool, # D-001810-10-05) and Mcl-1 (SMARTpool: ON-TARGETplus Mcl-1 siRNA, L-004501-00-0005) were purchased from Thermo Fisher Scientific (Pittsburgh, PA). MPNST cell lines were transfected as previously described [33]. Cells were plated on 12 wells plates. After 24 hours, they have been incubated with the formed complexes of Lipofectamine 2000 (Invitrogen, Carlsbad, CA, U.S.A.) and the respective siRNA (12-well condition) in DMEM without FBS and antibiotics. The day after, FBS was added to a total concentration of 2%.

Cell viability and caspase cleavage assays

Cellular proliferation was measured using CellTiter-Glo assays (Promega, Madison, WI), according to the manufacturer's instructions. Briefly, cells were plated in 96-well plates. After treatments, 100µl of CellTiter-Glo Reagent was added to each well containing 100µl medium and cells. Cell lysis was induced by shaking for 2 min on an orbital shaker. Then cells were incubated for 10 min at RT for stabilization of the signal prior to measuring luminescence. Luminescence was measured using a plate reader (SpectraMax i3x multi-mode detection platform, Molecular

Devices). Caspase activation was assessed with an *in vitro* caspase-3 like cleavage assay utilizing the chemical substrate DEVD-7-amino-4-methylcoumarin (AMC) (Enzo Life Sciences, Framingdale, NY #ALX-260-031). Assay was performed as previously described [34].

Measurement of apoptosis and mitochondrial membrane potential

For annexin V/propidium iodide (PI) staining the FITC Annexin V Apoptosis Detection Kit I (BD Pharmingen, U.S.A.) was used according to the manufacturer's instructions. TMRE staining was performed using CellSimple™ Mitochondrial Membrane Potential Assay Kit (II) (Cell Signaling #45898), in accordance with the manufacturer instructions. Fluorescence was measured using a BD FACSCalibur flow cytometer. The data were analyzed with the FlowJo software (version 8.7.1; Tree Star, Ashland, OR, U.S.A.).

Western blotting

Whole cell lysates were prepared by removing the media and lysing cells directly in Laemmli buffer, containing 5% 2-Mercaptoethanol (Bio-Rad #161-0710), 95% 2x Laemmli Sample Buffer (Bio-Rad #161-0737) and protease and phosphatase inhibitor cocktail (Thermo Scientific #1861281). Lysates were stored at -80ºC. Whole tumor lysates were prepared by lysing the tissues directly in RIPA buffer (Thermo Fisher #89900) with the addition of protease and phosphatase inhibitor cocktail (Thermo Scientific #1861281). Tumors were mechanically disaggregated followed by sonication. Insoluble material was removed by centrifugation at 12,000 r.p.m., and the supernatant was collected for protein quantification. Lysates were immediately stored at -80ºC.

Western blots were performed as described previously [35]. All primary antibodies were diluted to a final concentration of 1:500, except β-actin (1:8000). Secondary antibodies conjugated with horseradish-peroxidase were used at a dilution of 1:5000. For immunodetection, the Pierce ECL Western blotting substrate was utilized (Pierce ECL; Thermo Scientific, Waltham, MA). Membranes were developed using Azure c-300 gel doc & western blot Imaging (Azure Biosystem). Quantification of Western blot bands was performed with the open source image processing program ImageJ.

Transmission Electron Microscopy:

Cells were fixed with 2.5% glutaraldehyde in 0.1M Sorenson's buffer (PH 7.2) for at least one hour, then postfixed with 1% OsO4 also in Sorenson's buffer for one hour. After dehydration cells were embedded in a mixture of Lx-112 (Ladd Research Industries, Inc.) and Embed-812 (EMS, Fortwashington, PA). Thin sections (60nm) were cut on the MT-Power-Trome XL ultramicrotome. Sections were stained with uranyl acetate and lead citrate and examined under a JEOL JEM-1200 EXII electron microscope. Images were taken on an ORCA-HR digital camera (Hamamatsu) and recorded with the AMT Image Capture Engine.

Subcutaneous xenograft model

7×10^6 ST88-14 cells suspended 1:1 in Matrigel Matrix (Corning Inc., Corning, NY, U.S.A.) were implanted subcutaneously into one flank (first experiment) and into both flanks (second experiment) of 6-8 week-old SCID SHO mice as previously described [18]. 4 mice per experimental group were used. Vehicle or drug was injected intraperitoneally 3 times each week for 4 weeks during the first *in vivo* study, and for five of seven days, from Monday to Friday, for

2 weeks during the second *in vivo* experiment. For intraperitoneal application WP1130 were dissolved in a solution of 80% Cremophor EL (SIGMA, St. Louis, MO) and 20% Ethanol (Pharmco-Aaper, Brookfield, CT) (v/v), diluted 1:1 in sterile PBS.

Histological analysis

Subcutaneous tumors and samples from organs were removed from SCID SHO mice and fixed for at least 24h in 4% PBS-buffered formalin. Then tissues were embedded in paraffin and 4 μm thick sections were cut prior to staining with hematoxylin and eosin, TUNEL (Click-iT™ TUNEL Colorimetric IHC Detection Kit, Thermo Fisher #C10625) or cleaved caspase 3 (Cell Signaling #9661). Photomicrographs were taken at X40 and X60 magnification.

Statistics

All data points represent mean ± S.D. All experiments were repeated at least 3 times unless stated otherwise. Representative data is shown. Statistical significance was determined by one-way ANOVA test for multiple comparisons and student's t-test for two groups using Graphpad Prism 6 software. A p-value ≤ 0.05 was considered significant.

ACKNOLEDGMENTS

This work was supported by Department of Defense grants W81XWH-14-1-0073, W81XWH-12-1-0164 and X81XWH-15-1-0193, and by National Institutes of Health grants K08 NS083732, R01 NS095848, R01 NS102366 and Louis V. Gerstner, Jr. Scholars Program (2017-2020). Research reported in this publication was supported by the National Cancer Institute Cancer Center Support Grant P30 CA013696. We thank Dr. Kristy Brown with expert technical assistance with the TEM

acquisition and analysis. We thank Dr. Linda Sasset for the optimization of the protocol for protein extraction from tumors. Research reported in this publication was performed in the CCTI Flow Cytometry Core, supported in part by the Office of the Director, National Institutes of Health under award S10RR027050. The content is solely the responsibility of the authors and does not necessarily represent the official views of the National Institutes of Health.

Author contributions:

Conception and Design: EB, KAR and MDS

Development of methodology: EB, MDS and KAR

Acquisition of data: EB, SJB

Analysis and interpretation of data: EB, MDS and KAR

Administrative, technical and material support: EB, MDS, SLC and KAR

Writing, review and revision of the manuscript: EB, MDS, SLC and KAR

Study supervision: KAR

COMPETING INTEREST

The authors report no conflicts of interest.

Data availability statement: all the data are available upon request.

REFERENCES

1 Kim, A. *et al.* Malignant Peripheral Nerve Sheath Tumors State of the Science: Leveraging Clinical and Biological Insights into Effective Therapies. *Sarcoma* **2017**, 7429697, doi:10.1155/2017/7429697 (2017).

2 Graham, C. D. *et al.* BH3 mimetics suppress CXCL12 expression in human malignant peripheral nerve sheath tumor cells. *Oncotarget* **8**, 8670-8678, doi:10.18632/oncotarget.14398 (2017).

3 Kiuru, M. & Busam, K. J. The NF1 gene in tumor syndromes and melanoma. *Lab Invest* **97**, 146-157, doi:10.1038/labinvest.2016.142 (2017).

4 Brooks, D. G. The neurofibromatoses: hereditary predisposition to multiple peripheral nerve tumors. *Neurosurg Clin N Am* **15**, 145-155, doi:10.1016/j.nec.2004.02.008 (2004).

5 Brossier, N. M. & Carroll, S. L. Genetically engineered mouse models shed new light on the pathogenesis of neurofibromatosis type I-related neoplasms of the peripheral nervous system. *Brain Res Bull* **88**, 58-71, doi:10.1016/j.brainresbull.2011.08.005 (2012).
6 Karpel-Massler, G. *et al.* Inhibition of deubiquitinases primes glioblastoma cells to apoptosis in vitro and in vivo. *Oncotarget* **7**, 12791-12805, doi:10.18632/oncotarget.7302 (2016).
7 Yan, J. *et al.* Usp9x- and Noxa-mediated Mcl-1 downregulation contributes to pemetrexed-induced apoptosis in human non-small-cell lung cancer cells. *Cell Death Dis* **5**, e1316, doi:10.1038/cddis.2014.281 (2014).
8 Engel, K. *et al.* USP9X stabilizes XIAP to regulate mitotic cell death and chemoresistance in aggressive B-cell lymphoma. *EMBO Mol Med* **8**, 851-862, doi:10.15252/emmm.201506047 (2016).
9 Karpel-Massler, G. *et al.* TIC10/ONC201 synergizes with Bcl-2/Bcl-xL inhibition in glioblastoma by suppression of Mcl-1 and its binding partners in vitro and in vivo. *Oncotarget* **6**, 36456-36471, doi:10.18632/oncotarget.5505 (2015).
10 Nair, J. S. & Schwartz, G. K. Inhibition of polo like kinase 1 in sarcomas induces apoptosis that is dependent on Mcl-1 suppression. *Cell Cycle* **14**, 3101-3111, doi:10.1080/15384101.2015.1078033 (2015).
11 Karpel-Massler, G. *et al.* Inhibition of Mitochondrial Matrix Chaperones and Antiapoptotic Bcl-2 Family Proteins Empower Antitumor Therapeutic Responses. *Cancer research* **77**, 3513-3526, doi:10.1158/0008-5472.CAN-16-3424 (2017).
12 Milani, M. *et al.* DRP-1 is required for BH3 mimetic-mediated mitochondrial fragmentation and apoptosis. *Cell Death Dis* **8**, e2552, doi:10.1038/cddis.2016.485 (2017).
13 Wang, W. B. *et al.* Paraptosis accompanied by autophagy and apoptosis was induced by celastrol, a natural compound with influence on proteasome, ER stress and Hsp90. *J Cell Physiol* **227**, 2196-2206, doi:10.1002/jcp.22956 (2012).
14 Zhang, J. S. *et al.* gamma-Tocotrienol induces paraptosis-like cell death in human colon carcinoma SW620 cells. *PLoS One* **8**, e57779, doi:10.1371/journal.pone.0057779 (2013).
15 Peterson, L. F. *et al.* Targeting deubiquitinase activity with a novel small-molecule inhibitor as therapy for B-cell malignancies. *Blood* **125**, 3588-3597, doi:10.1182/blood-2014-10-605584 (2015).
16 Wang, S. *et al.* Ablation of the oncogenic transcription factor ERG by deubiquitinase inhibition in prostate cancer. *Proc Natl Acad Sci U S A* **111**, 4251-4256, doi:10.1073/pnas.1322198111 (2014).
17 Pham, L. V. *et al.* Degrasyn potentiates the antitumor effects of bortezomib in mantle cell lymphoma cells in vitro and in vivo: therapeutic implications. *Mol Cancer Ther* **9**, 2026-2036, doi:10.1158/1535-7163.MCT-10-0238 (2010).
18 Karpel-Massler, G. *et al.* Combined inhibition of Bcl-2/Bcl-xL and Usp9X/Bag3 overcomes apoptotic resistance in glioblastoma in vitro and in vivo. *Oncotarget* **6**, 14507-14521, doi:10.18632/oncotarget.3993 (2015).
19 Murtaza, M., Jolly, L. A., Gecz, J. & Wood, S. A. La FAM fatale: USP9X in development and disease. *Cell Mol Life Sci* **72**, 2075-2089, doi:10.1007/s00018-015-1851-0 (2015).
20 Yang, B. *et al.* Deubiquitinase USP9X deubiquitinates beta-catenin and promotes high grade glioma cell growth. *Oncotarget* **7**, 79515-79525, doi:10.18632/oncotarget.12819 (2016).
21 Cox, J. L. *et al.* Context-dependent function of the deubiquitinating enzyme USP9X in pancreatic ductal adenocarcinoma. *Cancer Biol Ther* **15**, 1042-1052, doi:10.4161/cbt.29182 (2014).
22 Perez-Mancera, P. A. *et al.* The deubiquitinase USP9X suppresses pancreatic ductal adenocarcinoma. *Nature* **486**, 266-270, doi:10.1038/nature11114 (2012).
23 Kapuria, V. *et al.* Deubiquitinase inhibition by small-molecule WP1130 triggers aggresome formation and tumor cell apoptosis. *Cancer research* **70**, 9265-9276, doi:10.1158/0008-5472.CAN-10-1530 (2010).

24 Oslowski, C. M. & Urano, F. Measuring ER stress and the unfolded protein response using mammalian tissue culture system. *Methods Enzymol* **490**, 71-92, doi:10.1016/B978-0-12-385114-7.00004-0 (2011).
25 Ishida, C. T. *et al.* BH3-mimetics and BET-inhibitors elicit enhanced lethality in malignant glioma. *Oncotarget* **8**, 29558-29573, doi:10.18632/oncotarget.16365 (2017).
26 Singleton, D. C. & Harris, A. L. Targeting the ATF4 pathway in cancer therapy. *Expert Opin Ther Targets* **16**, 1189-1202, doi:10.1517/14728222.2012.728207 (2012).
27 Schwickart, M. *et al.* Deubiquitinase USP9X stabilizes MCL1 and promotes tumour cell survival. *Nature* **463**, 103-107, doi:10.1038/nature08646 (2010).
28 Trivigno, D., Essmann, F., Huber, S. M. & Rudner, J. Deubiquitinase USP9x confers radioresistance through stabilization of Mcl-1. *Neoplasia* **14**, 893-904 (2012).
29 Leverson, J. D. *et al.* Potent and selective small-molecule MCL-1 inhibitors demonstrate on-target cancer cell killing activity as single agents and in combination with ABT-263 (navitoclax). *Cell Death Dis* **6**, e1590, doi:10.1038/cddis.2014.561 (2015).
30 Peddaboina, C. *et al.* The downregulation of Mcl-1 via USP9X inhibition sensitizes solid tumors to Bcl-xl inhibition. *BMC Cancer* **12**, 541, doi:10.1186/1471-2407-12-541 (2012).
31 Ryan, J. J. *et al.* Role for the stem cell factor/KIT complex in Schwann cell neoplasia and mast cell proliferation associated with neurofibromatosis. *J Neurosci Res* **37**, 415-432, doi:10.1002/jnr.490370314 (1994).
32 Stonecypher, M. S., Byer, S. J., Grizzle, W. E. & Carroll, S. L. Activation of the neuregulin-1/ErbB signaling pathway promotes the proliferation of neoplastic Schwann cells in human malignant peripheral nerve sheath tumors. *Oncogene* **24**, 5589-5605, doi:10.1038/sj.onc.1208730 (2005).
33 Siegelin, M. D. *et al.* Exploiting the mitochondrial unfolded protein response for cancer therapy in mice and human cells. *J Clin Invest* **121**, 1349-1360, doi:10.1172/JCI44855 (2011).
34 Geng, Y., Kohli, L., Klocke, B. J. & Roth, K. A. Chloroquine-induced autophagic vacuole accumulation and cell death in glioma cells is p53 independent. *Neuro Oncol* **12**, 473-481, doi:10.1093/neuonc/nop048 (2010).
35 Pareja, F. *et al.* PI3K and Bcl-2 inhibition primes glioblastoma cells to apoptosis through downregulation of Mcl-1 and Phospho-BAD. *Mol Cancer Res* **12**, 987-1001, doi:10.1158/1541-7786.MCR-13-0650 (2014).

Fig. 1: Usp9X inhibition causes massive reduction in cellular viability in MPNST cell lines. (a-c) ST88-14 (a), T265-2c (b), 90-8 cells (c) were treated with increasing concentrations of WP1130 for 72h. Cellular viability was determined by CellTiter-Glo assay and the IC_{50}-values were calculated based on a non-linear regression analysis. Data are presented as mean and SD, n=3. **(d-f)** Usp9X was silenced in ST88-14 (d), T265-2c (e), 90-8 cells (f) with non-targeting (NT) RNA or siUsp9X for 24, 48 and 72h. Cellular viability was determined by CellTiter-Glo assay and relative cell viability was calculated. Data are presented as mean and SD, n=3. * = 0.0129 *** ≤ 0.001. **(g-j)** Usp9X knock down was performed in ST88-14, T265-2c and 90-8 cells. Whole-cell extracts were examined by Western blot for Usp9X. ß-actin Western blot analysis was performed to confirm equal protein loading. Bar graphs show protein quantification analyzed through ImageJ. Data are presented as mean and SD, n=3.

Fig. 2: Usp9X inhibition induces cell death with features of apoptosis and loss of membrane potential in MPNST cell lines. (a-d) ST88-14 (a, c) and T265-2c cells (b, d) were treated with WP1130 at the concentration of 2.5 µM, or transfected either with non-targeting (NT)-siRNA or Usp9X-siRNA. **(a, b)** Staining for annexin V/Propidium Iodide was performed prior to flow cytometric analysis. Representative flow plots are shown. N=3. **(c,d)** Cells were stained with Mitochondrial Membrane Potential Assay Kit (TMRE), then flow cytometric analysis was performed. N=3. **(e-f)** ST88-14 cells were treated with WP1130 at the concentration of 2.5µM (e) or transfected either with non-targeting (n.t.)-siRNA or Usp9X-siRNA (f), then caspase 3-like enzymatic activity was measured at different time points. Column: mean. Error bar: SD, n=3. * = 0.0209 ** = 0.0026 *** ≤ 0.001. **(g)** T265-2c cells were treated with WP1130 at the concentration of 2.5µM prior to caspase 3-like activity measurement at different time points.

Fig. 3: Mcl-1 knock-down causes massive reduction in cellular viability, cell death with features of apoptosis and loss of membrane potential in MPNST cell lines. (a, d, e) ST88-14 (a) 90-8 (d), T265-2c (e) cells were transfected either with non-targeting (NT)-siRNA or Mcl-1-siRNA for 24, 48 and 72h. Cellular viability was determined by CellTiter-Glo assay and relative cell viability was calculated. Data are presented as mean and SD, n=3. *(a) = 0.0161, *(d) = 0.0015, *(e) = 0.0168, *** ≤ 0.001 **(b, f)** Staining for annexin V/Propidium Iodide was performed prior to flow cytometric analysis. Representative flow plots are shown. N=3. **(c, g)** Staining for

Mitochondrial Membrane Potential Assay Kit (TMRE) was performed prior to flow cytometric analysis. Representative flow plots are shown. N=3. **(h, i)** Knock down of Mcl-1 was confirmed in ST88-14 cells (h) and T265-2c cells (i) by Western blot analysis. ß-actin was used to ensure equal loading.

Fig. 4: Caspase-dependent apoptosis is not the exclusive MPNST cell death pathway activated after Usp9X and Mcl-1 knock down *in vitro*. (a, b) ST88-14 (a) and T265-2c (b) cells were transfected with non-targeting (NT)-siRNA with or without z-VAD as controls, or Usp9X-siRNA, or Mcl-1-siRNA for 72h. Cellular viability was determined by CellTiter-Glo assay and relative cell viability was calculated. Data are presented as mean and SD, n=3. **(c)** Caspase-3 like activity was measured at 24 h after treatments in ST88-14 cell line. Data are presented as mean and SD, n=3.

Fig. 5: Usp9X inhibition causes Noxa increase and ER stress in MPNST cell lines. Ultrastructural analysis shows features of paraptosis. (a, b) ST88-14 cells were transfected for 24 h with either non-targeting (NT)-siRNA or Usp9X-siRNA (a) or treated with WP1130 at the concentration of 1.25 and 2.5 μM (b). Whole cell extracts were collected prior to Western blot analysis for ATF3, Noxa and ß-actin. Numbers shows protein quantification analyzed through ImageJ. N=3. **(c-e)** Ultrastructural appearance of untreated control cells using TEM. **(f-h)** After treatment with WP1130 at the concentration of 2.5 μM (f, g, h) T265-2c cells showed extensive cytosolic vacuolization (f, red arrows) and swelling of ER (g, red arrowheads) and mitochondria (h, red arrows).

Fig. 6: Treatment with WP1130 reduces tumor size in a mouse MPNST model generated by subcutaneous injection of ST88-14 cell line. (a) Tumor growth curves showing the increase in tumor size for each treatment group. Data are presented as mean and SEM. Asterisks shown only for 25 mg/Kg dose, compared to control group. Asterisks values, from left to right: 0.0413, 0.0321, 0.0409, 0.0479 and 0.0162. **(b)** Quantification of the tumors volume among different treatment groups 35 days after tumor implantation. * = 0.0202, *[1] = 0.0198. **(c)** Quantification of

the tumors weight among different treatment groups 35 days after tumor implantation. * = 0.0458. **(d)** Representative photographs of the tumors. **(e, f)** Representative photomicrographs showing the histological morphology (H & E staining) of tumors from mice receiving either vehicle or WP1130 at the concentration of 12.5 mg/kg. Arrows indicate mitotic figures. Scale bar, 50 µm. **(g)** Whole tissue extracts from vehicle and 25 mg/kg WP1130 treated mice were collected prior to Western blot analysis for Mcl-1 and ß-actin served as loading control. Numbers shows protein quantification analyzed through ImageJ. N=3.

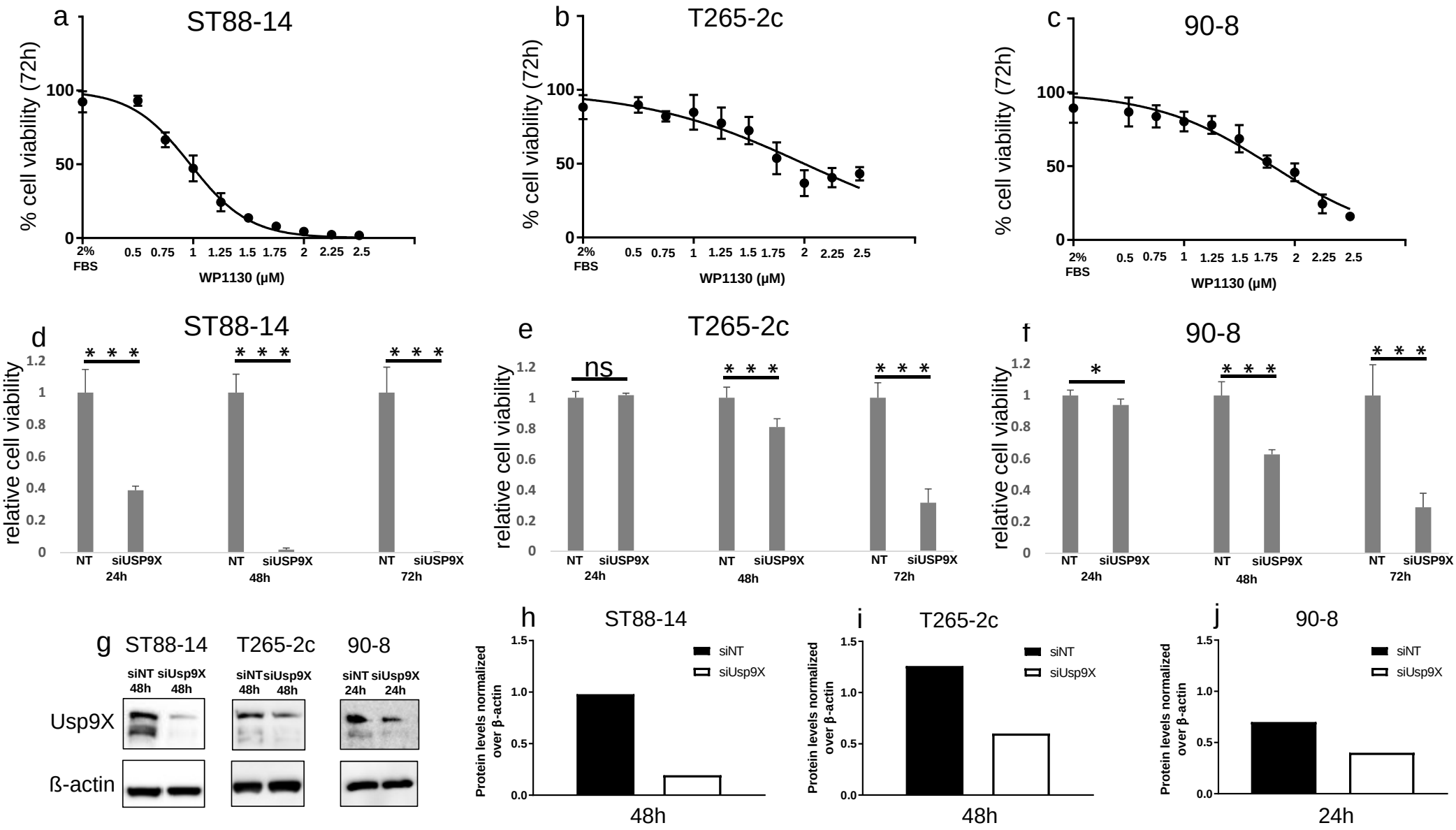
a
ST88-14
% cell viability (72h)
100
50
0
2% FBS
0.5 0.75 1 1.25 1.5 1.75 2 2.25 2.5
WP1130 (μM)
b
T265-2c
% cell viability (72h)
100
50
0
2% FBS
0.5 0.75 1 1.25 1.5 1.75 2 2.25 2.5
WP1130 (μM)
c
90-8
% cell viability (72h)
100
50
0
2% FBS
0.5 0.75 1 1.25 1.5 1.75 2 2.25 2.5
WP1130 (μM)
d
ST88-14
relative cell viability
1.2
1
0.8
0.6
0.4
0.2
0
* * *
* * *
* * *
NT siUSP9X
24h
NT siUSP9X
48h
NT siUSP9X
72h
e
T265-2c
relative cell viability
1.2
1
0.8
0.6
0.4
0.2
0
ns
* * *
* * *
NT siUSP9X
24h
NT siUSP9X
48h
NT siUSP9X
72h
f
90-8
relative cell viability
1.2
1
0.8
0.6
0.4
0.2
0
*
* * *
* * *
NT siUSP9X
24h
NT siUSP9X
48h
NT siUSP9X
72h
g
ST88-14
T265-2c
90-8
siNT siUsp9X
48h 48h
siNT siUsp9X
48h 48h
siNT siUsp9X
24h 24h
Usp9X
ß-actin
h
ST88-14
Protein levels normalized over β-actin
1.5
1.0
0.5
0.0
siNT
siUsp9X
48h
i
T265-2c
Protein levels normalized over β-actin
1.5
1.0
0.5
0.0
siNT
siUsp9X
48h
j
90-8
Protein levels normalized over β-actin
1.5
1.0
0.5
0.0
siNT
siUsp9X
24h

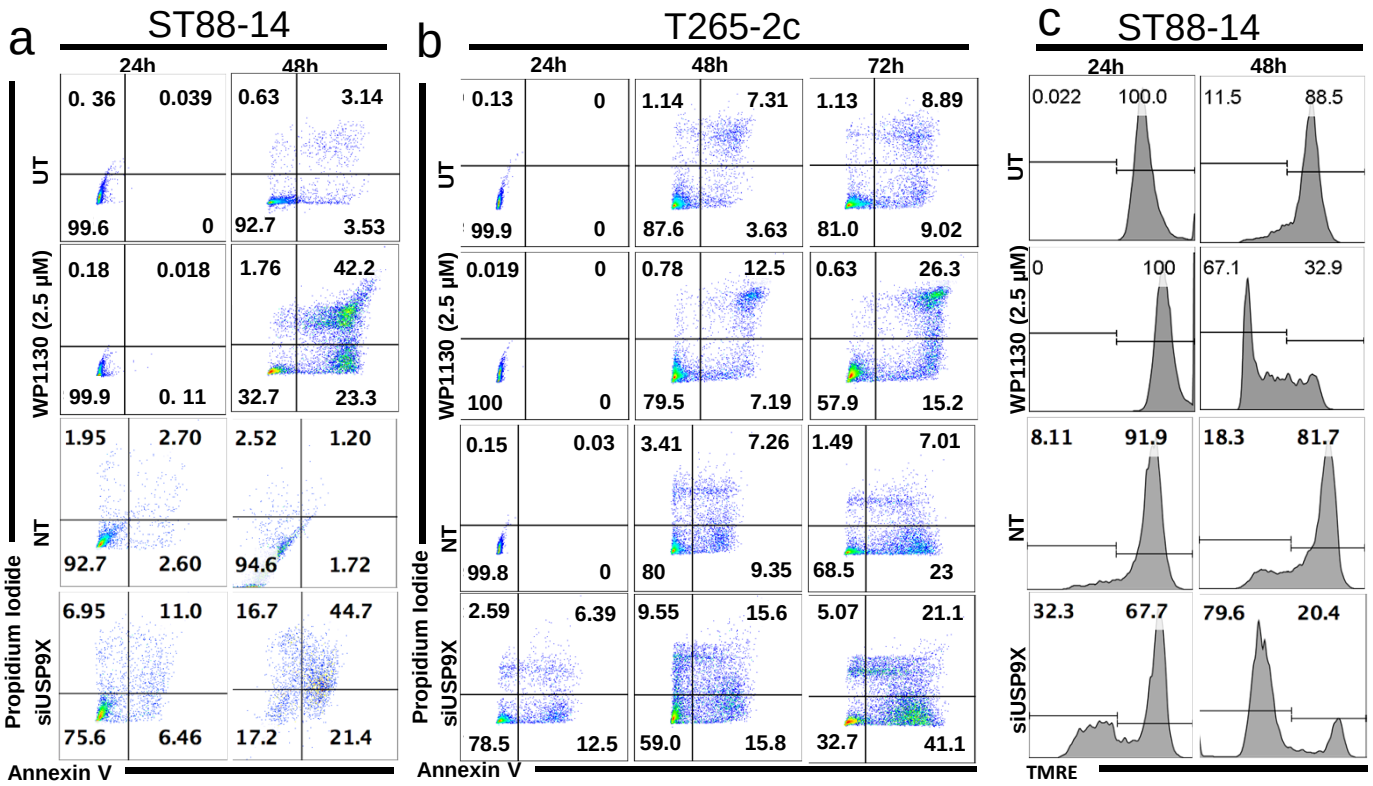
a
ST88-14
24h
48h
UT
WP1130 (2.5 µM)
NT
siUSP9X
Propidium Iodide
Annexin V
0. 36
0.039
99.6
0
0.63
3.14
92.7
3.53
0.18
0.018
99.9
0. 11
1.76
42.2
32.7
23.3
1.95
2.70
92.7
2.60
2.52
1.20
94.6
1.72
6.95
11.0
75.6
6.46
16.7
44.7
17.2
21.4
b
T265-2c
24h
48h
72h
0.13
0
99.9
0
1.14
7.31
87.6
3.63
1.13
8.89
81.0
9.02
0.019
0
100
0
0.78
12.5
79.5
7.19
0.63
26.3
57.9
15.2
0.15
0.03
99.8
0
3.41
7.26
80
9.35
1.49
7.01
68.5
23
2.59
6.39
78.5
12.5
9.55
15.6
59.0
15.8
5.07
21.1
32.7
41.1
c
ST88-14
24h
48h
0.022
100.0
11.5
88.5
0
100
67.1
32.9
8.11
91.9
18.3
81.7
32.3
67.7
79.6
20.4
TMRE

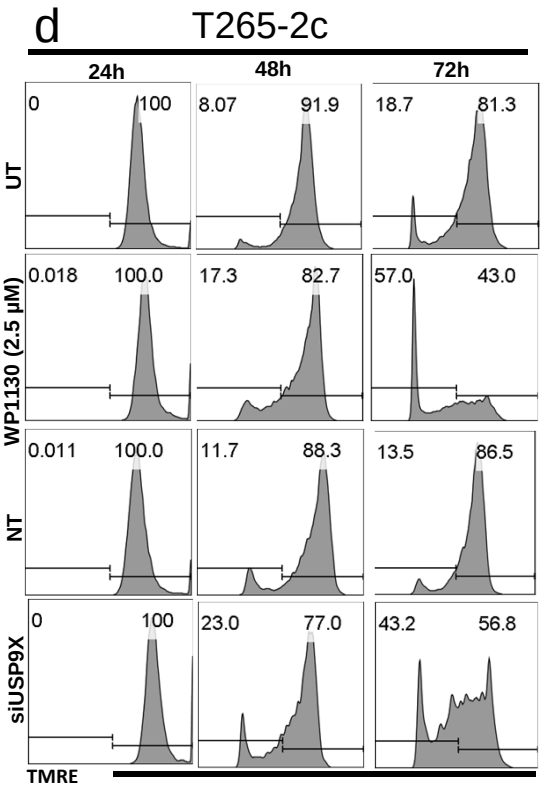
d
T265-2c
24h
48h
72h
UT
WP1130 (2.5 µM)
NT
siUSP9X
TMRE
0
100
8.07
91.9
18.7
81.3
0.018
100.0
17.3
82.7
57.0
43.0
0.011
100.0
11.7
88.3
13.5
86.5
0
100
23.0
77.0
43.2
56.8

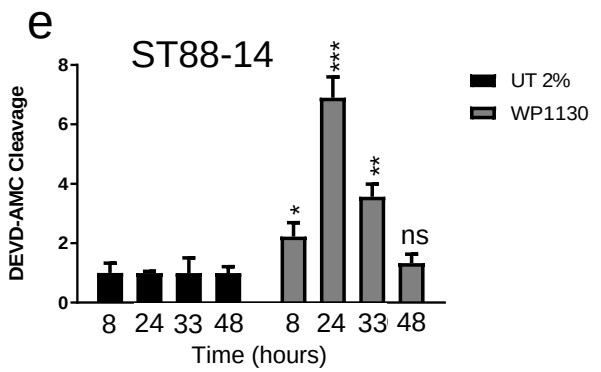
e
ST88-14
DEVD-AMC Cleavage
Time (hours)
UT 2%
WP1130
8 24 33 48 8 24 33 48
*
***
**
ns

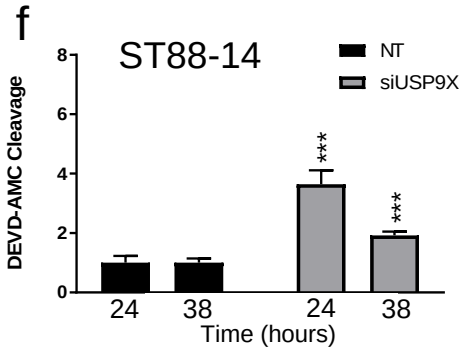
f
ST88-14
DEVD-AMC Cleavage
Time (hours)
NT
siUSP9X
24 38 24 38
***
***

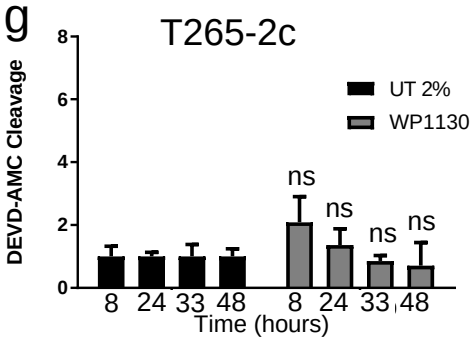
g
T265-2c
DEVD-AMC Cleavage
Time (hours)
UT 2%
WP1130
8 24 33 48 8 24 33 48
ns
ns
ns
ns

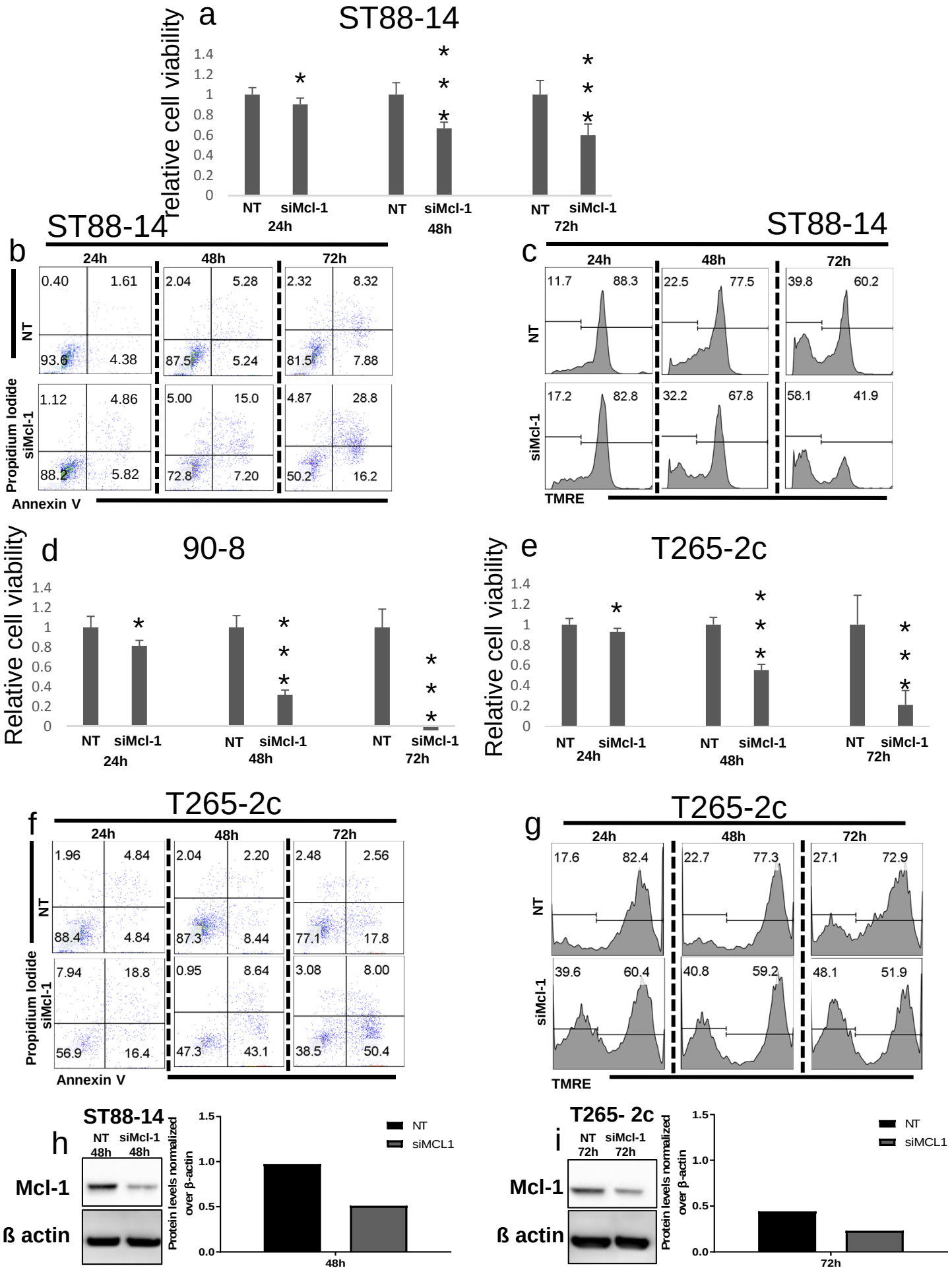
a
ST88-14
relative cell viability
1.4
1.2
1
0.8
0.6
0.4
0.2
0
NT
siMcl-1
24h
48h
72h
b
ST88-14
24h
48h
72h
0.40
1.61
93.6
4.38
2.04
5.28
87.5
5.24
2.32
8.32
81.5
7.88
1.12
4.86
88.2
5.82
5.00
15.0
72.8
7.20
4.87
28.8
50.2
16.2
Propidium Iodide
Annexin V
c
ST88-14
11.7
88.3
22.5
77.5
39.8
60.2
17.2
82.8
32.2
67.8
58.1
41.9
TMRE
d
90-8
Relative cell viability
e
T265-2c
f
T265-2c
1.96
4.84
88.4
4.84
2.04
2.20
87.3
8.44
2.48
2.56
77.1
17.8
7.94
18.8
56.9
16.4
0.95
8.64
47.3
43.1
3.08
8.00
38.5
50.4
g
T265-2c
17.6
82.4
22.7
77.3
27.1
72.9
39.6
60.4
40.8
59.2
48.1
51.9
h
ST88-14
Mcl-1
ß actin
Protein levels normalized over β-actin
siMCL1
i
T265- 2c

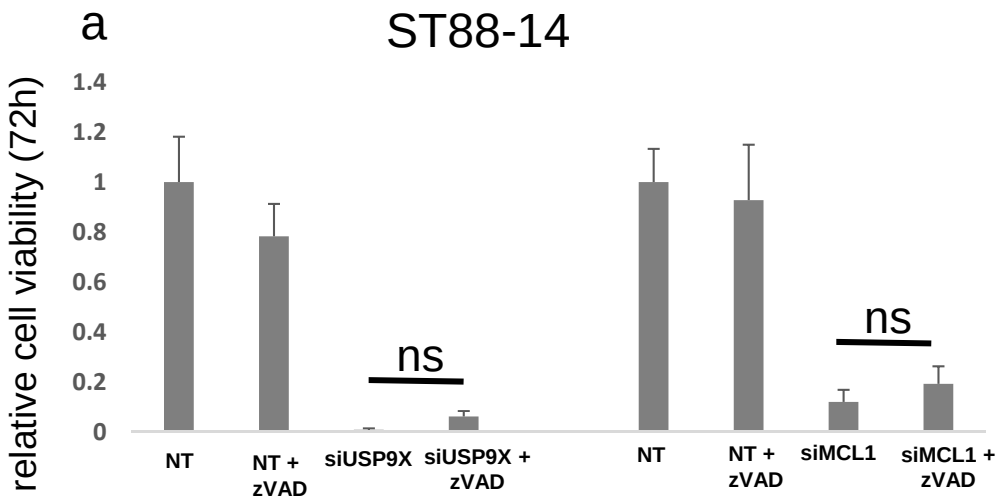
a
ST88-14
relative cell viability (72h)
1.4
1.2
1
0.8
0.6
0.4
0.2
0
ns
ns
NT
NT + zVAD
siUSP9X
siUSP9X + zVAD
NT
NT + zVAD
siMCL1
siMCL1 + zVAD

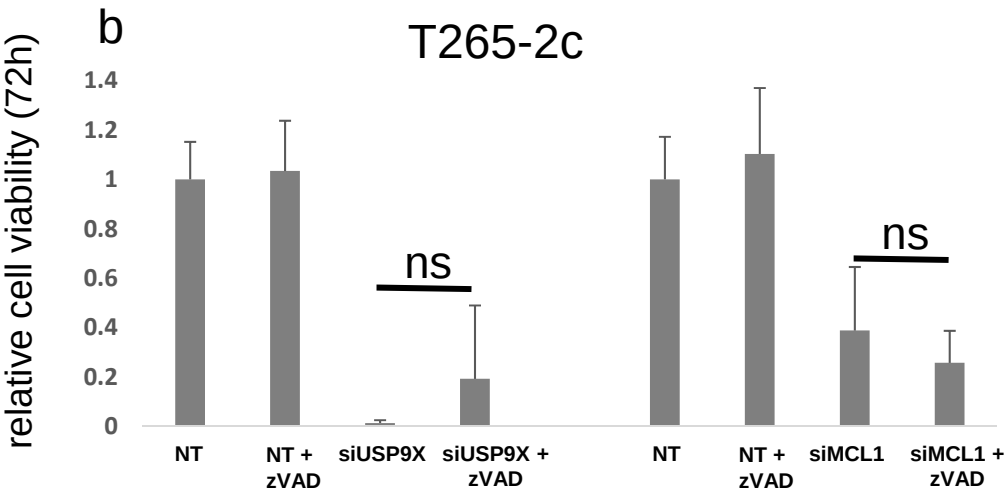
b
T265-2c
relative cell viability (72h)
1.4
1.2
1
0.8
0.6
0.4
0.2
0
ns
ns
NT
NT + zVAD
siUSP9X
siUSP9X + zVAD
NT
NT + zVAD
siMCL1
siMCL1 + zVAD

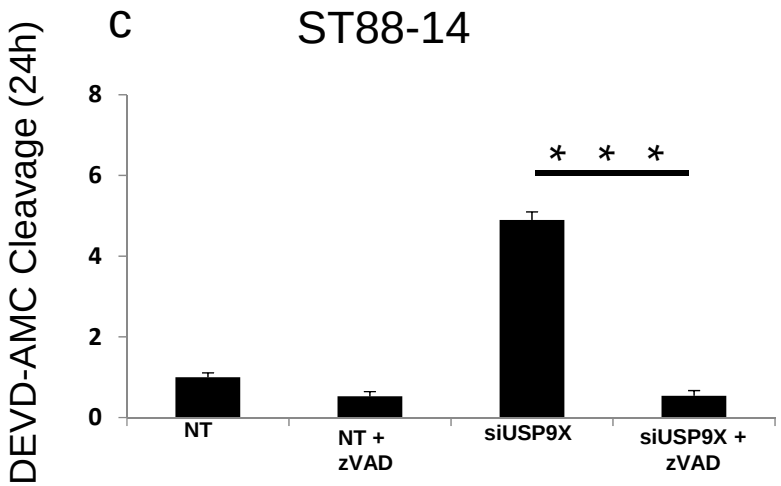
c
ST88-14
DEVD-AMC Cleavage (24h)
8
6
4
2
0
* * *
NT
NT + zVAD
siUSP9X
siUSP9X + zVAD

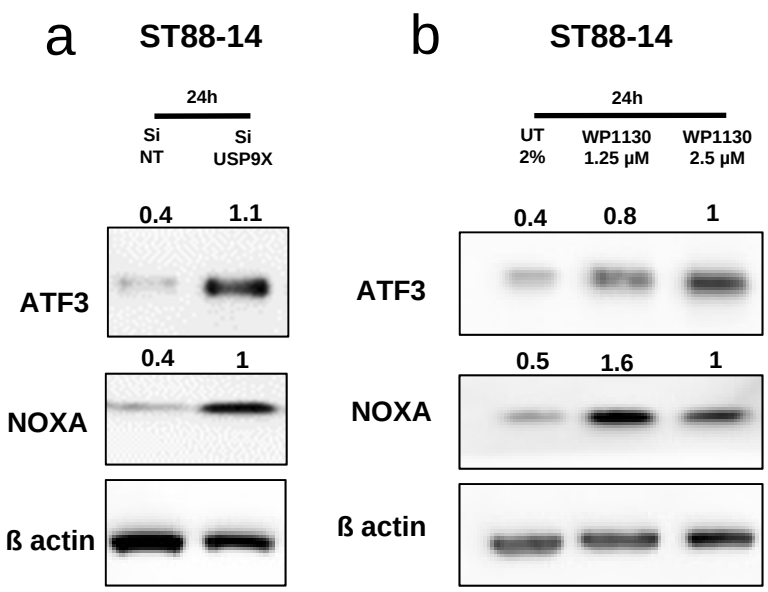
a
ST88-14
24h
Si NT
Si USP9X
0.4
1.1
ATF3
0.4
1
NOXA
ß actin
b
ST88-14
24h
UT 2%
WP1130 1.25 µM
WP1130 2.5 µM
0.4
0.8
1
ATF3
0.5
1.6
1
NOXA
ß actin

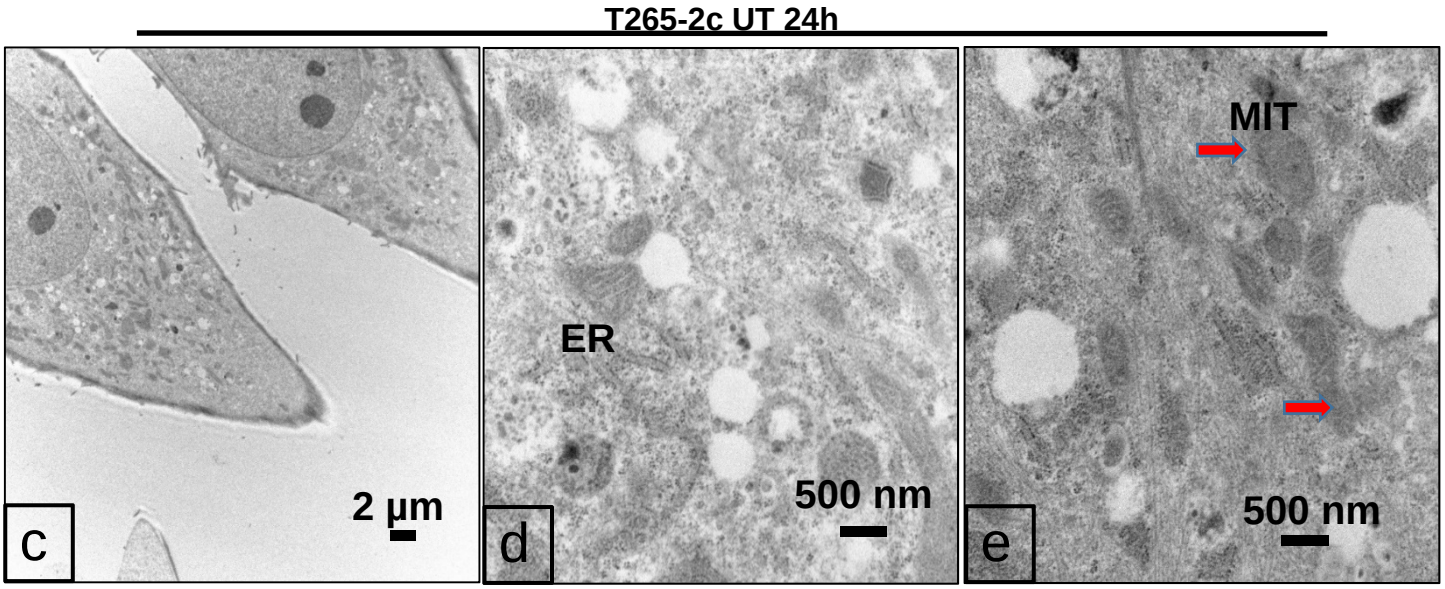
T265-2c UT 24h
2 µm
c
ER
500 nm
d
MIT
500 nm
e

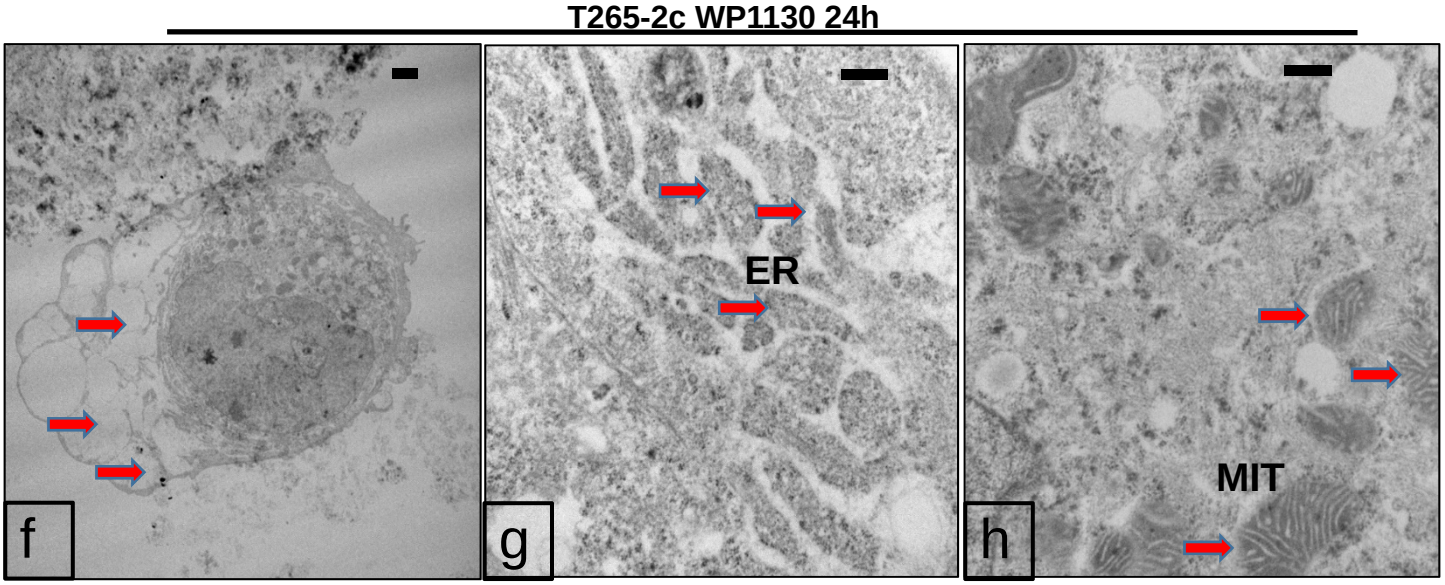
T265-2c WP1130 24h
f
ER
g
MIT
h

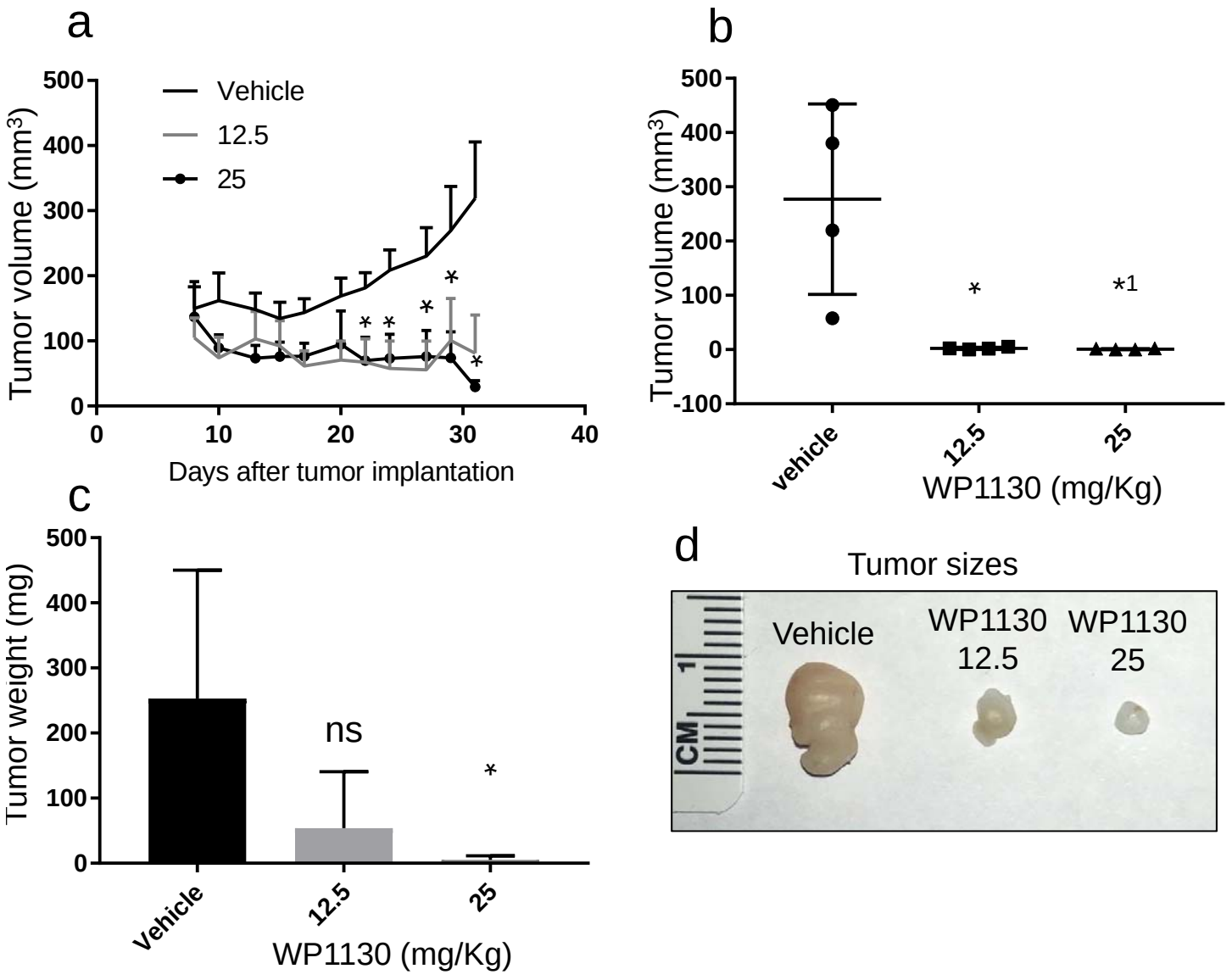
a
Vehicle
12.5
25
Tumor volume (mm3)
Days after tumor implantation
b
Tumor volume (mm3)
vehicle
12.5
25
WP1130 (mg/Kg)
*1
c
Tumor weight (mg)
ns
Vehicle
12.5
25
WP1130 (mg/Kg)
d
Tumor sizes
Vehicle
WP1130 12.5
WP1130 25
CM

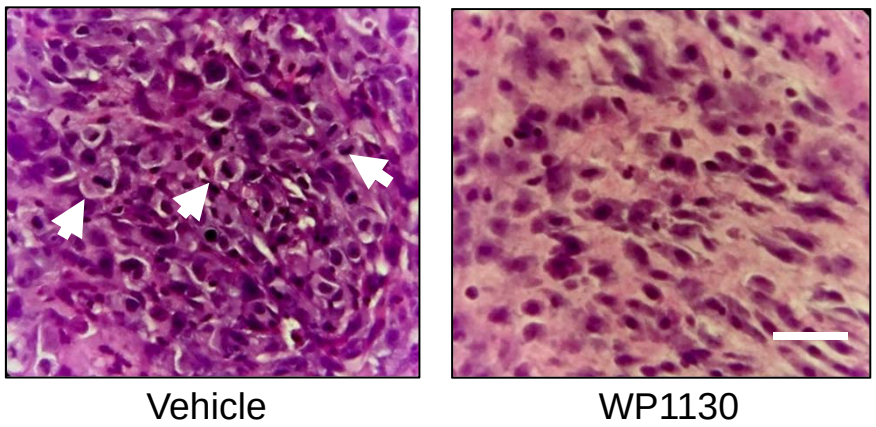
e
f
Vehicle
WP1130

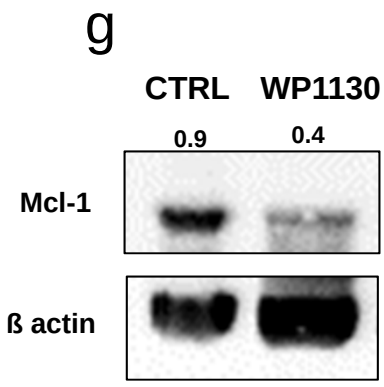
g
CTRL
WP1130
0.9
0.4
Mcl-1
ß actin

Usp9X Regulates Cell Death in Malignant Peripheral Nerve Sheath Tumors.

Bianchetti E, Bates SJ, Carroll SL, Siegelin MD, Roth KA

Fig. 1 g

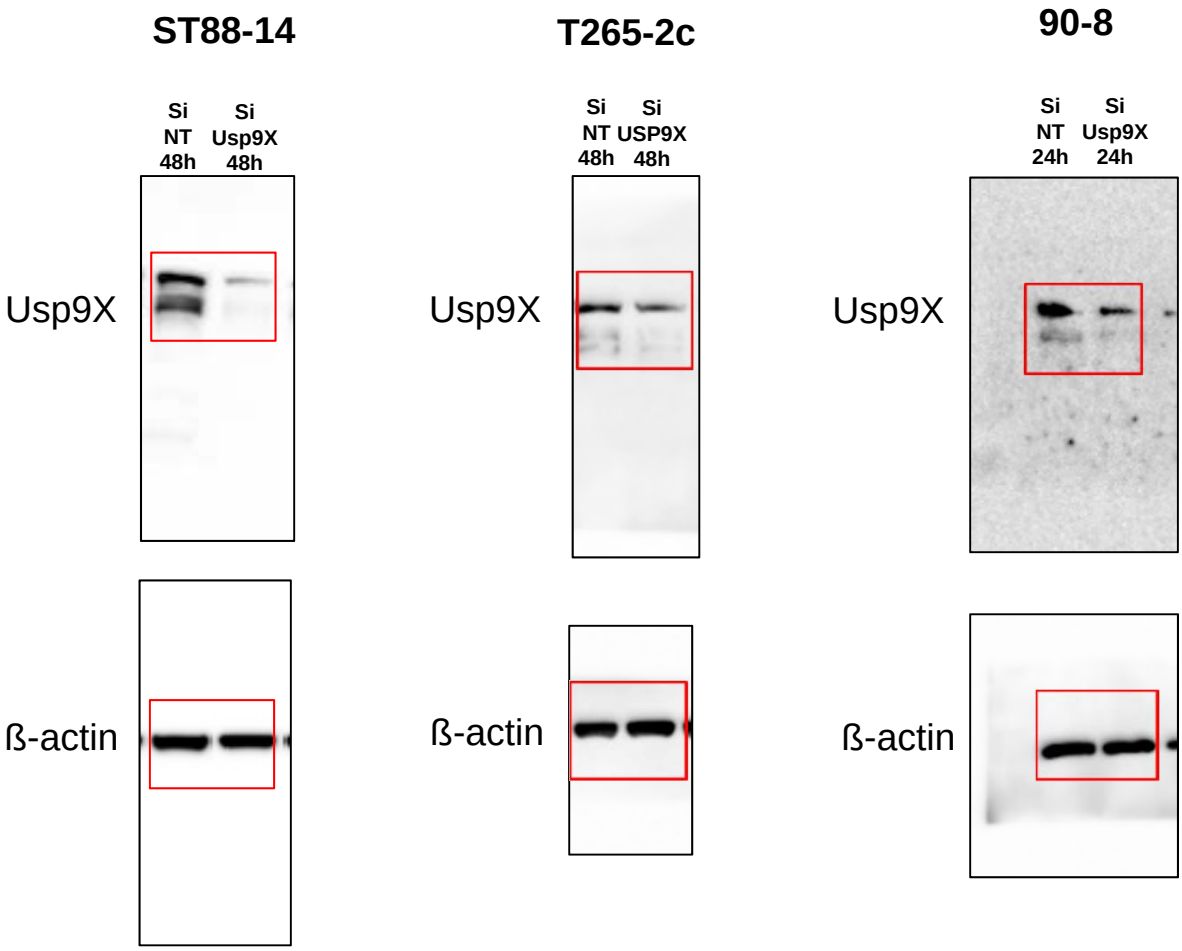
ST88-14
T265-2c
90-8
Si NT 48h
Si Usp9X 48h
Si NT 48h
Si USP9X 48h
Si NT 24h
Si Usp9X 24h
Usp9X
Usp9X
Usp9X
ß-actin
ß-actin
ß-actin

Fig. 3 h

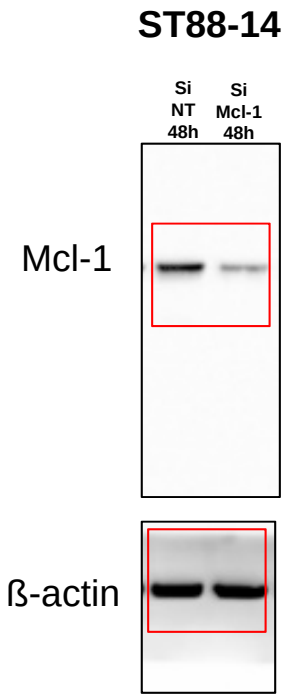
ST88-14
Si NT 48h
Si Mcl-1 48h
Mcl-1
ß-actin

Fig. 3 i

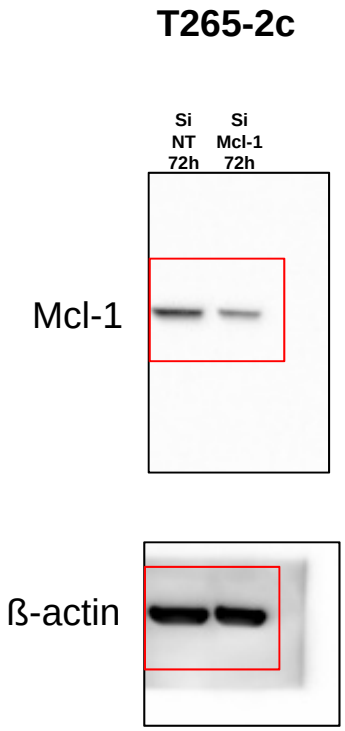
T265-2c
Si NT 72h
Si Mcl-1 72h
Mcl-1
ß-actin

Fig. 5 a

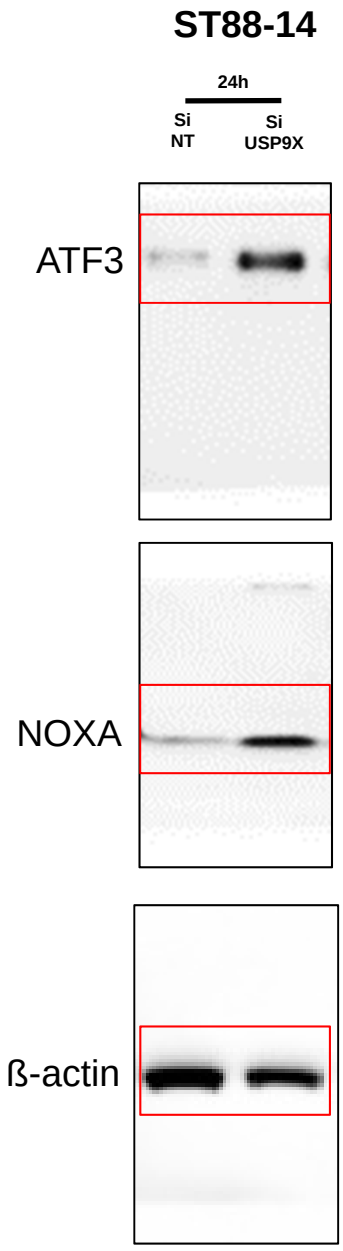
ST88-14
24h
Si NT
Si USP9X
ATF3
NOXA
ß-actin

Fig. 5 b

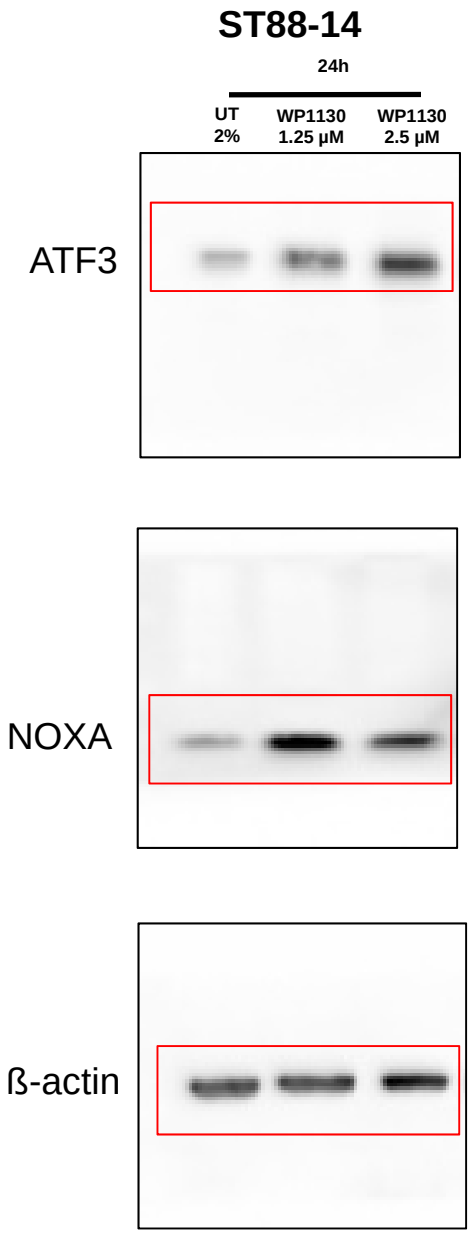
ST88-14
24h
UT 2%
WP1130 1.25 µM
WP1130 2.5 µM
ATF3
NOXA
ß-actin

Fig. 6 g

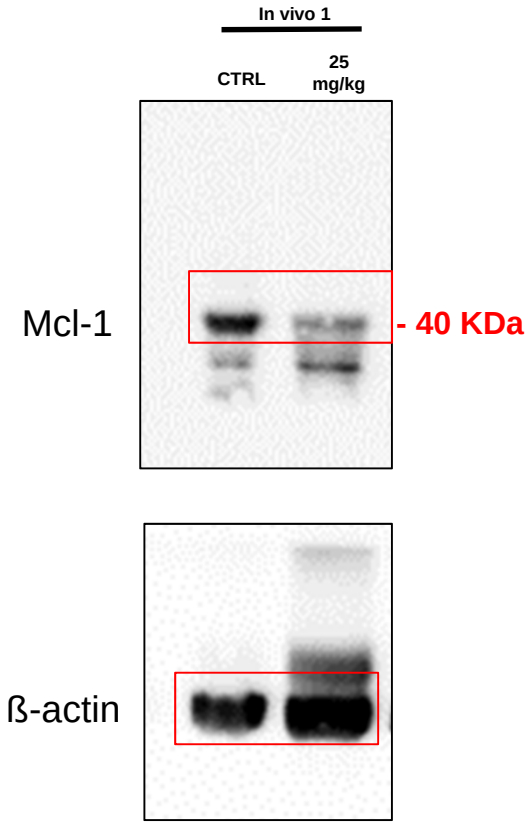

Suppl. Fig. 1 a

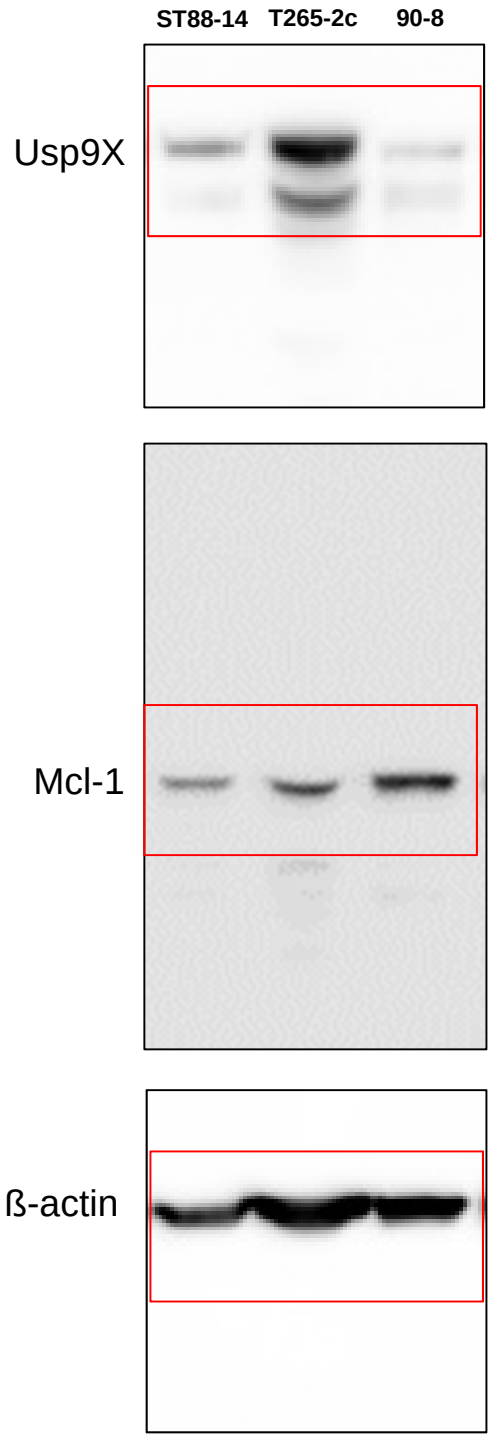

Suppl. Fig. 1 d

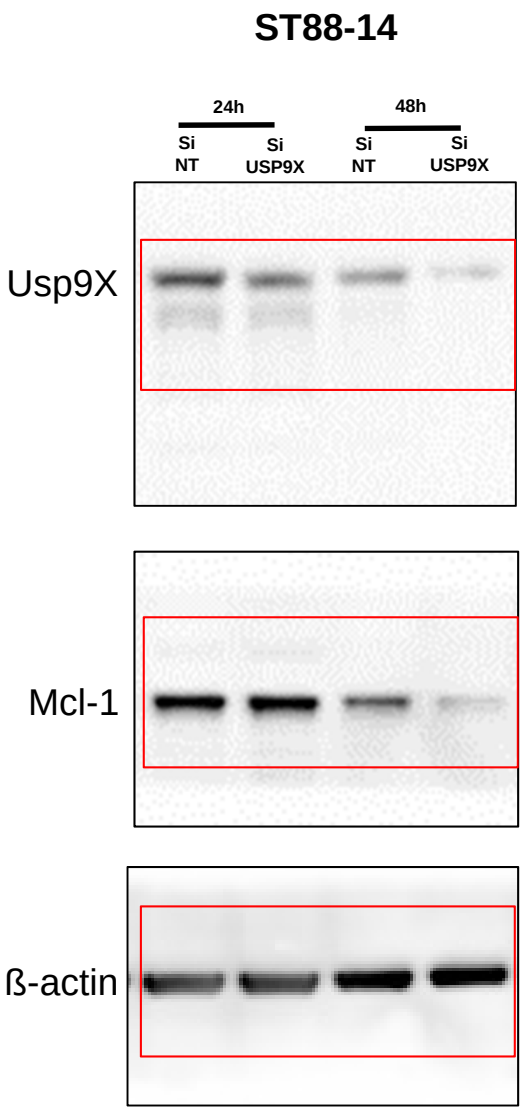

Suppl. Fig. 1 e

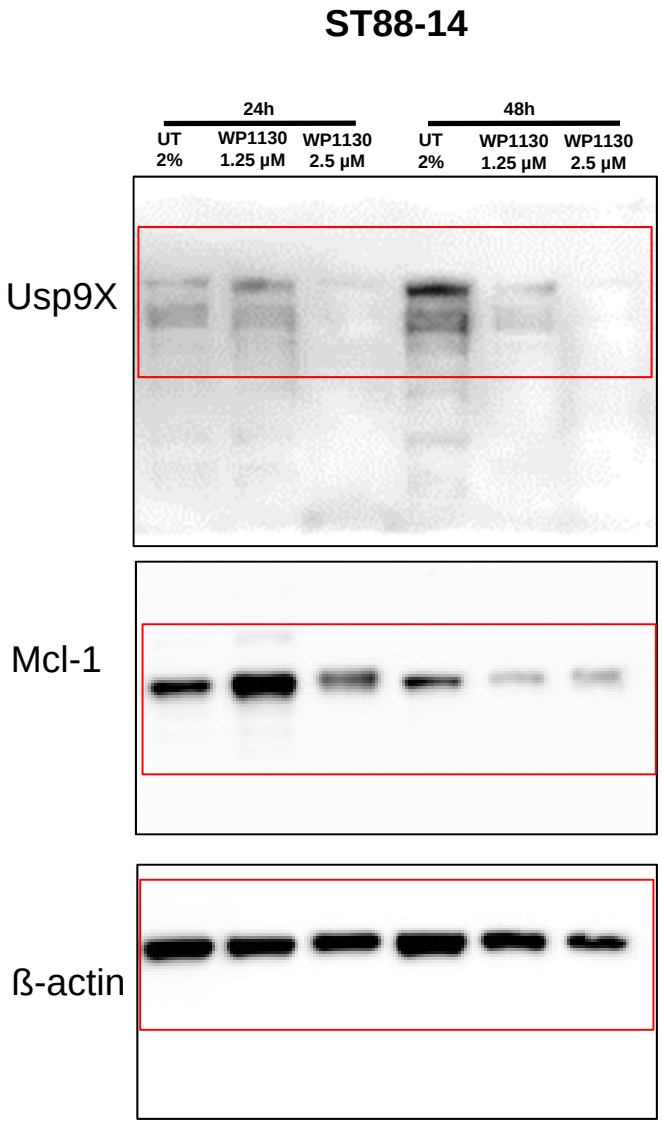

Usp9X Regulates Cell Death in Malignant Peripheral Nerve Sheath Tumors.

Bianchetti E, Bates SJ, Carroll SL, Siegelin MD, Roth KA

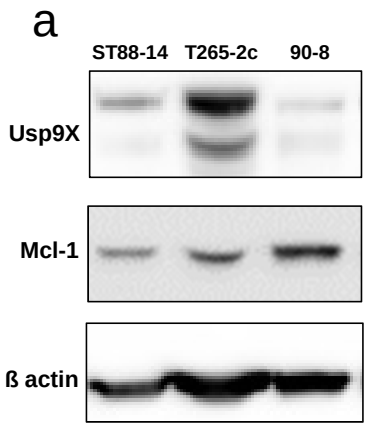
a
ST88-14
T265-2c
90-8
Usp9X
Mcl-1
ß actin

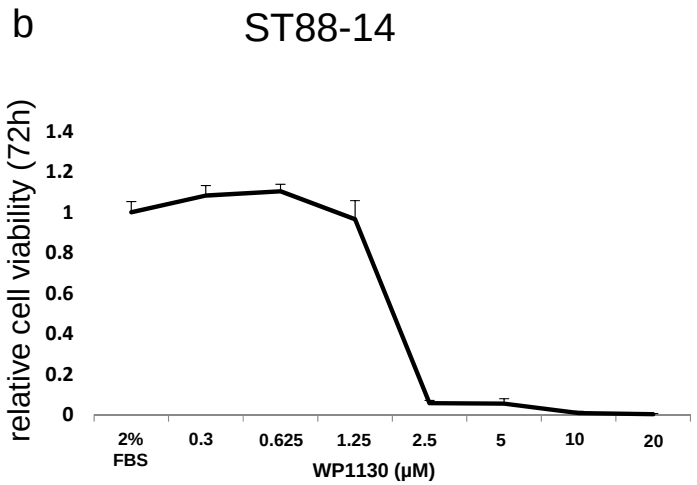
b
ST88-14
relative cell viability (72h)
1.4
1.2
1
0.8
0.6
0.4
0.2
0
2% FBS
0.3
0.625
1.25
2.5
5
10
20
WP1130 (µM)

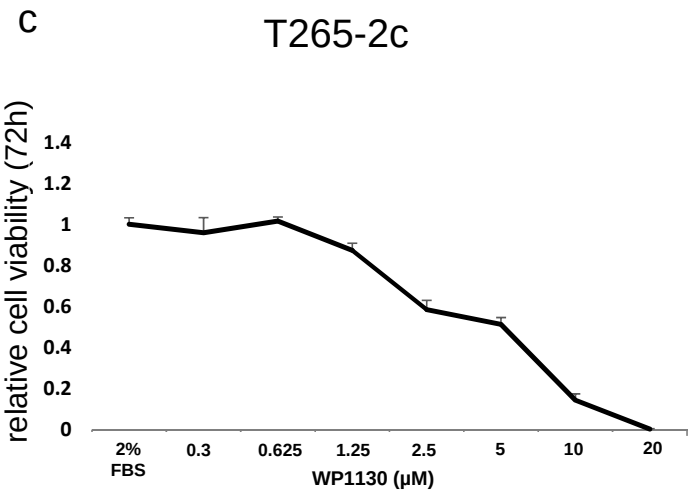
c
T265-2c
relative cell viability (72h)
1.4
1.2
1
0.8
0.6
0.4
0.2
0
2% FBS
0.3
0.625
1.25
2.5
5
10
20
WP1130 (µM)

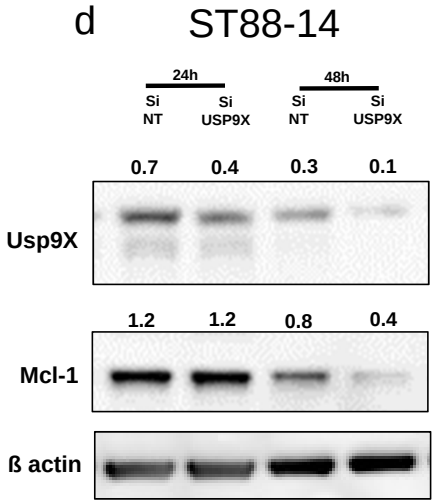
d
ST88-14
24h
48h
Si NT
Si USP9X
Si NT
Si USP9X
0.7
0.4
0.3
0.1
Usp9X
1.2
1.2
0.8
0.4
Mcl-1
ß actin

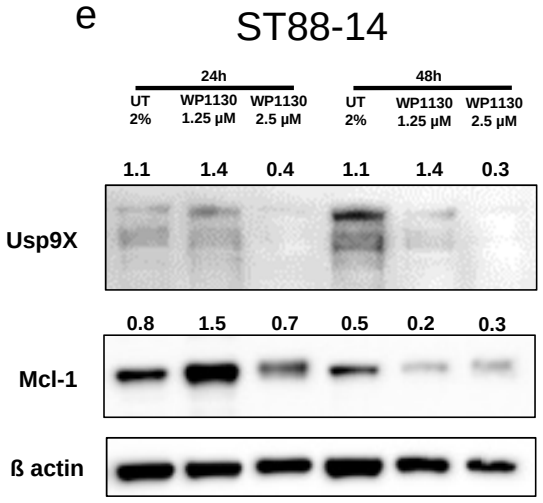
e
ST88-14
24h
48h
UT 2%
WP1130 1.25 µM
WP1130 2.5 µM
UT 2%
WP1130 1.25 µM
WP1130 2.5 µM
1.1
1.4
0.4
1.1
1.4
0.3
Usp9X
0.8
1.5
0.7
0.5
0.2
0.3
Mcl-1
ß actin

Supplementary Fig. 1: Usp9X expression and pharmacological inhibition in human NF1 patient-derived MPNST cell lines. Usp9X inhibition causes Mcl-1 depletion in MPNST cell lines. (a) A panel of human MPNST cell lines was analyzed for the expression of Usp9X and Mcl-1 by Western blotting. **(b, c)** ST88-14 (b), T265-2c (c) cells were treated with increasing concentrations of WP1130 for 72h. Cellular viability was determined by CellTiter-Glo® assay and the relative cell viability values were calculated normalizing data to untreated samples. Data are presented as mean and SD, n=1. **(d, e)** ST88-14 cells were transfected for 24 h and 48 h with either non-targeting (NT)-siRNA or Usp9X-siRNA (d) or treated with WP1130 at the concentration of 1.25 and 2.5 µM for 24 h and 48 h (e). Whole cell extracts were collected prior to Western blot analysis for Usp9X, Mcl-1 and ß-actin (loading control). Numbers shows protein quantification analyzed through ImageJ. N=3.

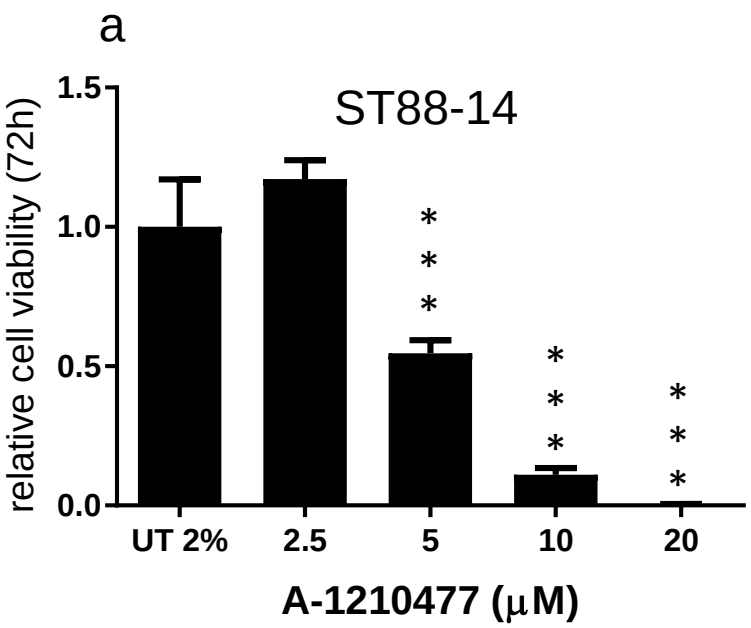
a
ST88-14
relative cell viability (72h)
1.5
1.0
0.5
0.0
UT 2%
2.5
5
10
20
A-1210477 (μM)

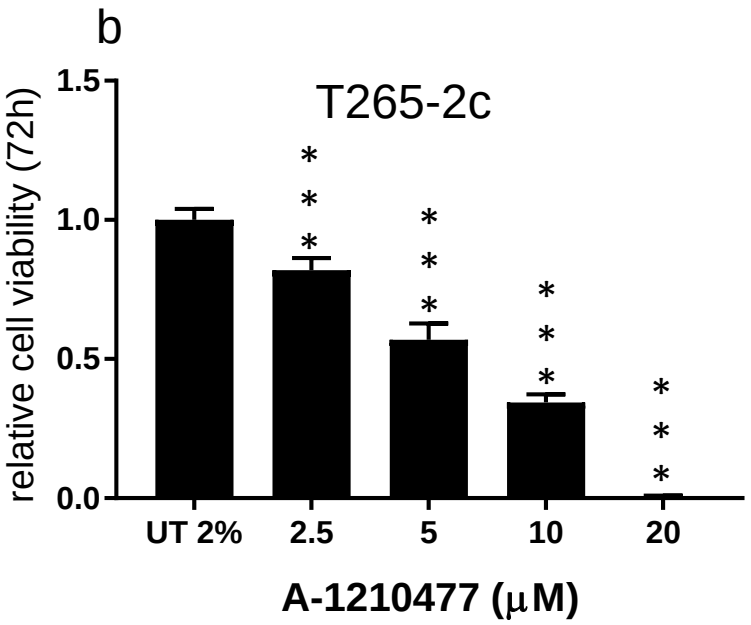
b
T265-2c
relative cell viability (72h)
1.5
1.0
0.5
0.0
UT 2%
2.5
5
10
20
A-1210477 (μM)

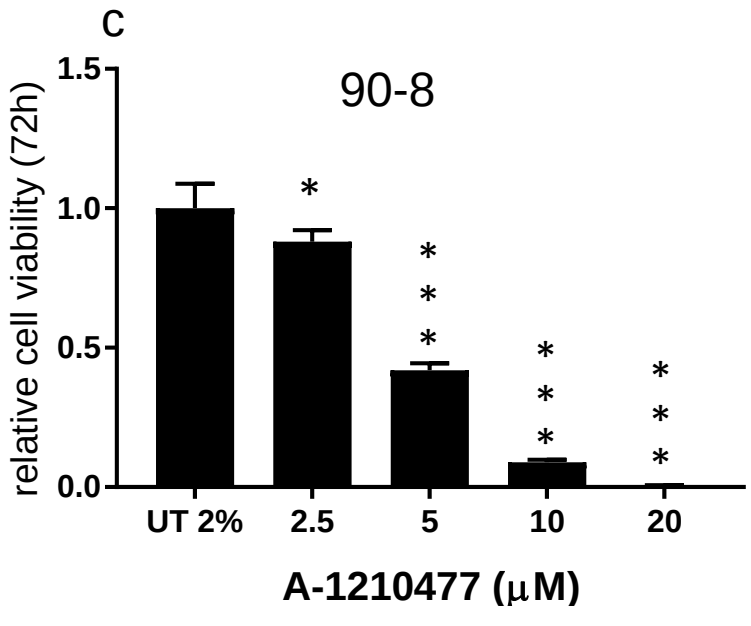
c
90-8
relative cell viability (72h)
1.5
1.0
0.5
0.0
UT 2%
2.5
5
10
20
A-1210477 (μM)

Supplementary Fig. 2: Mcl-1 pharmacological inhibition using A-1210477 reduces cell viability in MPNST cell lines. (a-c) ST88-14 cells (a), T265-2c cells (b) and 90-8 cells (c) were treated with increasing concentrations of A-1210477 for 72h. Cellular viability was determined by CellTiter-Glo® assay and the relative cell viability values were calculated normalizing data on the untreated samples. * = 0.0135, *** ≤ 0.001. Data are presented as mean and SD, n=3.

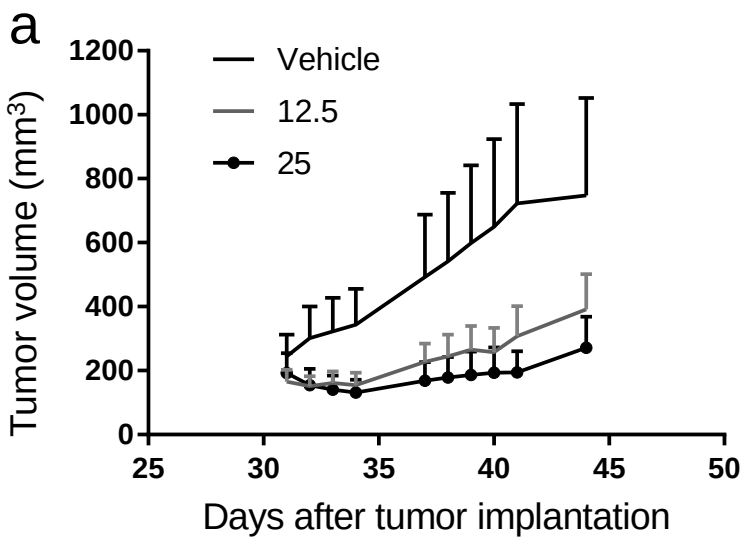

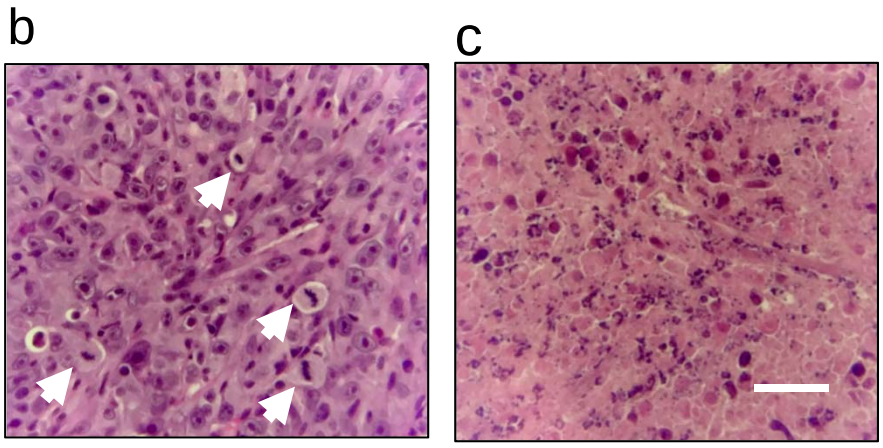

Vehicle WP1130

Supplementary Fig. 3: Delayed treatment with WP1130 reduces tumor size in a mouse model generated by subcutaneous injection of ST88-14 cell line. (a) Tumor growth curves showing the increase in tumor size for each treatment group. Data are presented as mean and SEM. One-way ANOVA test for multiple comparisons showed a statistically significant difference between groups, with $p \leq 0.001$. **(b, c)** Representative pictures, after H & E staining, showing the histological morphology of tumors from animals receiving either vehicle or WP1130 at the concentration of 12.5 mg/Kg. Mitotic figures are highlighted by arrows. Scale bar, 50 μm.

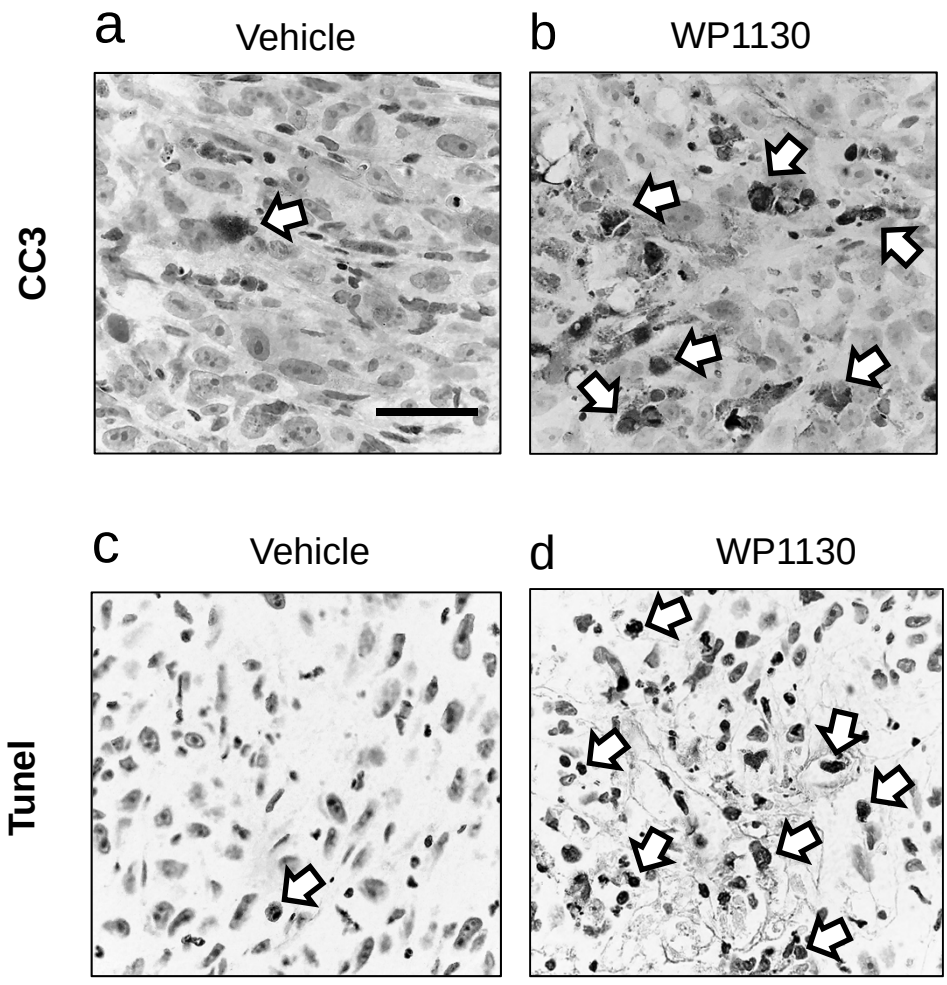
a
Vehicle
b
WP1130
CC3
c
Vehicle
d
WP1130
Tunel

Supplementary Fig. 4: WP1130 treatment *in vivo* increases cleaved caspase 3 immunoreactivity and TUNEL staining in MPNSTs. (a, b) Representative photomicrographs showing cleaved caspase 3 immunoreactivity (CC3) of tumors from mice receiving either vehicle or WP1130 at the concentration of 25 mg/kg. Arrows indicate positive cells. Scale bar, 60 µm. **(c, d)** Representative photomicrographs showing TUNEL staining of tumors from mice receiving either vehicle or WP1130 at the concentration of 12.5 mg/Kg. Arrows indicate positive cells. Scale bar, 60 µm.